SEISMIC RISK REDUCTION OF LOW DUCTILITY RC FRAMES USING YIELDING SHEAR PANEL DEVICE

FATEMA TUZ JOHORA

(BSc Engg., MIST)

A THESIS SUBMITTED

FOR THE DEGREE OF MASTER OF

SCIENCE IN CIVIL ENGINEERING

DEPARTMENT OF CIVIL ENGINEERING

MILITARY INSTITUTE OF SCIENCE AND TECHNOLOGY

2017

The thesis titled "Seismic Risk Reduction of Low Ductility RC Frames Using Yielding Shear Panel Device" submitted by Fatema Tuz Johora Roll No: 2014110029 Session 2014-2015 has been accepted as satisfactory in partial fulfillment of the requirement for the degree of Master of Science in Engineering (M.Sc. Engg.) on 21th August,2017.

BOARD OF EXAMINERS

1. Dr. Md Raquibul Hossain — Chairman
   Assistant Professor — (Supervisor)
   Department of Civil Engineering, BUET, Dhaka.

2. Dr. Mahmud Ashraf — (Co-Supervisor)
   Associate Professor
   Department of Civil Engineering. Deakin University, Australia.

3. Shah Md Muniruzzaman — Member
   Head of the Department — (Ex-Officio)
   Department of Civil Engineering, MIST, Dhaka.

4. _____ — Member
   Dr. Khondaker Sakil Ahmed
   Associate Professor
   Department of Civil Engineering, MIST, Dhaka.

5. _____ — Member
   Dr. Iftekhar Anam — (External)
   Professor
   Department of Civil Engineering, UAP, Dhaka.

DECLARATION

I hereby declare that this thesis is my original work and it has been written by me in its entirety. I have duly acknowledged all the sources of information which have been used in the thesis

This thesis has not been submitted for any degree in any university previously

Fatema Tuz Johora

21th August, 2017

ACKNOWLEDGEMENT

First of all, I am indebted to the Almighty Allah for overwhelming all the obstacles and predicament that faced during the whole research work and for bringing this thesis into its authenticity.

I am gratified to articulate my heartiest appreciation and heartfelt indebtedness to my supervisor, Dr. Md Raquibul Hossain, Asst. Professor, Department of Civil Engineering, BUET, co-supervisor Dr. Mahmud Ashraf, Associate Professor, School of Engineering Deakin University Geelong, Australia and Kamrul Islam, Assistant Professor, Department of Civil Engineering, MIST. Without their secure supervision this thesis would not be able to reach its triumph. Their efforts and encouragement in preparation of the manuscripts have made the work easier for me.

I would like to thank Shah Md Muniruzzaman, Head of the Department, Military Institute of Science & Technology for his collaboration during all the phases of this thesis.

I would like to thank to all the accompanying persons during all these research works.

DEDICATION

DEDICATED TO MY PARENTS AND SPOUSE

PREFACE

This thesis is a result of around two and half years research works from October 2014 to July 2017 under the supervision of Dr. Md Raquibul Hossain and Dr. Mahmud Ashraf. This thesis is presented in an integrated article format.

TABLE OF CONTENTS

ABSTRACT

Earthquake is a great threat for human lives as well as for the infrastructures. The loss of human lives and the socio-economic impact of the earthquake makes this hazard more important to analyze and identify the most cost effective and easy to adapt solutions to minimize the losses. The underlying principal for different control systems that are used to protect buildings from damaging earthquake effects is to dissipate the energy as such no or minimal damage occurs to the structure itself. Passive control device is one of the most suitable and reliable technologies as it does not require external power for being active to dissipate energy. The current research proposes the use of a passive energy dissipating device named Yielding Shear Panel Device (YSPD) for strengthening existing low ductility RC buildings. YSPD consists of a square hollow section (SHS) with a diaphragm plate. The basic concept of the YSPD exploits the in plane shear deformation of a steel plate to dissipate the energy introduced due to an earthquake. Bouc-Wen-Baber Noori (BWBN) material is used to simulate the pinching hysteretic force deformation relationship of YSPDs. YSPDs are modeled as spring elements connected between the beam and the V-brace. Static pushover analysis has been conducted to find out the change in capacity of the structure after installing YSPDs. Furthermore, eigen value analysis, time history analysis, incremental dynamic analysis and fragility analysis are done to find out the seismic performance of YSPDs. Three different sizes of YSPDs with three different arrangements are used for the seismic performance evaluation. The result obtained from the static and dynamic analyses for the bare frame and the frames with different sizes and arrangements of YSPDs are compared. The results from the simulations suggests installation of YSPDs has improved the capacity of the structure. The results also suggests that increased size of the YSPD dissipates more energy, and reduces the inter story and roof drift of the structure. The simulated structure shows better performance when YSPDs are installed in three story-three bay configuration compared to first story-three bay and three story-second bay configuration.

LIST OF TABLES

LIST OF FIGURES

CHAPTER 1: INTRODUCTION

1.1 General

Earthquake is one of the most life threatening natural hazards. Devastating earthquakes occurring in different parts of the world in the recent years pose a great risk for human lives. A severe earthquake can cause damages and destructions of civil engineering structures, national economic losses and more importantly, it can cause casualty. For example, a severe earthquake with a magnitude of 7 Mw occurred in Haiti on 12th January 2010 causing estimated 222,570 human lives and leaving another 1.3 million people homeless **[1]**. China also faced an earthquake of 6.9 Mw in 14th April 2010, due to this earthquake 2698 people were died and 12135 were injured **[1]**. More recently, a devastating earthquake hit Nepal in 25th April 2015. Nepal was shaken by this Gorkha earthquake (7.8 Mw), followed by two aftershocks on 26th April and 12th May, leaving approximately 9,000 and 22,000 people being killed and injured, respectively **[1]**. Figure 1.1 shows photographs of the severity and destructive effect of this earthquake.

Figure 1.1: The impact of earthquake in Nepal **[3].**

Table 1.1 below lists major earthquakes occurred from 2006 to 2016 **[1]**. Maximum intensities are indicated on the Mercalli and are sourced from United States Geological Survey (USGS) Shake Map Data. Table 1.2 lists the earthquakes that occurred in 2016 alone and resulted in 10 or more causalities.

Table 1.1: Number of earthquakes worldwide between 2006 -2016 **[1]**

Magnitude	2006	2007	2008	2009	2010	2011	2012	2013	2014	2015	2016
8.0+	2	4	0	1	1	1	2	2	1	1	0
7.0-7.9	9	14	12	16	23	19	2	17	11	18	16
6.0-6.9	142	178	168	144	150	185	108	125	143	127	130
5.0-5.9	1712	2074	1768	1896	2209	2276	1401	1453	1574	1413	1550

Table 1.2: Earthquakes with at least 10 dead ranked by death toll (Occurred in 2016) **[2]**

Rank	Death Toll	Magnitude	Location	MMI	Depth (Km)	Date
1	661	7.8	Ecuador	VIII	20.6	April 16
2	117	6.4	Taiwan	VII	23.0	February 6
3	40	7.0	Japan	IX	11.0	April 15
4	11	6.7	India	VII	55.0	January 3

1.2 Objectives of the thesis

The objectives of the present investigation are to find out the seismic vulnerability of low ductility RC building, retrofit the structure using YSPD as an energy dissipating tool and finally, to compare the seismic performances of the structures retrofitted with and without YSPD. The specific objectives of the thesis are:

1. To determine the seismic performance of the low-ductility RC frame and YSPD retrofitted RC frame.

2. To compare the performance in terms of base shear capacities, roof drift and maximum inter-story drift.
3. To evaluate the risk based seismic vulnerability assessment of the structure with YSPDs and without YSPDs through fragility analysis.
4. To determine the best configuration of YSPDs within a frame based on the results of the seismic performance of RC frames fitted with YSPD obtained from the nonlinear static and dynamic analyses.

1.3 Thesis organization

Chapter 1 illustrates the objective of the research work.

Chapter 2 provides literature review on retrofitting techniques and more specifically on YSPD.

Chapter 3 presents the description of the building taken for analysis. It also describes the finite element modeling of the moment resisting frame with YSPDs. This chapter illustrates the static pushover, dynamic time history, incremental dynamic analysis (IDA) and fragility analysis of the moment resisting frame and summaries the results obtained from these analyses. Finally, this chapter describes the seismic performance evaluation of the moment resisting frame with YSPDs and compares the performance of the structure with YSPDs and without YSPDs.

Chapter 4 provides the conclusions as well as the limitations of the study and recommendations for possible future development in this field.

CHAPTER 2: LITERATURE REVIEW

2.1 Introduction

Previous studies studied the behavior of low-rise and mid-rise reinforced concrete frame buildings against earthquake load. Erberic and Cullu identified several causes of heavy damage, and even collapse in the worst case, of reinforced concrete buildings as a result of earthquakes **[4]**. The causes, as identified in the study, were:

a) Not following the current codes/regulations by most designers.
b) Not considering the Seismic behavior of the structure in architectural design and during the selection of the structural system.
c) Failure to maintain Construction quality properly.

To improve the quality of the structures and make the structures safer the evaluation of seismic performance of these building is a must. Fragility is the most important parameter In order to determine the seismic performance of these structure. Fragility is a key indicator of infrastructure performance and seismic risk assessment. Fragility is a function of demand on the system, which means the probability of failure in order to meet a performance objective **[5].** In other words, fragility is the ability of an engineering system to withstand a specified demand **[6].** Padgett and DesRoches describes the fragility as a given ground motion intensity (IM), it is conditional probability for the seismic demand (D) which will exceed the capacity (C) of the structure.

$$\text{Fragility} = P\,[D \geq C|IM] \qquad (2.1)$$

Nielson (2005) describes fragility as a conditional probability and demonstrates that a structure will meet or exceed a specified damage level for a known ground motion intensity.

$$\text{Fragility} = P[LS|IM = y] \qquad (2.2)$$

Where LS is the limit state or damage level of the bridge or bridge components, IM is the ground motion intensity and y is the realization of the chosen ground motion intensity. Damage limit demonstrated the following things global drift ratio (maximum roof drift normalized by the building height), inter story drift ratio (maximum lateral displacement between two consecutive stories normalized by the story height), maximum roof displacement or story shear force etc and

the ground motion intensity used in the fragility functions is one of the followings spectral quantities, peak ground motion values, modified Mercalli scale etc **[7].**

Fragility not only finds out the probability of a specified damage state but also describes the maximum probable losses **[5].** Fragility is helpful for the owners as it offers tools to evaluate alternative retrofit measure for the structure **[5].**In order to optimize the seismic design of structures and compare different seismic rehabilitation technique fragility curves are used **[8].**

There are various kinds of methods for fragility development, one of these is empirical method using empirical data from past earthquake events. **[4]**. Fragility curves are also developed based on experts' opinion. For example, sufficient data was not available when the Applied Technology Council (ATC) developed the ATC-13 report; therefore, ATC put together a panel of 42 experts to provide information. Analytical method can also be used for fragility analysis. In analytical method, structural demands or capacities are used in order to find out the failure probability **[5].** A large number of analytical fragility curves have been developed by many researchers. For example, Mander and Basozn developed analytical fragility curves for HAZUS using finite element technique **[10]**. Similarly, Karim and Yamazaki developed analytical fragility curve for the Kobe earthquake **[11]**. Kurian et al. developed analytical fragility curves for a railway overbridge **[12].** Kurian et al. used analytical fragility curves for typical three span two lane railway over bridge which is situated in highly seismic region. They developed analytical fragility curve assuming lognormal distribution and found that sensitivity of fragility curve is high for high damage level of the structural modeling. Neilson et al. also developed analytical fragility curves for different classes of highway bridges **[13].** Kibboua et al. determined the seismic vulnerability for reinforced concrete bridge piers using analytical fragility curves **[14].** Mander developed a basis for fragility curves that can be used to find out the vulnerability of highway bridges **[15].** Sbinozuka and Kim developed analytical fragility curves for concrete bridges retrofitted with steel jacketing and adjusted the empirical fragility curves obtained for the unretrofitted bridges **[16].** Elnashai developed analytical fragility curve and showed a comparison with the empirical curves for Northridge and Kobe earthquake **[17]**. Using analytical methods Neilson (2006) developed fragility curves for nine types of bridges. He created 3-D analytical models. After that he generated probabilistic seismic demand models (PGMD). From these models he developed fragility curves specific level of damage **[9].** Mackie and Stojabinovic developed analytical and numerical fragility

curves for single bent reinforced concrete highway overpass bridges **[18].** Kibboua et al. generated analytical fragility curves for typical Algerian reinforced concrete bridge piers **[19].**

Structural demand and capacity models are need to be developed before generating analytical fragility curves **[20].** Two different methods are used to develop probabilistic seismic demand model (PGMD), the scaling method and the cloud approach **[20].** In the scaling method scaled earthquake data are used and incremental dynamic analysis (IDA) is done at each intensity level on the other hand cloud method uses unscaled earthquake data after that nonlinear time-history analysis is done to developed PGMD model **[20]**

Limit state capacities are used in order to describe the fragile condition of a structure. Limit state capacity is the ability of a structure to withstand the demand during seismic excitation **[20].** It is the performance of structure ranging from uncertainty to various damage levels including collapse. ASCE 41 (ASCE 2007) and FEMA 356 provide guidance on three performance levels **[20]** as discussed section below.

Structure falls into immediate occupancy (IO) category if structural damages are within limit (such as yielding of steel, significant cracking of concrete, nonstructural damage). Occupants are permitted for the immediate access in to the structure.

In life safety (LS) category structure may be collapse partially or totally but the risk and injury will be minimum and occupants are protected from loss of life.

For collapse prevention (CP) category there is no margin against collapse and structure supports gravity loads.

Limit states capacity follows a lognormal distribution **[21, 22, 23].** Here is a closed form solution for the fragility in lognormal form given bellow-

$$\text{Fragility} = \emptyset\left(\frac{\ln\left(\frac{Sd}{Sc}\right)}{\sqrt{\beta^2 D|IM + \beta^2 c}}\right) \qquad (2.3)$$

Where Sc is the median value of the structural capacity (for the limit state) and βc is its associated logarithmic standard deviation of structural capacity.

According to FEMA 356 the limit state capacities for IO, LS, CP are 1%, 2%, 3% maximum allowable drift ratios for concrete building **[25]**. The fragility $F_r(x)$ and seismic hazard H(x) are calculated using the following formula:

$$F_r(x) = \frac{\varphi\,[\,(\ln x - \ln Sa)}{\beta_R} \qquad (2.4)$$

$$H(x) = k_0 x^{-k} \qquad (2.5)$$

where,

S_a = median value of the fragility of the structure in units of S_a

β_R = lognormal standard deviation of the system fragility

Φ = standard normal cumulative distribution function

K_0 and k = constant depend on the site of the building

The uncertainties associated with seismic demand and structural capacity is defined by dispersion parameter β_R. β_R is calculated using the following formula

$$\beta_R = \sqrt{\beta_{D|S_a}{}^2 + \beta_c{}^2} \qquad (2.6)$$

$\beta_{D|S_a}$ = uncertainty in seismic demand

β_c = uncertainty in structural capacity

No wonder that the severity and disastrous effects of earthquakes has drawn the attention of the academia and the industries to find out easy to adapt and cost-effective solutions to minimize impacts of earthquake and save the lives of the people **[26]**. Comprehensive researches have been conducted in this regard and different types of retrofitting techniques have been proposed and

utilized to strengthen the structures against earthquake loads. Some of these techniques are discussed here.

Olivato and Marletta reviewed different types of retrofitting techniques including traditional and innovative methods **[29]**. They suggest that traditional methods such as increase of strength and stiffness, mass reduction can be ineffective as these methods do not consider seismic design criteria. They categorized stiffness reduction, ductility increase, damage controlled structures, composite materials and active control as innovative methods. Stiffness reduction method was discussed briefly. They showed that stiffness reduction method is very effective to minimize the effect due to the earthquake.

Ranjan and Dhiman used three different types of jacketing techniques, named Reinforced Concrete (RC), Fiber Reinforced Polymer Jacketing (FRP) and Steel Fiber Reinforced Concrete (SFRC), to increase the strength of columns of existing building **[27]**. The researchers also described the design procedures the for RC, FRP, SFRC jacketing of concrete columns. They concluded that FRP jacketing is advantageous than RC and SFRC but slightly expensive.

Kunisue et al. used elasto–plastic steel dampers in existing buildings to increase the energy dissipation **[28]**. They conducted experimental analysis to determine the effectiveness of the frames with dampers and performed response analysis of the frames with dampers. The study reported that, based on the experimental and response analyses performed, the elasto-plastic steel dampers were able to dissipate earthquake energy.

Rizkalla and Hasan conducted experiments to evaluate the performance of pre-stressed concrete bridge fitted with different types of retrofitting techniques **[30]**. Five different retrofitting techniques, named as extremely bonded CFRP strips, near surface mounted leadline bars, near surface mounted C-Bar CFRP bars, near surface mounted CFRP strips, extremely bonded CFRP sheets were used in this study. They compared different retrofitting techniques in terms of construction cost in USA and % of increase in capacity. They showed that extremely bonded CFRP sheets are most cost effective and can increase the capacity of the structure more than the other technics. Extremely bonded CFRP strips are also low cost and capability of increasing capacity of the structure is slightly lower than extremely CFRP sheets. Near surface mounted C-Bar CFRP bars is costly and capable of increasing capacity of the structure. Near surface mounted leadline bars and near surface mounted CFRP strips are more costly than the others but % of increase in

capacity is almost similar to the other technics. They also suggested the development length should not be less than 800 mm for 10 mm diameter near surface mounted C-BAR CFRP bars, 850 mm for near surface mounted CFRP strips (25 x 1.2 mm), 500 mm for CFRP sheets bonded to the soffit of concrete specimens.

Vaghani et al. also reviewed different types of retrofitting techniques and structural control systems **[31]**. They discussed about jacketing of existing beams, columns or joints with the use of friction damper, metal shear panels and fiber reinforced cement, the method of confinement of column by embedded composite grid, use of steel fiber reinforced mortar, steel bracing etc. They recommended that steps should be taken to update design manuals and codes of practice considering various strengthening methods and current structure has to be assessed properly before applying any retrofitting techniques.

The retrofitting techniques discussed above are often very expensive and complicated process to adapt for practical purposes. Recently different types of control devices such as active, semi-active passive control devices have been used both in research and industrial purposes to dissipate the earthquake energy. Control devices are easy and relatively inexpensive to install. Generally, the energy introduced by earthquake is transferred to the super-structure through the foundation **[30]**. Part of this energy can be dissipated through the use of supplementary energy dissipation devices to save the super-structure from damages **[31]**. Use of control systems to dissipate the earthquake energy is very common solution to the earthquake engineers. Three categories of control devices, such as active control device, semi- active control device and passive control device, are used **[32]**. These devices are categorized based on their working procedure. Active control devices require external source of power to dissipate the energy. Extensive research have been done on active control device. Currently Japan is using active control devices to protect structures from wind and earthquakes **[33]**. Semi-active devices require small amount of external power. On the other hand, passive control devices do not require any external source of power to be activated which makes it a very reliable method of control system **[34].** Different categories of structural control systems and the working mechanisms of active and passive energy devices are shown in Figure 2.1 and Figure 2.2, respectively **[35]**.

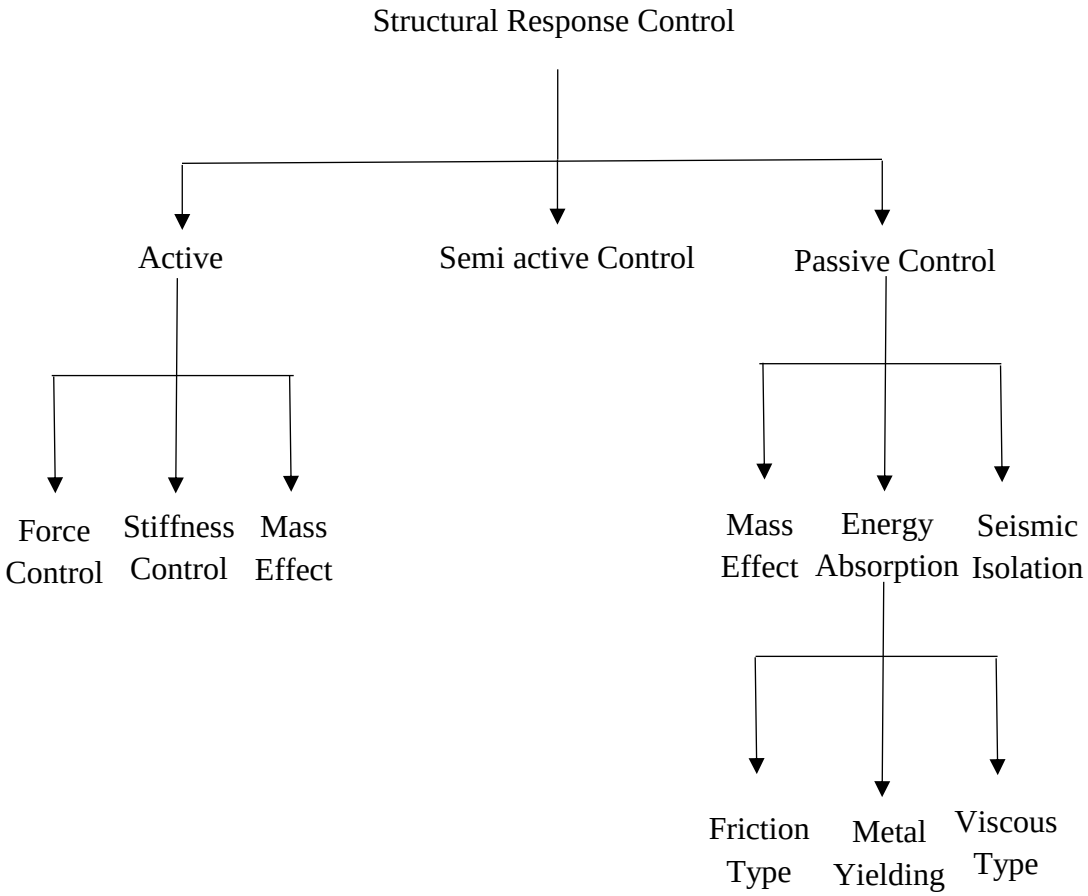

Figure 2.1: Categories of structural control system **[37]**.

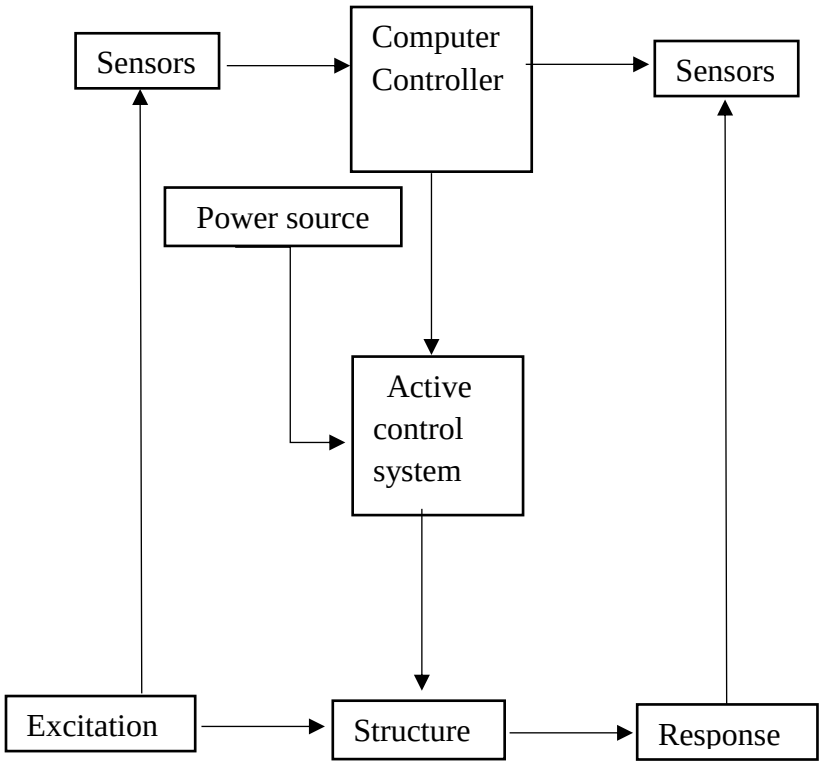

(a)

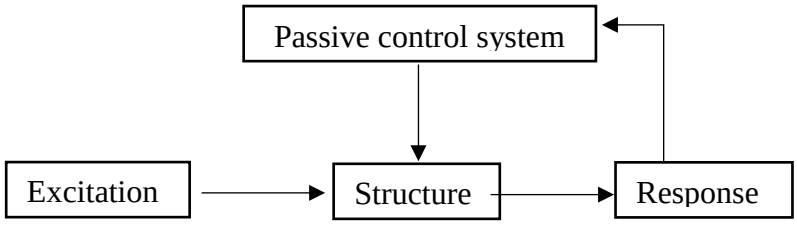

(b)

Figure 2.2: Flow diagram of the working steps of structural control systems--(a. structure with active control system. –b-. structure with passive control system-) [**35]**.

There are different kinds of passive control devices, such as, named metal yielding, seismic isolation, sliding friction, shearing and viscous fluid [**36]**, some of these are briefly discussed below:

Friction dampers dissipate energy through the friction occurring due to the relative sliding of two solid bodies **[36]**. Different types of friction damper have been developed to improve energy dissipation capacity of the structure. Pall et al. worked on variety of samples with different surface treatments and performed static and dynamic tests **[37]**. Pall and Marsh proposed X-braced friction damper and used a simple elasto-plastic model to represent the behavior of the damper **[38]**. Subsequently Filiatrault and Cherry developed more detailed macroscopic model for the friction damper **[39]**. Other types of friction dampers, such as three stage friction grip elements, the slotted bolted connections, have also been developed by the researchers [**40, 41]**.

Viscoelastic dampers were used to control the vibration of the structure against wind **[37]**. Recently it has been used for seismic control. Comprehensive experimental work has been carried out on viscoelastic dampers by many researchers for steel frames **[42-44]**. Chan et al. carried out shaking table test on the visco-elastically damped structure for El Centro earthquake **[45]**. Chan et al. also conducted experiments on three story lightly reinforced concrete frame equipped with viscous dampers **[46]**. They found that viscoelastic damper can reduce the overall response and the risk of developing damaging mechanism near collapse.

2.2 Metal yielding passive energy dissipating device

A good metallic device should possess certain characteristics i.e. it should have sufficient elastic stiffness and yield strength to withstand the in service lateral load. It should also have capability to dissipate large amount of energy and normally representable stable hysteretic force-displacement response **[47]**. The energy dissipating device is connected between the V-brace and beam in series **[47]**. The total in-plane stiffness ($k_{bd)}$ of the brace –device assembly is given by Equation 2.7.

$$k_{bd} = \frac{1}{\frac{1}{k_b} + \frac{1}{k_d}} = \frac{k_b\, k_d}{k_b + k_d} \tag{2.7}$$

where, k_b = stiffness of the brace

k_d = stiffness of the device

Equation 2.7 represents that the brace stiffness is compromised with the incorporation of flexible damper.

Various types of yielding passive energy dissipating devices, such as, Added Damping and Stiffness (ADAS), Triangular Added Damping and Stiffness (TADAS), Buckling Restrained Brace (BRB) and Yielding Shear Panel Device (YSPD) are used by many researchers to absorb the earthquake energy.

ADAS device consists of several X-shaped tapered mild steel plates. The plates are connected together using bolts. It is connected together between the V-brace and the bottom of beam **[48]**. ADAS dissipate energy through flexural deformation. X shape prevents the possibility of stress concentration and the corresponding failure.

TADAS consists of triangular steel plate which dissipate energy through hysteretic flexural deformation. One end of the TADAS is kept fixed while other end is pin supported. The concept of energy dissipation of TADAS is it absorbs energy through hysteretic flexural deformation. It shows stable hysteretic response due to its simple geometric configuration **[49]**.

BRB has two distinct elements; one is the load carrying element and the other is the lateral support element. Load carrying element deforms inelastically due to the diagonal tension and compression resulting from lateral movement of the frame. The lateral support system protects the central load carrying element from buckling **[57]**.

2.3 Single degree of freedom system fitted with energy dissipating device

So far many researchers worked on the energy dissipating device to absorb the energy induced due to earthquake. Soong and Dargush explained the energy dissipation mechanism of yielding energy dissipating device through Single Degree of Freedom (SDOF) system **[50]**. Figure 2.3 (a) depicts a single degree of freedom system along with an energy dissipating device. The force displacement relationship of energy dissipating device is shown in Figure 2.3 (b)

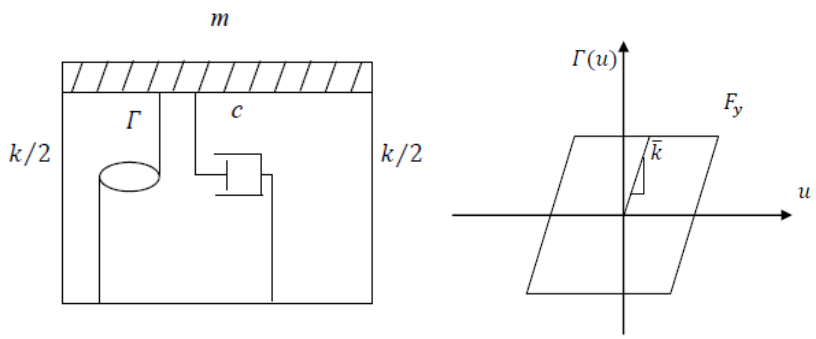

(a) (b)

Figure 2.3: (a) Single degree of freedom system with energy dissipating device. (b) Force displacement relationship of energy dissipating device **[49]**.

The equation of a SDOF in combination of an energy dissipating device can be expressed as:

$$m\ddot{u} + c\dot{u} + ku + \Gamma(u) = -(m + m_d)\ddot{u}_g \quad (2.8)$$

where, m, k, c are mass, stiffness and damping coefficient of parent structure consequently.

Γ (u) is force acting on the energy dissipating device as a function of lateral displacement

$\ddot{u}_g$ is ground acceleration

m_d is the mass of energy dissipating device, which can be neglected. So the Equation (2.8) becomes

$$m\ddot{u} + c\dot{u} + ku + \Gamma(u) = -m\ddot{u}_g \quad (2.9)$$

The balanced equation of SDOF with energy dissipating device is represented by the Equation 2.10.

$$E_I = E_K + Es + E_V + E_D \quad (2.10)$$

where,

Earthquake input energy, $E_I = -\int_0^u m\ddot{u}_g\, du = -\int_0^t m\ddot{u}_g \dot{u} dt$ (2.10.a)

Kinetic energy, $E_k = \int_0^U m\ddot{u}\, du = mu^{\cdot 2}/2 E_k = \int_0^U m\ddot{u}\, du = mu^{\cdot 2}/2$ (2.10.b)

Elastic strain energy, $E_s = \int_0^u kudu = ku^2/2 E_s = \int_0^u kudu = ku^2/2$ (2.10.c)

Viscous damping energy, $E_v = \int_0^u c\dot{u}\, du = \int_0^t c\, u^{\cdot 2} dt$ (2.10.d)

Dissipated hysteretic energy by energy dissipating device, $E_D = \int_0^U \Gamma(u) du$ (2.10.e)

From the Equation 2.10 it is observed that the energy dissipating device is able to dissipate more energy induced during earthquake.

Chan investigated the energy dissipation capacity of SDOF system equipped with energy dissipating device for EI Centro earthquake **[32]**. He found that 60% of the earthquake energy may be dissipated by energy dissipating device and the rest energy is dissipated through viscous damping. Energy dissipation of the SDOF system fitted with energy dissipating device is shown in Figure 2.4.

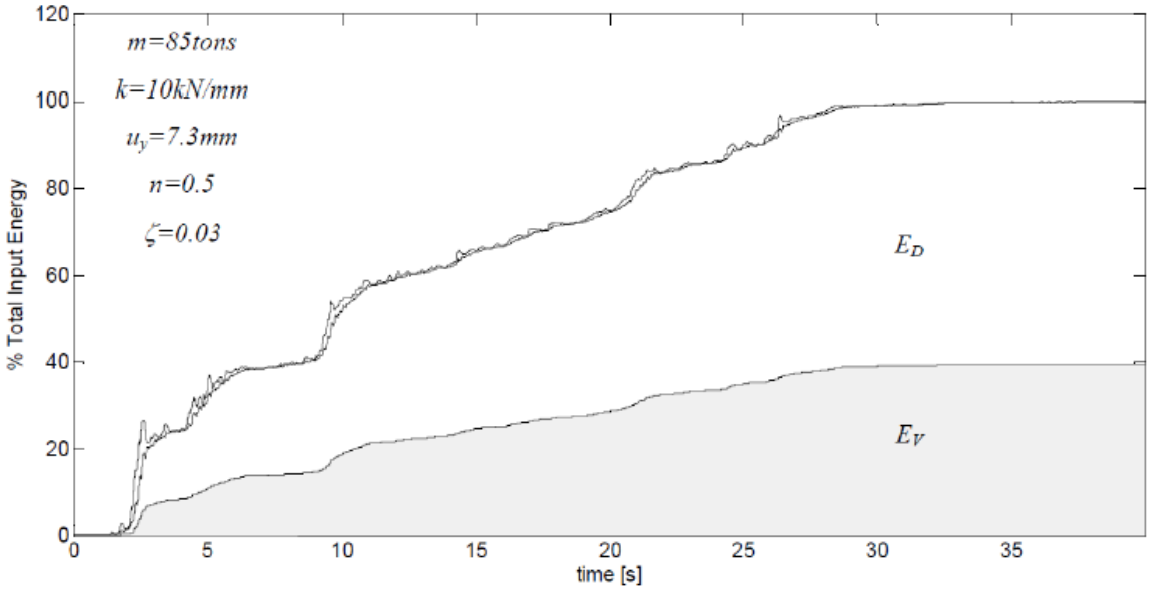

Figure 2.4: Energy dissipation of SDOF system equipped with energy dissipating device **[33]**

2.4 Background of yielding shear panel device (YSPD)

Yielding shear panel device is a passive energy dissipating device consisting of a square hollow section (SHS, dimension D x D x T) and diaphragm plate (thickness, t). Figure 2.5(a) shows the real image of YSPD. Square section is more effective in developing 45° tension field than the rectangular section **[47]**. The steel diaphragm plate is welded inside the square hollow section and it deforms in shear to dissipate earthquake energy due to the relative horizontal displacement of the top and the bottom part of the section. Deformed Shape and schematic diagram showing the geometric parameters of YSPDs are shown in Figure 2.5 (b) and Figure 2.5 (c). YSPD is a very simple and inexpensive device and its installation and replacement is easier than other control devices **[47]**.

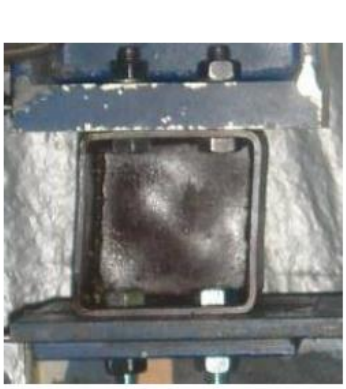

(a)

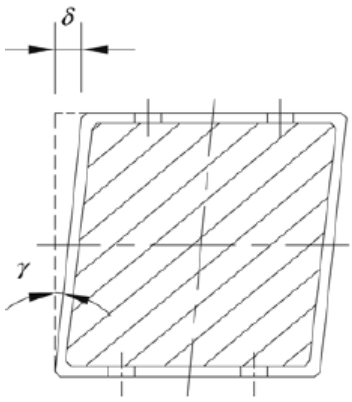

(b)

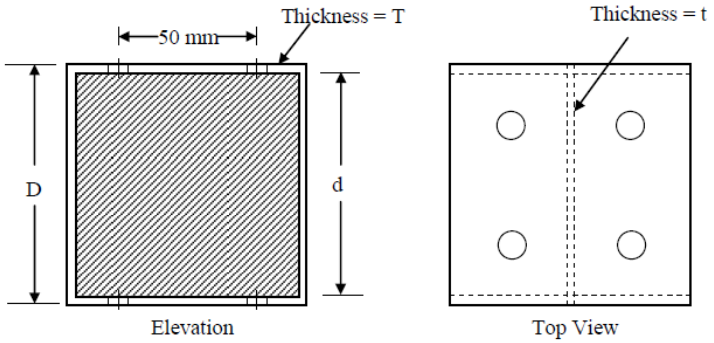

(c)

Figure 2.5: (a) Yielding shear panel device (b) Deformed Shape (c) Schematic diagram showing the geometric parameters of YSPDs **[33]**.

YSPD was first designed by U. Dorka at the University of Kassel, Germany to dissipate the earthquake energy **[52]**. YSPD was first introduced by Williams and Albermani using the design proposed by Dorka **[53].**

Figure 2.5 (a) shows a real image of yielding shear panel device that was tested by Chan **[34]**. He connected YSPDs with the test set up using bolt in a similar way when YSPDs are connected with the beam and V-brace. There were four bolts spaced at a centre-to-centre distance of 50 mm connected on each of the opposite flanges of square hollow sections, shown in Figure 2.5 (c).

Chan et al. conducted nineteen monotonic and cyclic tests to evaluate the performance of YSPD **[32]**. They used total 19 specimens with 6 different combinations of diaphragm plate to SHS. These set of experiments showed that the slenderness ratio of the diaphragm plate and in-plane rigidity of the surrounding SHS influences the performance of YSPD. They also found that energy dissipation, strength and ductility was proportional to the slenderness of diaphragm plate. The device with slenderness ratio 49.5 offered good energy dissipation and strength. They observed that the device with high slenderness ratio buckled while the device with low slenderness ratio did not buckle. However, the performance of the device with low slenderness ratio was poor in terms of strength and energy dissipation due to localized deformation of the SHS.

Chan et al. derived a preliminary design of YSPD to conduct experimental analysis and find out the capability to dissipate earthquake energy **[47]**. Figure 2.5 (b) shows the deformed shape of YSPD. The equation for the theoretical elastic in-plane lateral stiffness of the device considering minor contribution from the square hollow section can be written as:

$$k_d = \frac{Gtd}{d} = Gt \tag{2.12}$$

where, G= shear modulus

t = thickness of the diaphragm plate

Assuming von Mises yield criterion for a compact diaphragm plate the yield strength can be taken as shear yield strength.

$$F_y = \frac{f_y}{\sqrt{3}} td \tag{2.13}$$

where, d = width of the steel plate

f_y = tensile yield stress

Yield displacement of the device can be written as

$$u_y = \frac{F_y}{k_d} = \frac{f_y\ d}{\sqrt{3}\ G} \tag{2.14}$$

Elastic shear buckling will take place for a device with slender diaphragm plate. The equation 2.15 represents the critical shear stress for a simply supported plate.

$$\tau_\sigma = k_s \frac{\pi^2 E}{12\ (1-\upsilon^2)} \left(\frac{t}{d}\right)^2 \tag{2.15}$$

where,

k_s = 9.35 for square plate

E = Young's modulus

υ = Poisson's ratio

Taking E =205 Gpa and υ =0.3 the limiting plate slenderness ratio at which buckling occurs is

$$\left(\frac{d}{t}\right) = \frac{1732}{\sqrt{fy}} \tag{2.16}$$

Where f_y is the yield strength of the diaphragm plate (MPa).

Chan et al. conducted experiments to evaluate the seismic performance of perforated yielding shear panel device (PYSPD) **[55]**. Perforations on the diaphragm plate affect the stress patterns. From the finite element model it was found that tension field was developed under shearing action. Figure 2.6 shows the von Mises yield criterion stresses of the models with perforation diameter d_p = 5.5 mm deformed at 0.25% strain. From the Figure 2.6 it is observed that stress is high along the tension field diagonally on the plate. They concluded that perforations clearly interrupt the stresses. They also found that the PYSPD reduced elastic stiffness and yield strength and produced a stable hysteretic behavior.

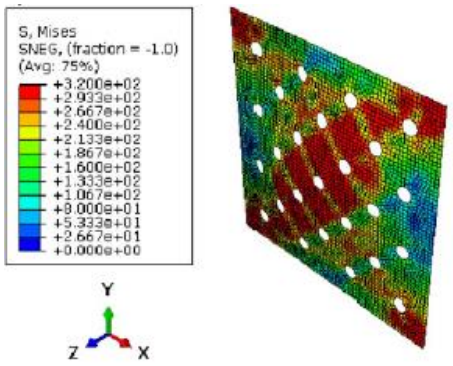

(a)

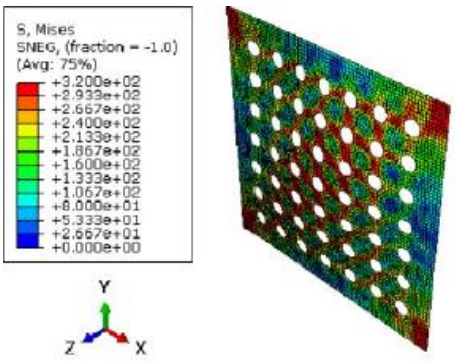

(b)

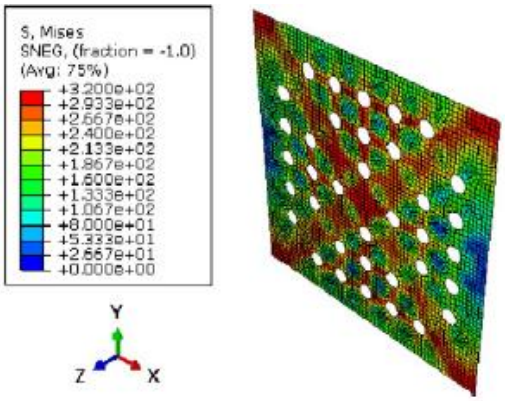

(c)

Figure 2.6: Mises stress distribution of (a) FE-1-5.5; (b) FE-2-5.5 and (c) FE-3-5.5 at 0.25% average strain **[55]**.

Zhengying et al. developed a modeling technique in order to describe the hysteretic response of YSPD **[56]**. They developed a BWBN model of the YSPD that accounts for pinching using Simulink and calibrated the hysteretic parameters they used experimental results of the YSPD. They incorporated the model in state-space approach to evaluate the response of the structure in terms of energy dissipation. In this study they used six different types of specimen. They showed that the energy dissipation of YSPD is 10% less when pinching is included in the model. Figure 2.7 shows the comparison of total energy dissipation ratio at each story using 100-2C and 100-3CS YSPDs. It is observed from Figure 2.7 that BWBN model with pinching shows less energy dissipation than the BW model without pinching. The incorporation of pinching showed better agreement with the experimental results for both of the specimens.

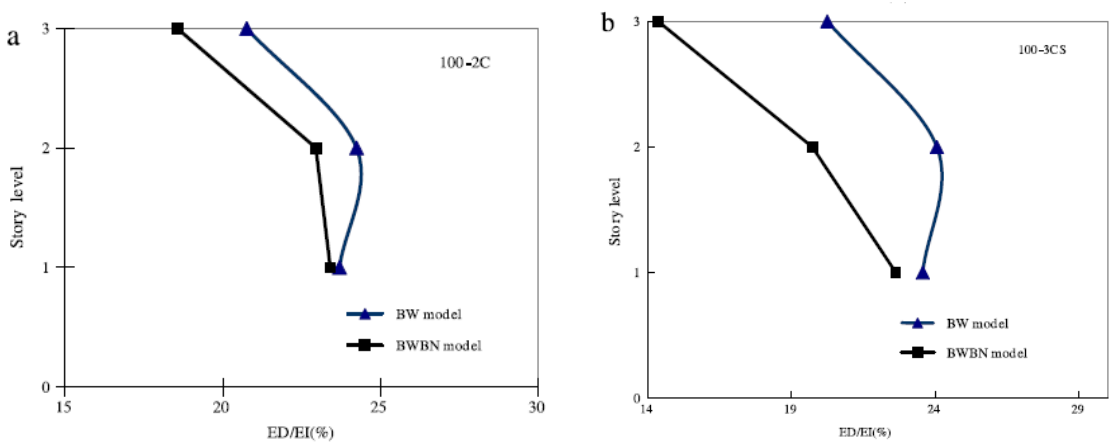

(a) (b)

Figure 2.7 : Variation of total energy dissipation E_D/E_I over the building (with and without pinching) using : (a) 100-2C and (b) 100-3CS **[56].**

Hossain et al. developed a finite element model for YSPD by using finite element software ANSYS **[26]**. They emphasized importance on modeling appropriate support conditions, initial geometric imperfections and residual stresses. Monotonic and cyclic test results were also used to verify the model. They also proposed theoretical formulas in order to predict the initial stiffness of load-deformation response which includes individual stiffness of the diaphragm plate and SHS.

Theoretical predictions for monotonic loading were almost similar with both FE and the experimental results.

Hysteresis response of YSPD was demonstrated using mathematical model developed by Hossain et al. **[33].** In order to simulate the response of energy dissipating device Bouc-Wen model was used earlier **[36].** One limitation of the Bouc-Wen model (BWBN) model was that it did not consider the effect of pinching and degradation of strength and stiffness. Therefore, a new model was developed by Baber and Noori to include strength degradation, stiffness degradation and pinching characteristics **[54].** They used a unified simple formulation technique for all the BWBN model parameters in order to use the easily obtainable physical properties such as plate thickness, size of the YSPD and material strength could be used in mathematical modeling. The mathematical model was able to simulate the performance of YSPD in terms of energy absorption **[33].** No detail modeling is required to show the effect of YSPD if this mathematical model is used. This mathematical model is used to develop design methods to find out the appropriate size, location and numbers of YSPD.

Hossain et al. performed a risk based seismic performance assessment of YSPDs in case of steel moment resisting frame. They considered a three story steel moment resisting frame which is designed for the SAC phase II steel project. They used three different types of YSPDs with two different types of arrangements. They installed YSPDs in the middle bay three story (case 1) and three bay three story (TT, case 2) and conducted incremental dynamic analysis and fragility analysis to evaluate the performance of YSPDs. Figure 2.8 shows the reduction in inter story drift demands (%) and dispersion of seismic demand ($\beta_{D|Sa}$) for different combination and cases. Table 2.1 illustrates the annual exceedance probability of different limit states. One of the outcomes of their research is increased size of YSPDs show better energy dissipation capacities. The increased size of YSPD is capable to reduce the median fragility and the limit states annual exceedance probability. Among two different types of arrangements TT arrangements shows better energy dissipation in comparison to the three story single bay arrangements **[58]**.

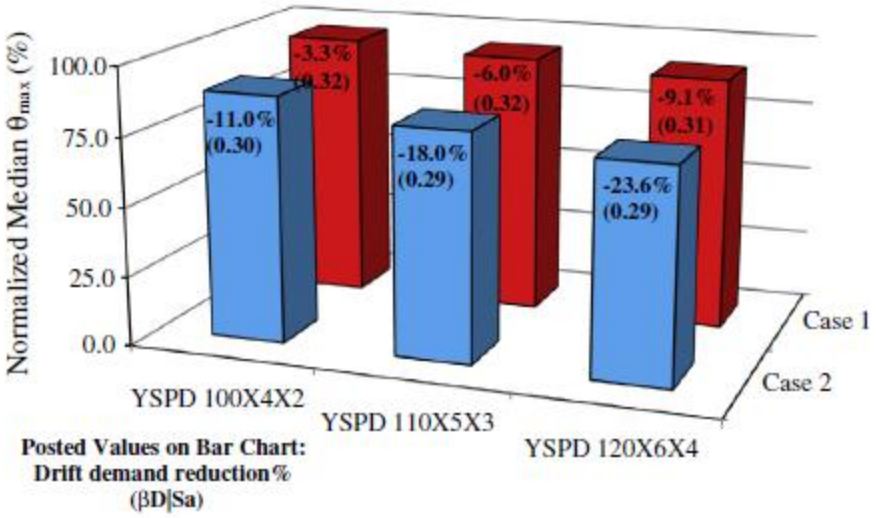

Figure 2.8: Reduction in inter story drift demands (%) and dispersion of seismic demand ($\beta_{D|Sa}$) for ground motions with design hazard level of LA **[58].**

Table 2.1: Annual exceedance probability of different limit states ($P_{LS)}$ with and without YSPDs **[58].**

	P_{LS} for different performance limit states		
	IO	LS	CP
No YSPD	1/6	1/250	1/1550
YSPD 100x4x2(case 1)	1/7	1/290	1/1560
YSPD 110x5x3(case 1)	1/10	1/310	1/1680
YSPD 120x6x4(case 1)	1/13	1/350	1/1860
YSPD 100x4x2(case 2)	1/15	1/360	1/2206
YSPD 110x5x3(case 2)	1/22	1/480	1/2360
YSPD 120x6x4(case 2)	1/29	1/585	1/2760

The current research focuses on evaluating the energy dissipating capacity of YSPD for the case of concrete building. Hossain et al. conducted incremental dynamic analysis and fragility analysis for evaluating the performance of YSPD in case of concrete building. So far no research has been

conducted to evaluate the seismic performance of concrete building equipped with YSPDs. A low ductility RC frame has been chosen to evaluate the performance of the structure when YSPDs are installed. This type of RC building without YSPD is very common in eastern and central U.S. It is only designed for gravity loads, no earthquake loads are considered **[51].**

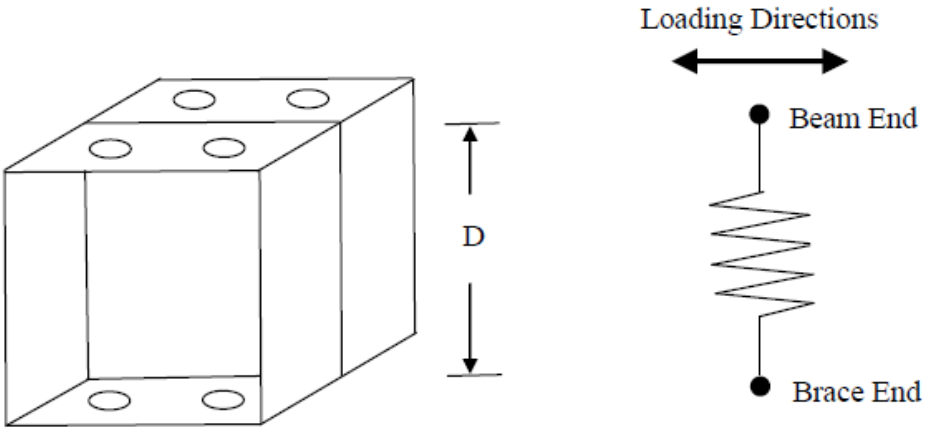

Figure 2.9: Representation of YSPD as a spring element **[35]**.

The Figure 2.9 shows the representation of YSPD as a spring element. The YSPD is connected between the v- bracing and the beam and modeled as a spring element. YSPD is a passive energy dissipating device which dissipates energy through shear deformation. The installation and replacement of YSPD is very simple and inexpensive **[34]**. Therefore, it is envisioned that incorporating YSPD in already build up low ductility RC can be a simple and cost effective solution to improve its seismic performance.

CHAPTER 3: SEISMIC PERFORMANCE OF LOW DUCTILITY RC FRAMES EQUIPPED WITH YIELDING SHEAR PANEL DEVICE

3.1 Introduction

The worst effect of earthquake is the loss of human lives caused by the collapse of structures. Comprehensive research is necessary to ensure that structures withstand design earthquake forces. There are lots of buildings around the world that are poor in construction quality and seismic design. These buildings are very vulnerable to earthquakes. Over the last few decades, researchers' have developed various retrofit techniques for non-ductile RC frames **[59]**. The main purpose of these previous retrofit techniques was to improve the strength, stiffness and ductility of the RC frames which was achieved by RC Jacketing, Steel Jacketing, Concrete fiber reinforced polymer (CFRP) Jacketing and Buckling Resistant Bracing to improve its seismic performance **[59-62]**. However, there are other techniques of retrofitting measures to improve the seismic performance without intervening the structural elements. The use of damper can reduce the vibration, lateral displacement and drift of the building. Control devices, which work as dampers, are used to dissipate the earthquake energy to save the structures from being damaged **[58].** The energy dissipating device not only works as a damper but also increase the stiffness of the building **[58].** Energy introduced due to earthquake is transferred to the super structure through foundation. The structural damage can be minimized by dissipating the energy as such various kinds of systems has been developed to serve this purpose. All systems can be categorized into three types, such as active control system, semi-active control system and passive control system.

The active control device requires external power to operate and the mechanical properties of these systems are typically adjusted based on the feedback from the structural system. Semi- active control system requires a very small amount of external energy and its mechanical properties are typically adjusted on feedback from the structural system. The major advantage of the passive control system is that no external power source is required to operate such systems **[63].** The mechanical properties of these systems cannot be modified and it dissipates energy by utilizing the motion of the structure to produce relative motion within damping device. For this reason use of passive control device is advantageous, reliable and relatively inexpensive to minimize the impact of earthquake **[64].**

Different categories of passive control devices e.g. metal yielding, seismic isolation, sliding friction, shearing and viscous fluid etc. have been developed by many researchers for the purpose of energy dissipation **[50].** These categories also have various types of sub-divisions. In Recent years, the use of metal yielding devices are more common for their simplicity and large energy dissipation capability. Several yielding devices, such as, i.e. Added Damping and Stiffness (ADAS), which dissipates energy through flexural dissipation and the modification of ADAS is Triangular Added Damping and stiffness (TADAS), Steel Slit Damper (SSD), Buckling Restrained Brace (BRB) and Yielding Shear Panel Device (YSPD) have been developed by researchers **[50]**. YSPD is a passive energy dissipating device which dissipates energy through shear deformation. The installation and replacement of YSPD is very simple and inexpensive **[26]**.

Large number of RC buildings around the world are vulnerable to earthquake due to poor seismic detailing. However, no attempt has been made to use the YSPD as a damper for investigating the performance of concrete building so far. In this research a low ductility RC building has been modelled to explore its performance against earthquake and to observe the improvements in seismic performance after incorporating YSPDs. The building was designed for the gravity loads only without using any seismic provision **[51]**. This type of building is very common in U.S.A. To evaluate the performance of YSPDs against earthquake static pushover, time history analysis, incremental dynamic analysis and fragility analysis has been conducted for three different types of YSPDs along with three different arrangements. Finally all results are compared for the frame with and without YSPDs.

3.2 Description of the building

In this study a three story low ductility RC moment resisting frame is modelled which has been experimentally tested by Bracci et al. **[51]**. The building has been designed before the introduction of modern seismic codes. During the design of the building only the gravity loads are considered without following any kind of seismic provision. This type of building is very common in the eastern and central U.S.A. The buildings are highly vulnerable to earthquakes because these are designed only for gravity loads following ACI- 318-89[2] without considering any seismic detailing requirements **[51]**.

The study frame consists of three stories each **3.66 m** high and three equal bays of **5.49m** wide. The columns and the beams are of equal size at each floor having the cross sections **300 x 300 mm^2** and **230 x 460 mm^2** respectively. Concrete with compressive strength **fc' = 24 MPa** and **40 grade** steel with yield strength **fy = 276 MPa** are used in the design. The general layouts of the structure and beam reinforcements are shown in Figure 3.1.

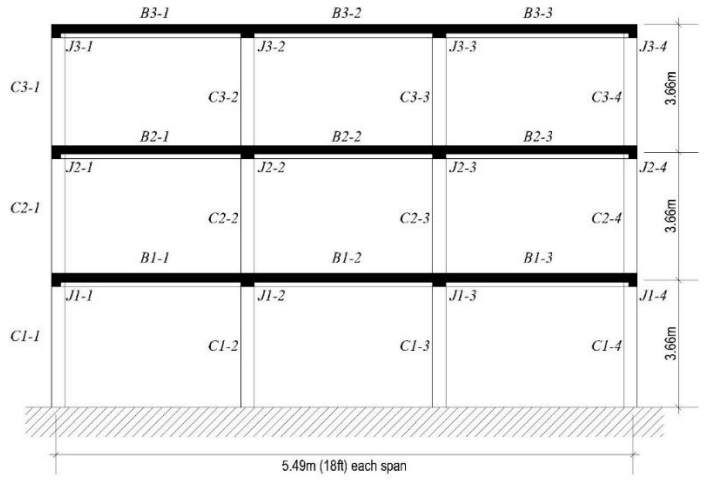

(a)

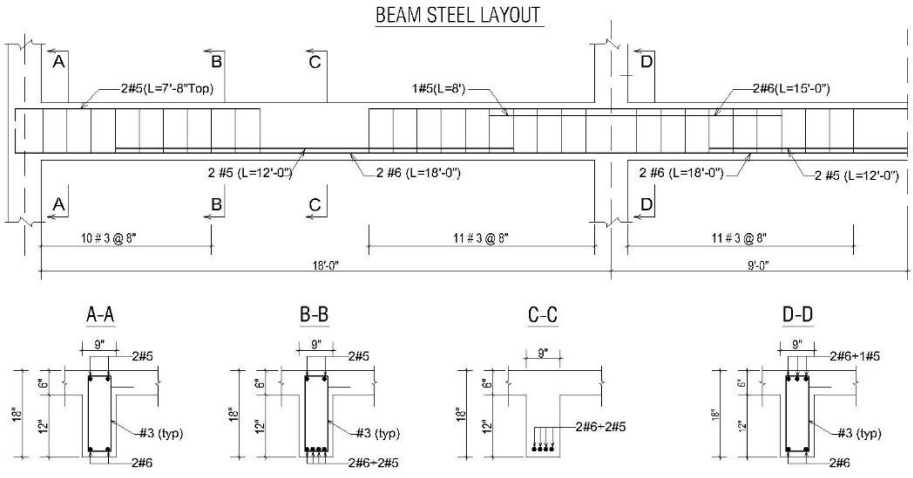

(b)

Figure 3.1: (a) General layout, (b) beam reinforcements of the structure **[68]**

3.3 Theoretical evaluation of YSPD

For strengthening the building against seismic loading passive energy device named YSPDs are used in the moment resisting RC frame along with V- bracing. YSPD device is a passive energy dissipating device **[58].** It consists of a square hollow section (SHS) with a diaphragm plate. The diaphragm plate is welded inside the square hollow section. SHS supports the diaphragm plate by providing a boundary as well as provides an interface to connect with the main structure**.** YSPD dissipates energy through shear deformation of the diaphragm plate**.** Tension field is developed **due** to post buckling of the diaphragm plate and SHS helps to resist the tension strips and tension field formation **[47].** YSPD is placed in a framed structure with a beam through an inverted V-brace connection **[58].** YSPD, bracing and the connection pattern of YSPD are shown in the Figure 3.2.

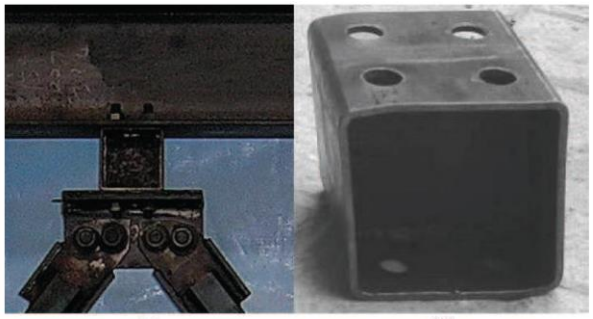

(a) (b)

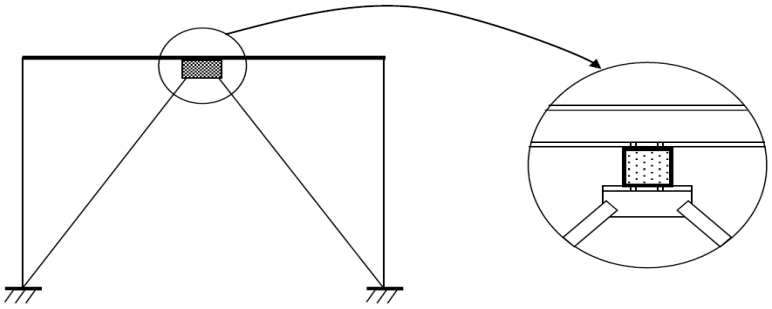

(c)

Figure 3.2: (a) Typical YSPD-brace assembly (b) Yielding Shear Panel Device **[47]**,

(c) Typical YSPD brace connection **[26]**.

YSPD resists two equal and opposite forces when load is applied. The two forces are created through the bolted connections and that's why YSPD's initial stiffness would be equal to the force required to produce unit horizontal displacement at the loaded flange **[68]**. Figure 3.3 shows the undeformed shape and the deformed shape of YSPD due to two equal and opposite force.

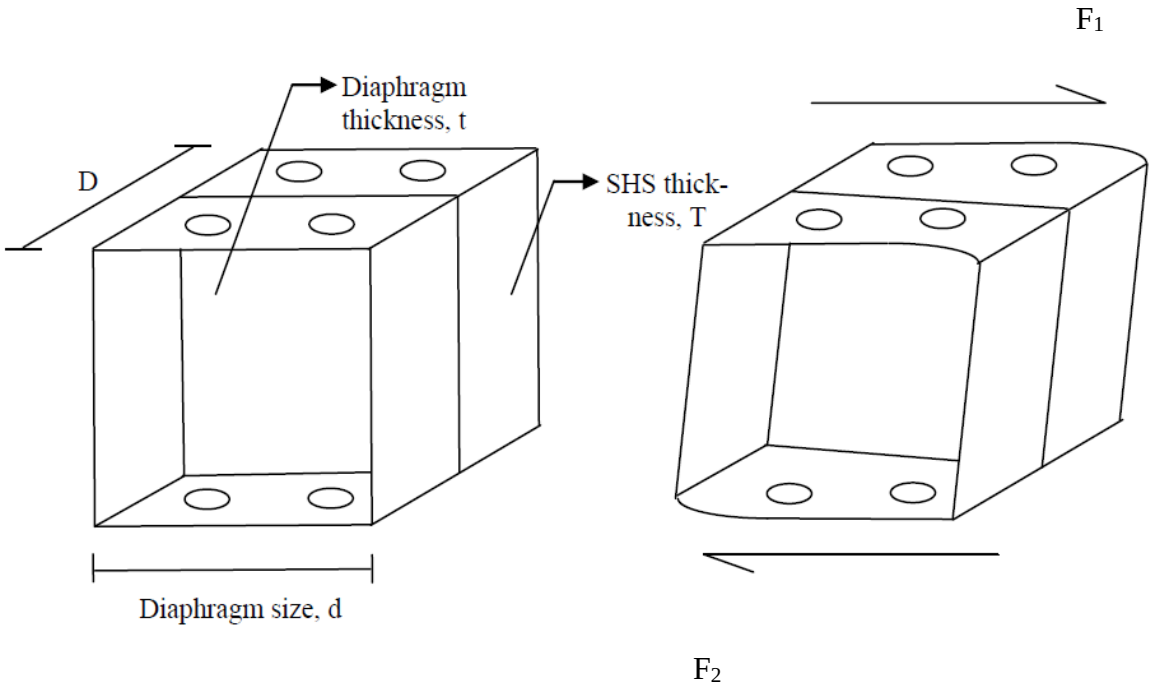

Figure 3.3: Undeformed and deformed shapes of a YSPD device **[26]**

The equation shows the overall stiffness of the YSPD:

$$\frac{1}{k_{YSPD}} = \frac{1}{k_{dia}} + \frac{1}{k_{SHS}} \tag{3.1}$$

For elastic deformation, the shear stress in diaphragm plate is

$$\tau = G\gamma \tag{3.2}$$

So the elastic stiffness of diaphragm plate in pure shear can be written as

$$K_{dia} = \tau dt = Gt \tag{3.3}$$

Due to the in-plane compression of the diaphragm plate and the vertical flanges the bolted flanges of the SHS experience flexural deformation. Figure 3.3 depicts the assumed deformation with acting force F_1 and F_2.

Bolted flanges undergo bending about an axis perpendicular to the loading direction due to F_1. neglecting the effects of the bolts hole and assuming a zero rotation along the line passing through the centre of nearby bolts, the F_1 force can be calculated as follows

$$F_1 = \frac{3EI_1}{d_1^3} = \frac{DT^3E}{4\,(\alpha+R)^3} \tag{3.4}$$

Where, $I_1 = (DT^3/12)$, r is the radius of the bolt hole.

The acting force F_2 is responsible for the deformation along the line joining the flange and the diaphragm plate is assumed to have a triangular distribution due to the large in-plane rigidity of the diaphragm plate. The deformation of the bolted flanges is shown in Figure 3.4.

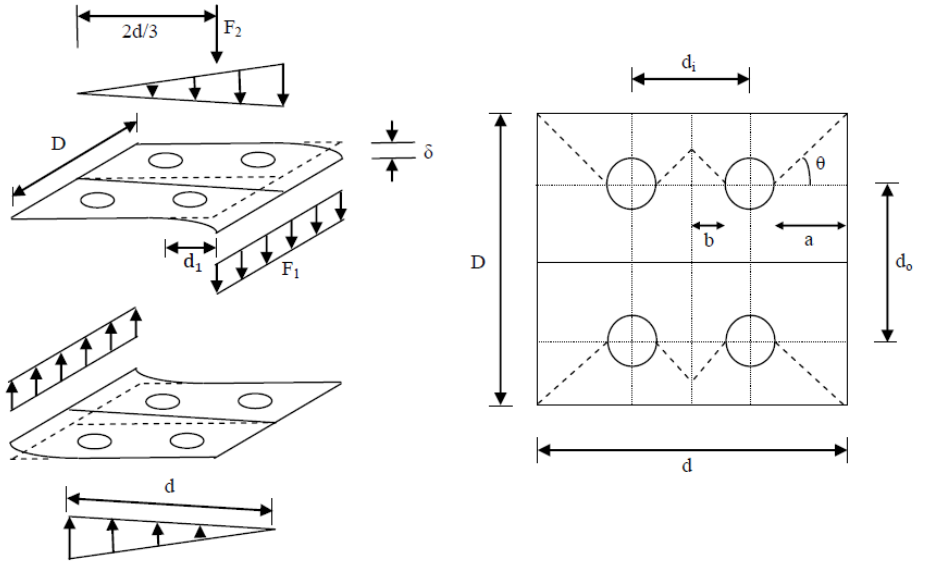

(a) (b)

Figure 3.4: (a) Deformation of the bolted flanges. (b) Dimensions of the bolted flanges [**26]**.

The resultant of the triangular force considering the deformation can be written as

$$F_2 = 2\left(\frac{6E\,I_2/d_2^3}{2}\right) = \frac{6EI_2}{d_2^3} = \frac{dT^3E}{2d_2^3} \quad (3.5)$$

Where, $I_2 = (dT^3/12)$,

Forces F_1 and F_2 are calculated for the bending of the flange in two orthogonal directions neglected the effect on each other. A reduction in the total calculated force is required to incorporate this effect. The reduced force can be calculated as follows

$$F_r = 2\left(\frac{6EI_3}{d_2^3}\right)\frac{3}{8} = \frac{3\,E\,(a+r)T^3}{8d_2^3} \quad (3.6)$$

Where, $I_3 = \frac{((a+r)T^3)}{12}$

The compression of the diaphragm plate and the vertical flanges in an YSPD is similar to the deformation of an I-section as shown in Figure 3.5

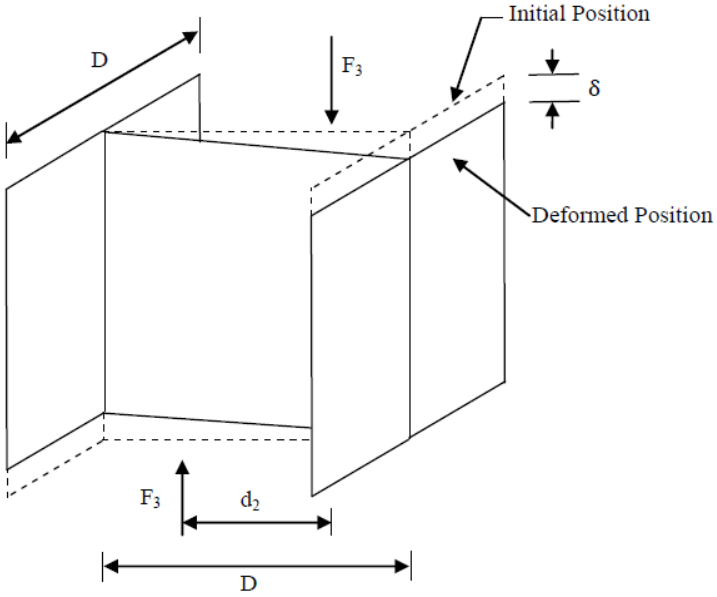

Figure 3.5: Compressive deformation of diaphragm plate and vertical flanges **[26]**.

The force required to make them a unit deformation at the end of the flange

$$F_3 = DT \times \frac{E}{d} + \frac{dt}{2} \times \frac{E}{d} \quad (3.7)$$

The distance between the zero deformation and the time of action of the force

$$d_3 = \frac{DTE + dtE/3}{F_3}$$

The stiffness of the SHS can be calculated by the moment balance of these force and thus may be expressed as follows

$$K_{SHS} = F_1 + \frac{F_2}{3} - \frac{F_r(2d_r - d)}{d} + \frac{F_3(2d_3 - d)}{d} \quad (3.8)$$

3.4 Modeling of the building and YSPDs

A 2D three story-three bay moment resisting low ductility RC frame as shown in Figure 3.8 is modeled using Opensees software **[Appendix A]**. Freddi et al. modeled the same frame for probabilistic seismic demand modeling of local level response parameters of that RC frame **[59]**. The same modeling approach is used in this analysis. T sections are considered during the modeling of the beams. "Beams with hinges" elements are used to incorporate nonlinear behavior of beam and column **[65]**. Panagiotakos and Fardis methods are used to calculate the plastic hinge length of beam and columns **[66]**. In plastic hinge zone Concrete-02 and Hysteretic material model is used to simulate the behavior of concrete and steel respectively. Beam column joints are considered as rigid. High axial stiffness of beams are used to incorporate the behavior of rigid-floor diagram.

YSPDs are used in the moment resisting frame to dissipate the earthquake energy through shear deformation. Geometric nonlinearity is incorporated in the modeling of YSPD to analyze post buckling behavior of YSPD. The first buckling mode of deformation is used as initial geometric imperfection. The first buckling deformation is scaled as a function of plate thickness and it was applied at 0.2t amplitude (t was the thickness of the diaphragm plate). Detail modeling and connection of YSPD with the steel base plate are given in Hossain et al. **[26]**.

The Bouc-Wen-Baber Noori (BWBN) model is used to show the pinching hysteretic force deformation relationship of YSPDs **[67].** Two types of parameters are used to construct non-degrading pinching hysteretic BWBN model named hysteretic parameters and pinching

parameters. Hysteretic parameters represent the shape of the force-displacement curve and the pinching parameters illustrates the pinching effect**.** Table 3.1 illustrates the BWBN model parameters of YSPD.

Table 3.1: BWBN material parameters for the YSPDs **[71]**

YSPD (D x T x t)	Fy (MPa)	K_t (KN/mm)	F_i (KN)	A	β	γ	n	q	ξ_{10}	P	Ψ_0	δ_ψ	λ
100 x 4 x 2	250	0.33	26.76	1.0	0.5	0.5	1.213	0.52	0.96	0.`18	0.41	0.00001	0.0300
110 x 5 x 3	300	0.42	54.22	1.0	0.5	0.5	0.54	0.38	0.95	0.1`5	0.27	0.00001	0.0014
120 x 6 x 4	350	0.49	93.51	1.0	0.5	0.5	0.300	0.30	0.95	0.12	0.22	0.00001	0.0002

D is the size of YSPD (mm)

T is the thickness of SHS plate (mm)

t is the thickness of diaphragm plate (mm)

F_y is the yield strength of SHS and diaphragm plates (MPa)

K_t is the tangential stiffness of YSPD after tension field formation (kN/mm)

F_i, A, β, γ, n are hysteretic parameters and are pinching parameters and q, ξ_{10}, p, Ψ_0, δ_ψ, λ are pinching parameters

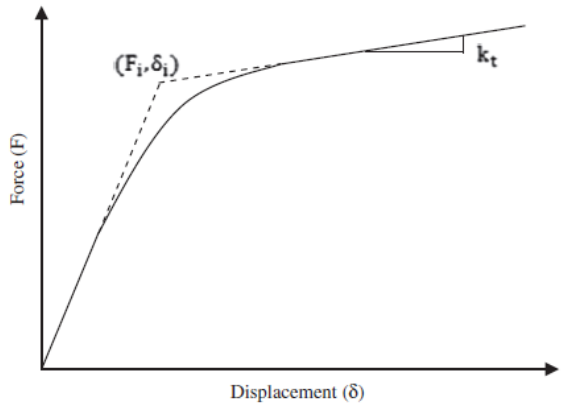

Figure 3.6**:** Nonlinear force displacement (F-δ) relationship of YSPD **[71]**

Figure 3.6 depicts the restoring force produced in the YSPD **[71]** and can be expressed according to BWBN model as follows

$$F=F_e+F_h=\alpha F_i\delta+(1-\alpha)F_i z \tag{3.9}$$

where, F_e = Elastic components of the restoring force

F_h = hysteretic component of the restoring force

Eq. (2.9) represents a nonlinear force displacement (F-δ) relationship based on the parameters F_i, α and z. F_i is well-defined as the force representing the intersecting point of the bilinear envelope of the force displacement relationship at a unit displacement of δ_i. K_t is the tangential stiffness of YSPD whereas $\alpha = k_t/F_i$. The non-degrading pinching hysteretic response depends on the hysteretic displacement z, which is represented by the following first order nonlinear differential equation.

$$\dot{z} = \delta h(z)\{A-[\gamma+\beta \mathrm{sgn}(\dot{\delta}z)]\,|z|^n\} \tag{3.10}$$

where A, β, γ and n are hysteretic model parameters which control the shape of the curve. Value of sgn($\dot{\delta}z$) depends on the sign of $\dot{\delta}z$ and the value becomes +1 if $\dot{\delta}z$ is positive or becomes -1 if $\dot{\delta}z$ is negative. Pinching inducing function h(z) is stated by following equations as

$$h(z)=1.0-\zeta_1 e(-(z.sgn(\delta)-(qz_n)^2\,/\,\zeta_2^2 \tag{3.11}$$

$$z_u=\left[\frac{1}{\beta+\gamma}\right]^{\frac{1}{n}} \quad (3.12)$$

Where $0 \leq \zeta_1 < 1$controls the severity of the pinching, ζ_2 causes the pinching region to spread, z_u is the ultimate value of z and q are model parameters. Depending on the hysteretic energy (ε), ζ_1, ζ_2 are written as follows

$$\zeta_1 = \zeta_{10}[1.0 - e^{(-p\varepsilon)}] \quad (3.13)$$

$$\zeta_2 = (\psi_0 + \delta_{\psi\varepsilon})(\lambda + \zeta_1) \quad (3.14)$$

where p controls the rate of initial drop in the slope, ζ_{10} is the total slip, ψ_0 contributes to the amount of pinching, δ_ψ controls the rate of pinching spread, λ controls the rate of change of ζ_2 as ζ_1 changes. The rate of hysteretic energy is given by following equation,

$\dot{\varepsilon} = (1 - \alpha)\, F_i z \dot{\delta}$ (3.15)

Three different sizes of YSPDs along with the three different bracings are used for the current study shown in Table 3.2. Cold formed welded Hollow Structural Section (HSS) are selected for the bracing system. HSS is made of ASTM A500 Grade B steel. The force displacement relationships of the three different sizes of YSPDs are shown in Figure 3.7. YSPDs are modeled as spring element which is connected between the V-bracing and mid span of the beam. Three different arrangements for the three different categories of YSPDs are used in this current study. The different types of frames and the considered modeled frames are shown in Table 3.2 and Figure 3.8 respectively.

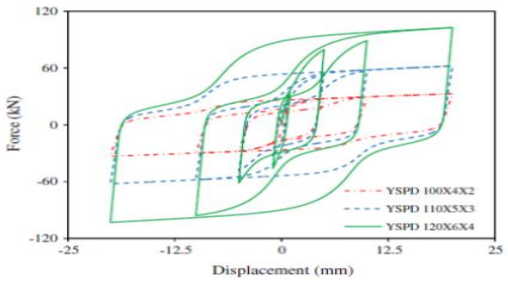

Figure 3.7: Cyclic force displacement relationship of the YSPDs generated using the BWBN models **[19]**

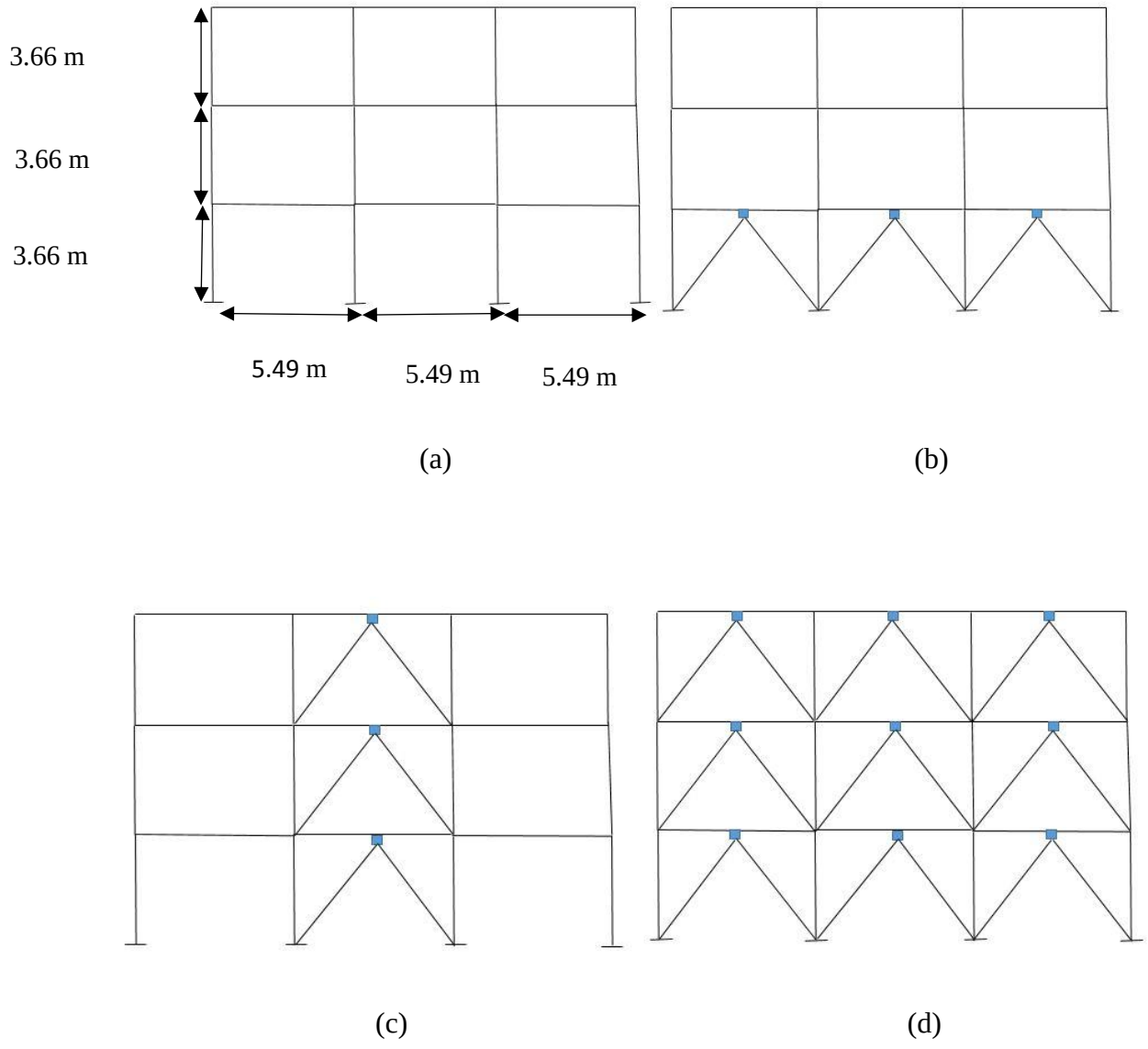

Figure 3.8: Types of frame considered for analysis (a) Bare frame (b) Frame with YSPDs in first story three bay (c) Frame with YSPDs in three story second bay (d) Frame with YSPDs in three story three bay configurations.

Table 3.2: Considered frames

Frame ID	Types of frame
BR	Bare frame
FT-C1	Frame with YSPDs (C1) in first story three bay
FT-C2	Frame with YSPDs (C2) in first story three bay
FT-C3	Frame with YSPDs (C3) in first story three bay
TS-C1	Frame with YSPDs (C1) in three story second bay
TS-C2	Frame with YSPDs (C2) in three story second bay
TS-C3	Frame with YSPDs (C3) in three story second bay
TT-C1	Frame with YSPDs (C1) in three story three bay
TT-C2	Frame with YSPDs (C2) in three story three bay
TT-C3	Frame with YSPDs (C3) in three story three bay

Table 3.3: Different sizes of YSPDs and bracing

ID	YSPDs (mm)	Bracing (in)
C1(Category-01)	YSPD 100 x 4 x 2	HSS 4 x 4 x 1/8
C2(Category-02)	YSPD 110 x 5 x 3	HSS 4 x 4 x ¼
C3(Category-03)	YSPD 120 x 6 x 4	HSS 4 x 4 x ½

3.5 Static pushover analysis

The static pushover analysis is very well-known method to find out the seismic force deformation relationship in order to evaluate the performance of existing and new structures. Sometimes pushover provides much useful information that cannot find out from dynamic analysis. To predict the force deformation demands produced on structures as well as on their elements due to earthquake ground motion, pushover analysis is considered as a simple intermediate solution.

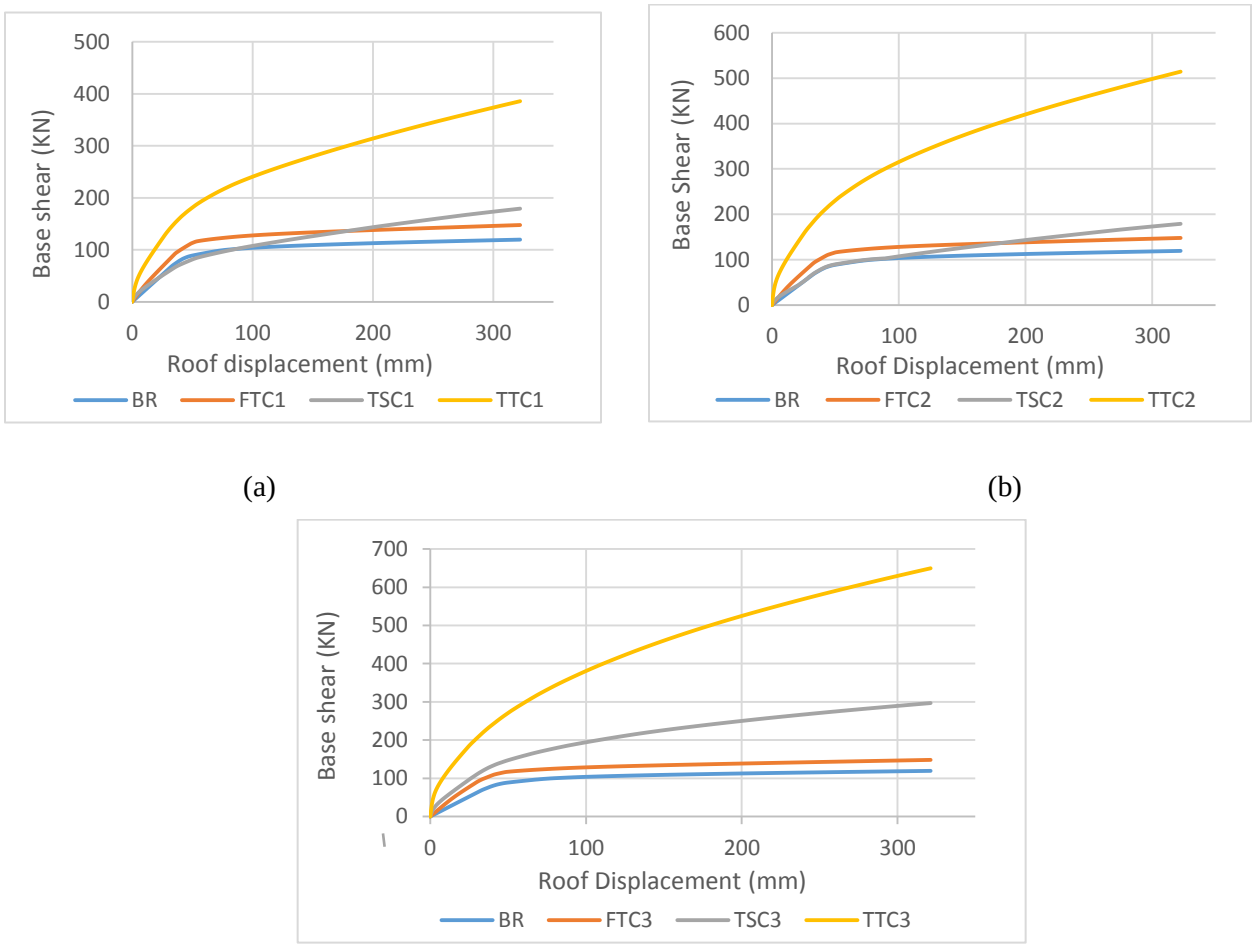

Figure 3.9: Pushover curves showing the comparison of the three different arrangement of YSPDs with the bare frame (a.For category-01, b. for category-02, c. for category-03)

In this current study pushover analysis has been performed for each type of frame using opensees finite element software. Type of the frame considered for the simulation are listed in Table 3.1. 2D finite element models are developed for each type of frames. Total ten pushover analyses have

been performed for the ten individual frames. A triangular lateral load distribution has been considered for the analysis, where the top and bottom of the loads are at the roof level and base of the building, respectively **[Appendix B]**. The pushover response curves are shown in Figure 3.9 for three different sizes of YSPDS. In the Figure 3.10 the bare frame is compared with the other types of frames i.e. YSPDs in the FT, YSPDs in the TS, YSPDs in TT.

Figure 3.9 (a-c) and Figure 3.10 (a-c) represents the resistant capacity of ten different types of frames. From the Figure 3.9 (a-c) it is observed that with the increase of the size of YSPDs the resistance capacity of the frames is also increased. The higher resistance capacity is observed for the YSPDs in TT than the YSPDs in FT and TS arrangements. TS arrangement shows large base shear capacities than FT arrangements with the increased roof displacements. Figure 3.9 (c) shows that the base shear capacity is large for YSPD category C3. Figure 3.9 (a) and (b) depict that for YSPD category C1 and C2 TS shows less base shear capacity initially than FT but finally the base shear capacities are large for TS arrangements than FT arrangements. It is observed from figure 3.9 (a) that for C1 category of YSPD the base shear capacity increases 23% for FT, 50% for TS and 223% for TT arrangements than the bare frame and from figure 3.9 (b) and (c) for C2 and C3 categories of YSPDs the performance increases further. For example, for C3 category base shear capacities increase 24% for FT, 149% for TS and 445% for TT arrangements than the bare frame. From Figure 3.10 (a) it is observed that for the FT arrangement the increase size of YSPDs does not affect much in the resistance capacity. But Figure 3.10 (b) and (c) showed that significant amount of increase in resistance capacity is observed with the increased size of YSPDs in case of YSPDs in TS and TT arrangements.

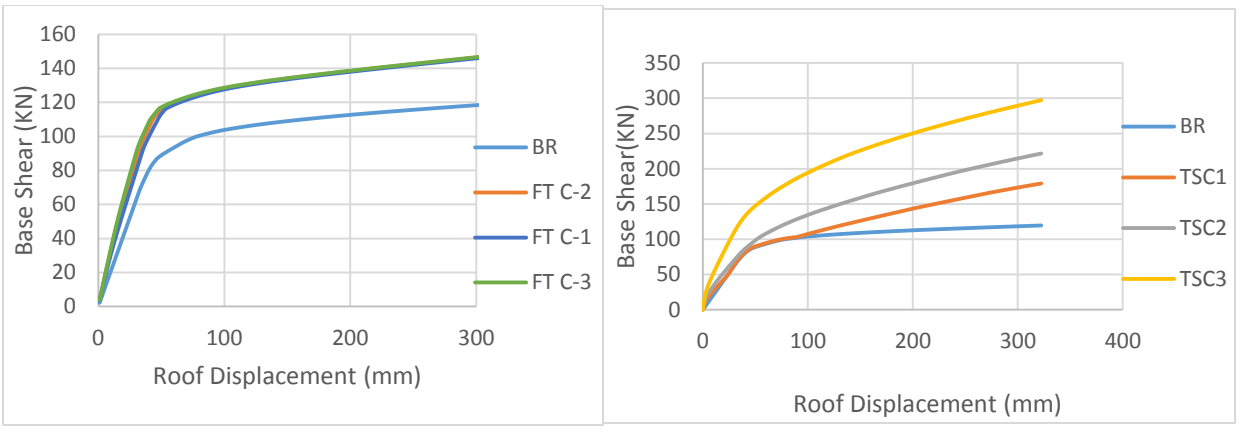

(a) (b)

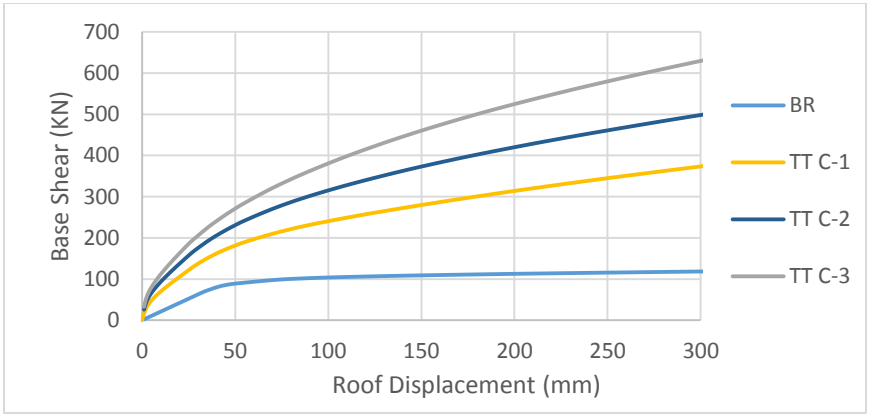

(c)

Figure 3.10: Pushover curves showing the comparison of the three different categories of YSPDs with the bare frame (a.For YSPDs in the FT, b. for YSPDs in the TS, c. for YSPDs in the TT)

Figure 3.11 describes the inter story drift demand for the ten types of frames obtained from pushover analysis. For the BR frame the maximum inter story drift is at first floor level. After installing YSPDs the inter story drift is lower in first floor level but the inter story drift in the second and third floor level is higher for FT arrangements. For TS and TT arrangements inter story drift is lower for all the floors than bare frame except for TS-C1 combination. TS-C1 does not show better performance than bare frame in terms of inter story drift. So YSPDs can be installed in TS arrangement but for YSPDs category C2 and C3 and in TT arrangement for all the category but best performance has been observed for TT-C3 arrangement.

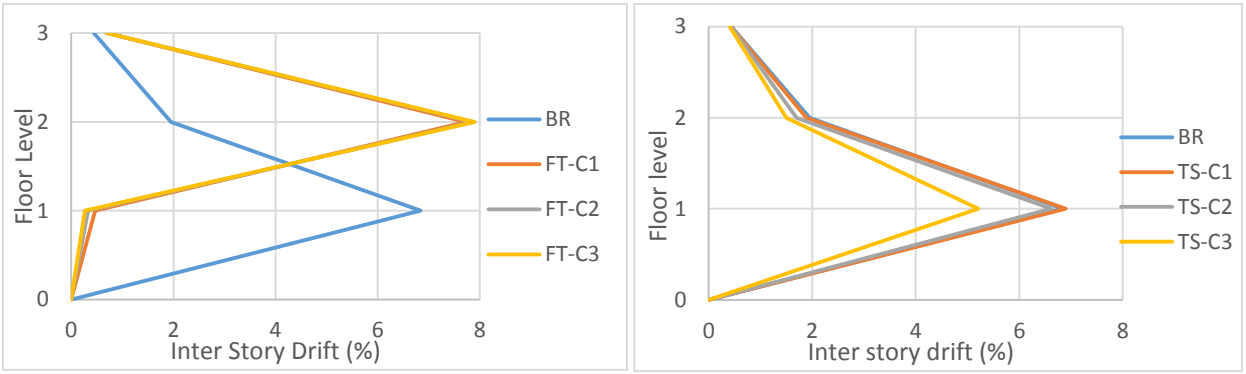

(a) (b)

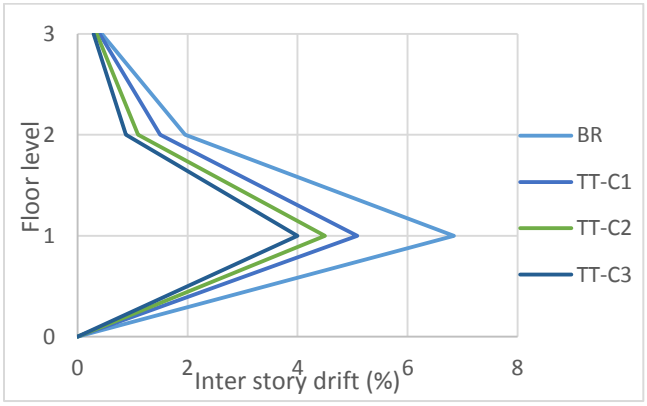

(c)

Figure 3.11: Inter story drift demand (a.For YSPDs in the FT, b. for YSPDs in the TS, c. for YSPDs in the TT)

3.6 Dynamic time history analysis

Time history analysis is very effective method to generate realistic dynamic sceneries of seismic damage **[47]**. Nowadays time history analysis method is widely used by many researchers to find out the seismic vulnerability of different structures **[65]**. In this research nonlinear time history analysis has been performed for ten different earthquake records including fault normal and fault parallel earthquake values for every earthquake. Earthquake records are listed in Table 3.4.

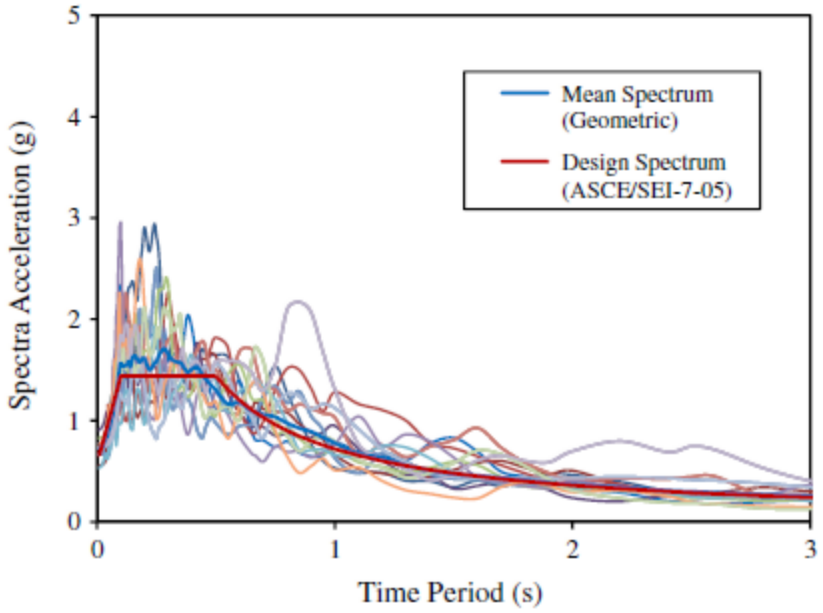

Figure 3.12: Response spectrum of the scaled ground motion records and design response spectrum at downtown Los Angeles for the site class D (stiff soil).

As part of this current study time history analysis has been performed for twenty earthquakes which matches the design. Figure 3.12 shows the response spectrum of the scaled ground motion records and design response spectrum at downtown Los Angeles for the site class D. Analyses were performed for the ten different types of frames and the results are compared. Eigen value analyses were performed to find out the fundamental time periods of the ten different types of frames. The results of the eigen value analyses are shown in the Table 3.5. The results show that the time periods have decreased with the increased size of YSPDs, and decreased gradually when the YSPDs are installed in orientation of FT, TS and TT.

Table 3.4: Selected ground motion records used in the current study **[26]**)

PGMD record no	Earthquake name	Year	Station name	Earthquake magnitude	Distance to rupture (Km)
1838	Hector Mine	1999	Whitewater Trout Farm	7.13	62.9
1153	Kocaeli, Turkey	1999	Botas	7.51	127.1
1511	Chi-Chi Taiwan	1999	TCU076	7.62	2.8
2112	Denali Alaska	2002	TAPS Pump Station #08	7.90	104.9
169	Imperial Valley-06	1979	Delta	6.53	22
804	Loma Prieta	1989	So.San Francisco Sierra Pt.	6.93	63.1
880	Landers	1992	Mission Creek Fault	7.28	27
143	Tabas, Iran	1978	Tabas	7.35	2.1
719	Superstition hills-02	1987	Brawley Airport	6.54	17
284	Irpinia,Italy-01	1980	Auletta	6.90	9.6

Table 3.5: Time periods of the first three modes for different types of frames

Time periods (sec)	BR	FT-C1	FT-C2	FT-C3	TS-C1	TS-C2	TS-C3	TT-C1	TT-C2	TT-C3
T_1	1.26	0.99	0.96	0.94	0.76	0.55	0.44	0.45	0.33	0.26
T_2	0.40	0.31	0.30	0.29	0.26	0.19	0.16	0.16	0.12	0.09
T_3	0.23	0.16	0.13	0.10	0.16	0.12	0.10	0.10	0.08	0.06

Inter story drift demands are determined out through non-linear time history analysis for the ten types of frames using twenty different earthquakes**.** The results of the inter story drift demands are shown in Figure 3.13 to 3.22. The Figure 3.13 shows that for the bare frame the inter story drift demand is higher at the first floor level than the other two floor levels and it is also true for both fault normal and fault parallel earthquakes. For fault normal earthquakes the inter story drifts of the structure are larger than the fault parallel earthquakes.

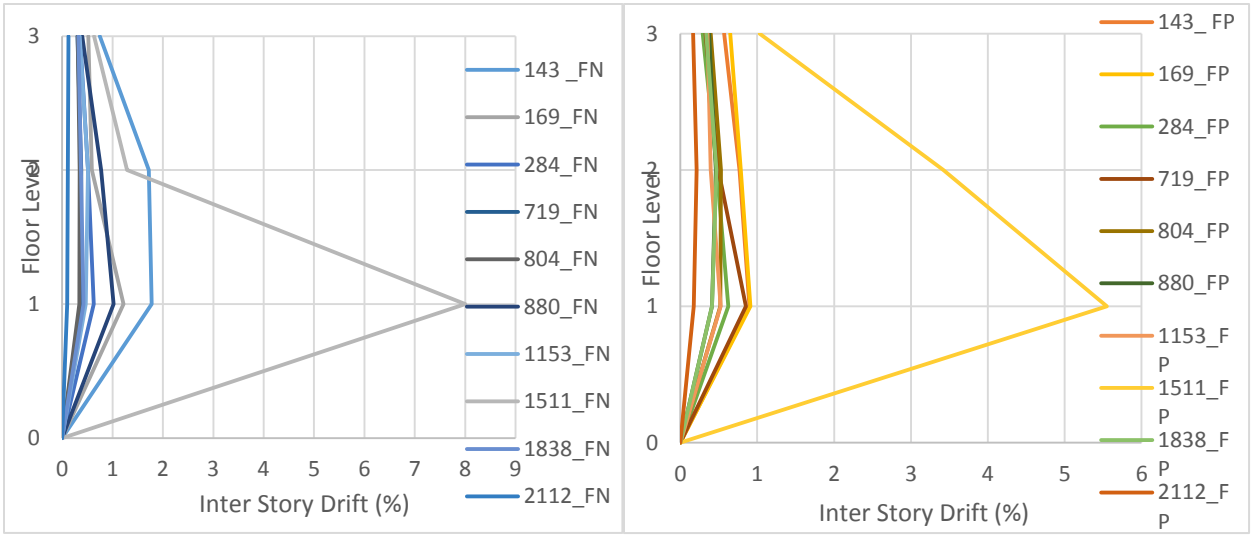

(a) (b)

Figure 3.13: Inter story drift demand for bare frame (a). Fault normal, (b). Fault paralllel

Figure 3.14, 3.15 and 3.16 show that for FT arrangement the inter story drift demand has decreased after installing the YSPDs in the first story but the inter story drift demand has increased largely in the second story. It is observed that the inter story drift demand has decreased with the increase of the sizes of YSPDs both for the fault normal (FN) and fault parallel (FP) earthquake data. The similar results are observed for three categories of YSPDs.

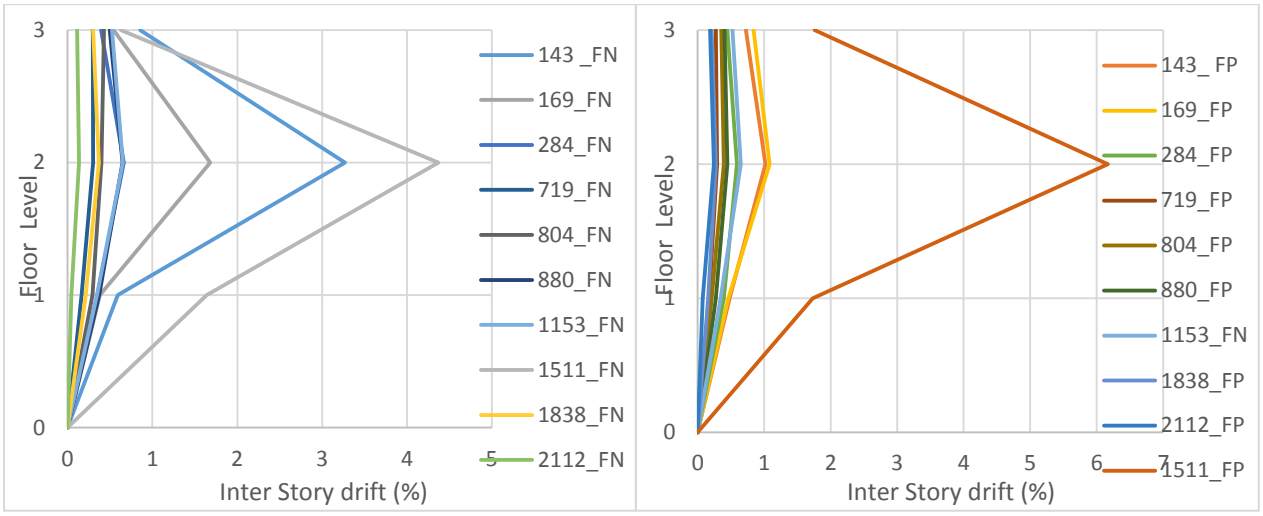

(a) (b)

Figure 3.14: Inter story drift demand for FT-C1 (a). Fault normal, (b). Fault paralllel

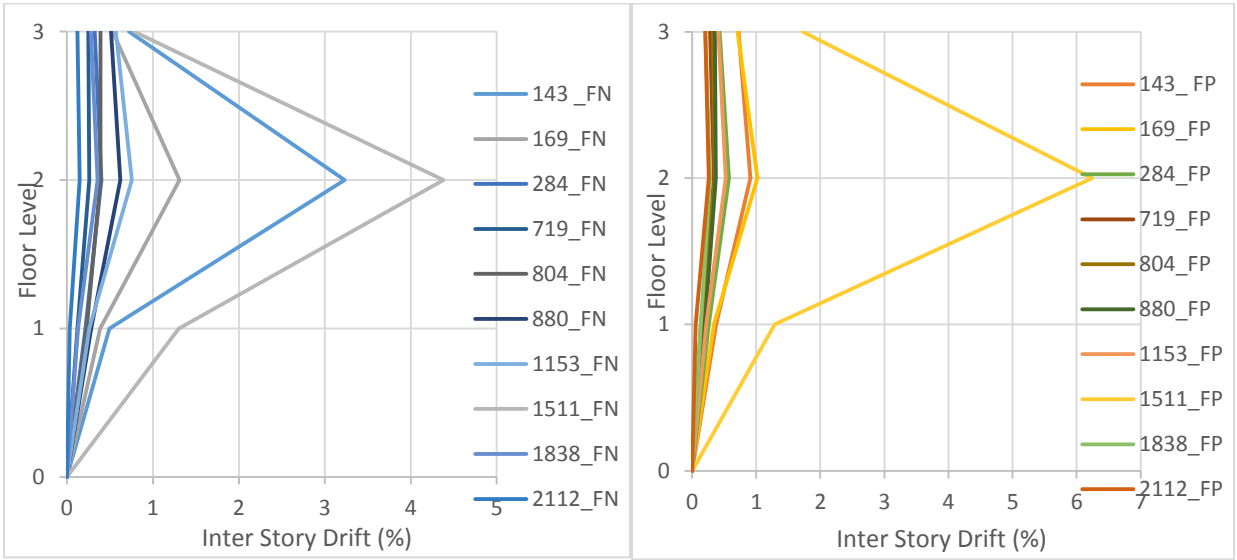

(a) (b)

Figure 3.15: Inter story drift demand for FT-C2 (a). Fault normal, (b). Fault paralllel

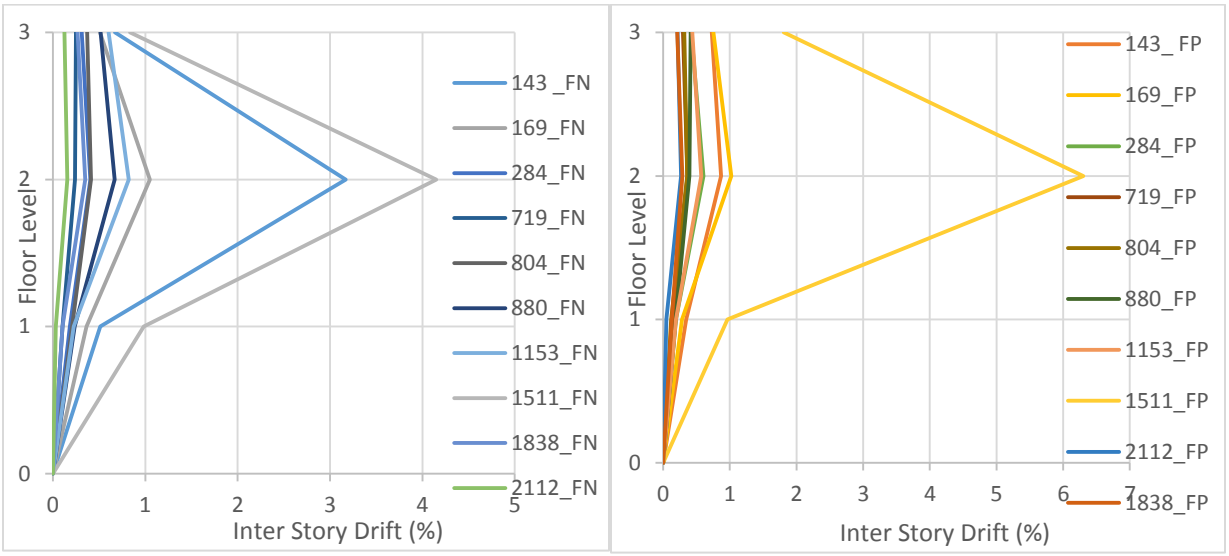

(a) (b)

Figure 3.16: Inter story drift demand for FT-C3 (a). Fault normal, (b). Fault paralllel

Figure 3.17, 3.18 and 3.19 represents the inter story drift demand for TS-C1, TS-C2 and TS-C3 arrangements. The results of the time history analysis show that after installing YSPDs the inter story drift demand decreases for TS-C2 and TS-C3 arrangements. But for TS-C1 arrangement inter story drift demands do not decrease at first floor level in comparison to the bare frame. However, inter story drift demand decreases at second and third floor level for most of the earthquake data for TS-C1 arrangement in comparison to bare frame.

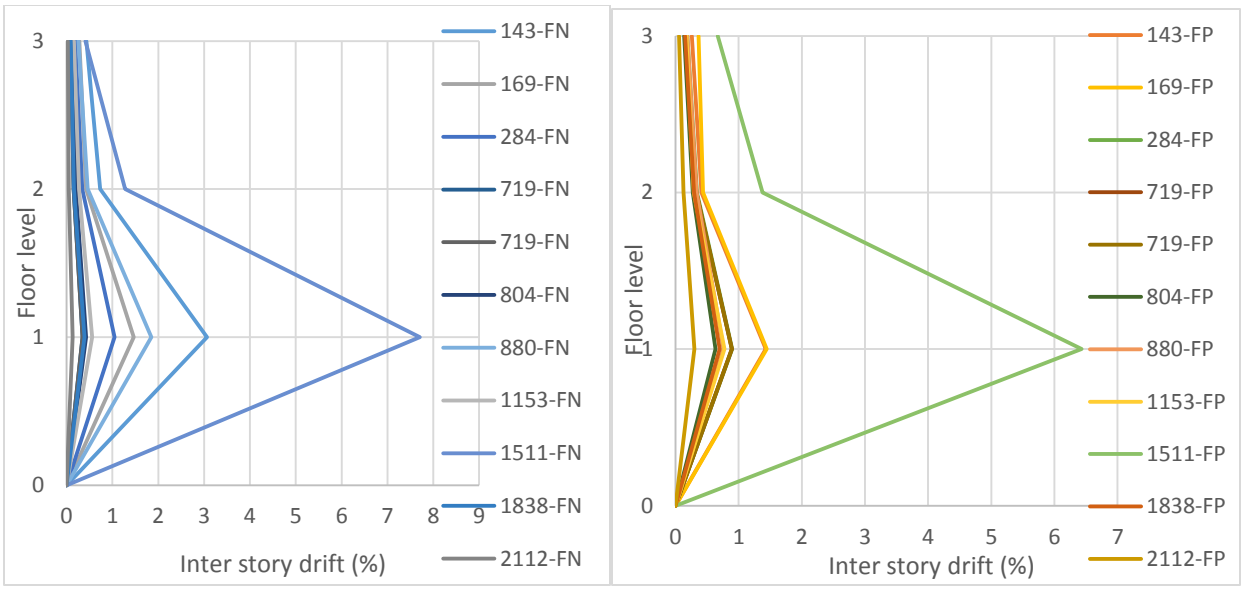

(a) (b)

Figure 3.17: Inter story drift demand for TS-C1 (a). Fault normal, (b). Fault paralllel

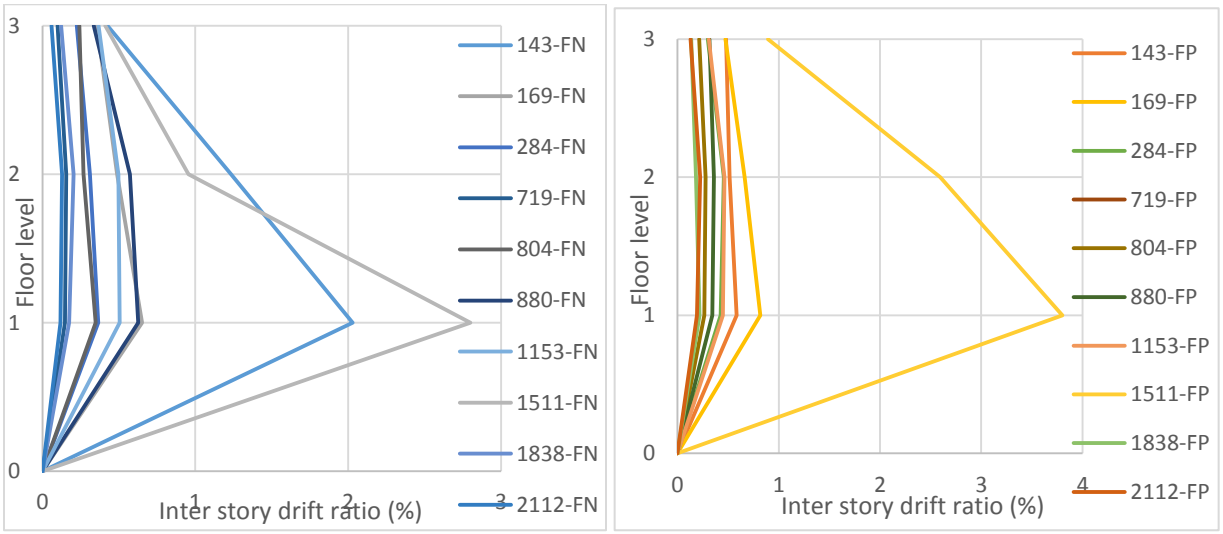

(a) (b)

Figure 3.18: Inter story drift demand for TS-C2 (a). Fault normal, (b). Fault paralllel

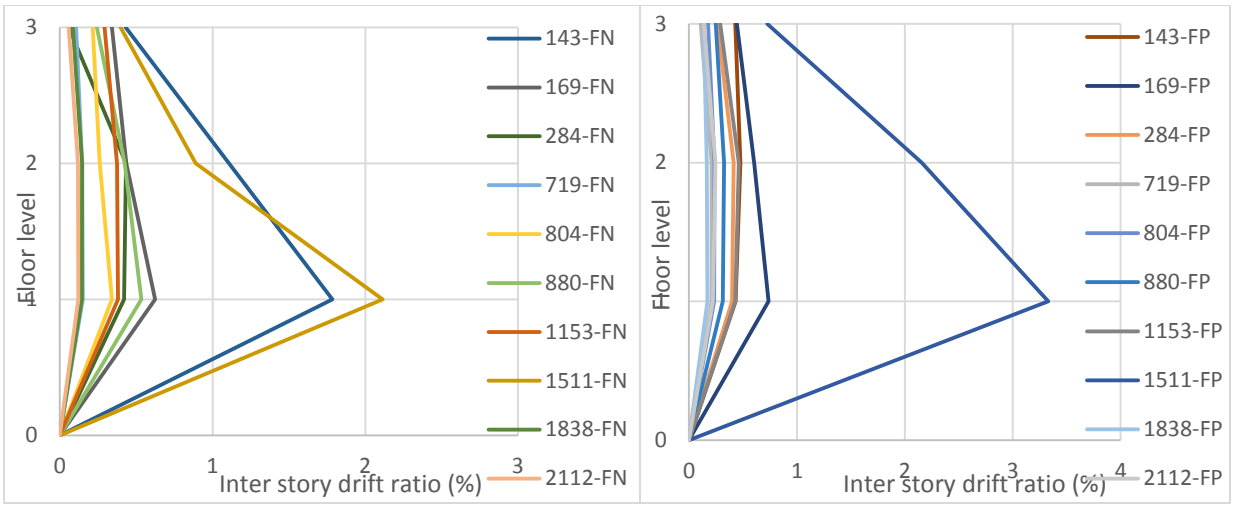

Figure 3.19: Inter story drift demand for TS-C3 (a). Fault normal, (b). Fault paralllel

Figure 3.20, 3.21 and 3.22 shows that the inter story drift demand is decreased considerably after installing YSPDs in the TT than the bare frame. Figure 3.17, 3.18 and 3.19 also show that the increased sizes of the YSPDs are helpful to decrease the inter story drift demand for the TT arrangements as well.

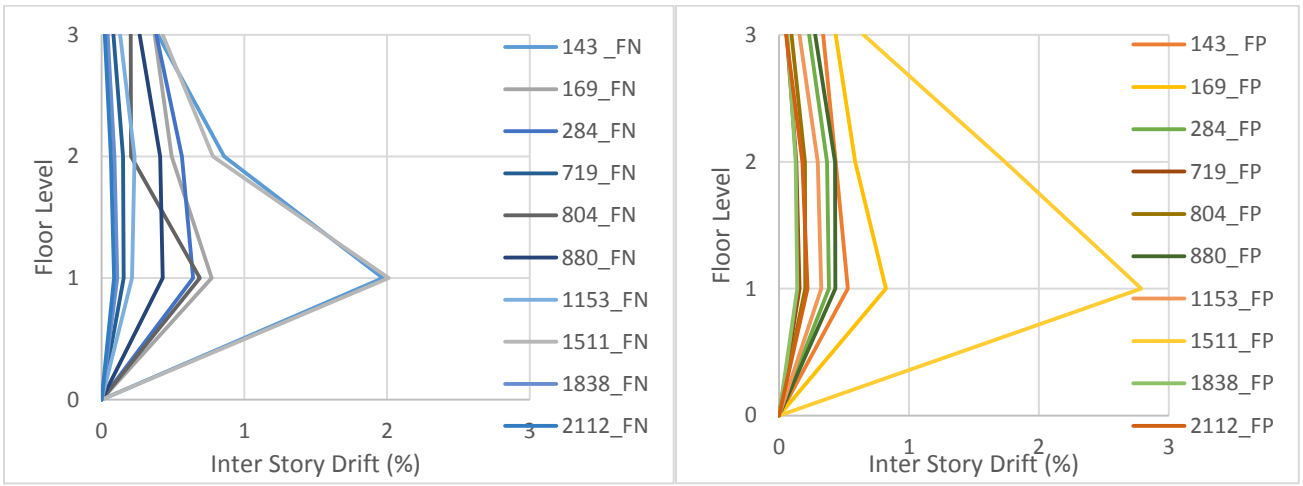

(a) (b)

Figure 3.20: Inter story drift demand for TT-C1 (a. Fault normal, b. Fault paralllel)

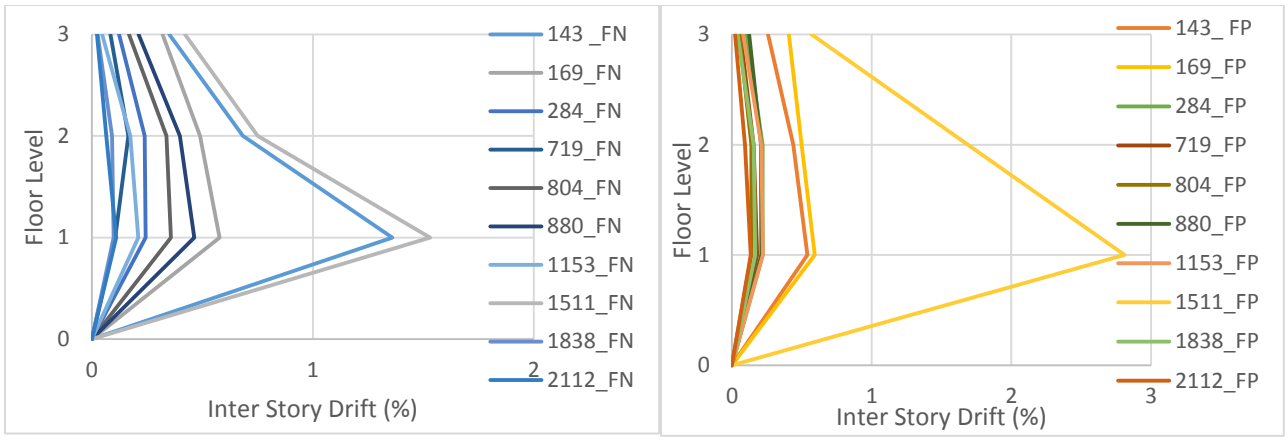

(a) (b)

Figure 3.21: Inter story drift demand for TT-C2 (a. Fault normal, b. Fault paralllel)

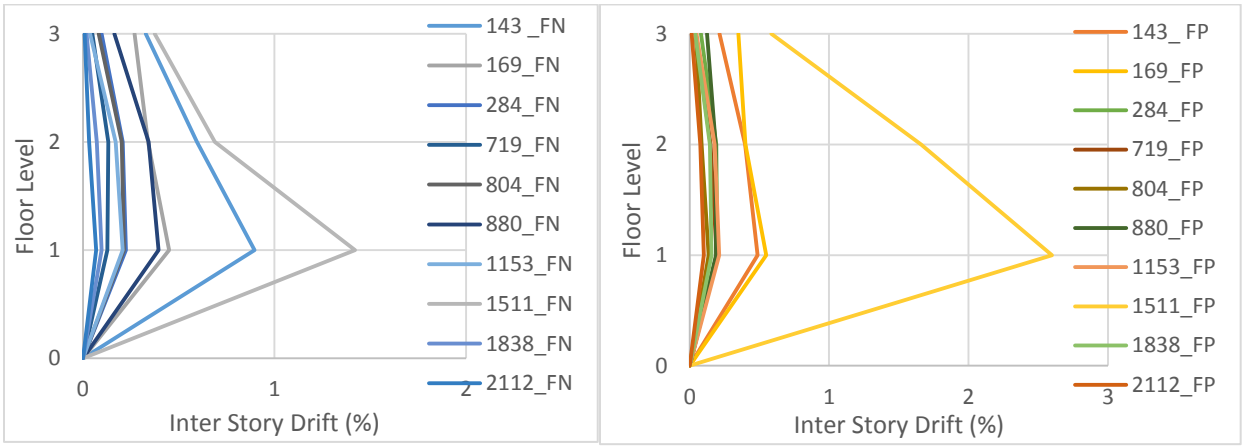

(a) (b)

Figure 3.22: Inter story drift demand for TT-C3 (a. Fault normal, b. Fault paralllel)

Figure 3.23, 3.24, 3.25 depict the location of maximum inter story drift demand for three categories of YSPDs along with considered frames (total ten) for ten earthquakes including fault normal and fault parallel . Figure 3.23 represents the maximum inter story drift location for YSPDs Category-01. Figiure 3.23 shows that for bare frame maximum inter story drifts occurs at first story. This condition is valid for both fault normal and fault parallel earthquake

data.Variation occurs for two to three earthquake data. In case of YSPDs in FT arragements the maximum inter story drift occur at second story level for both fault normal and fault parallel values. For TS arrangement maximum inter story drift occur at first floor level for TS-C1 arrangements. For TS-C2 and TS-C3 arrangents for most of the earthquakes maximum inter story drift occur at first floor level but for same earthquakes maximum inter story earthquake occurs at second floor level. For TT arrangements of YSPDs the maximum inter story drift happens in first floor level for most of the earthquake data. For YSPDs Category-02 and Category-03 similar trends are observed.

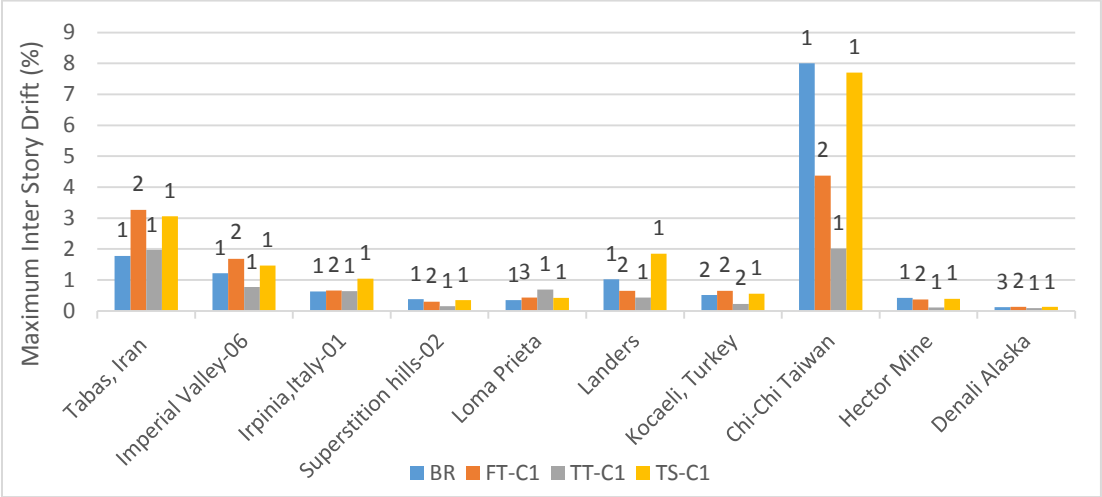

(a)

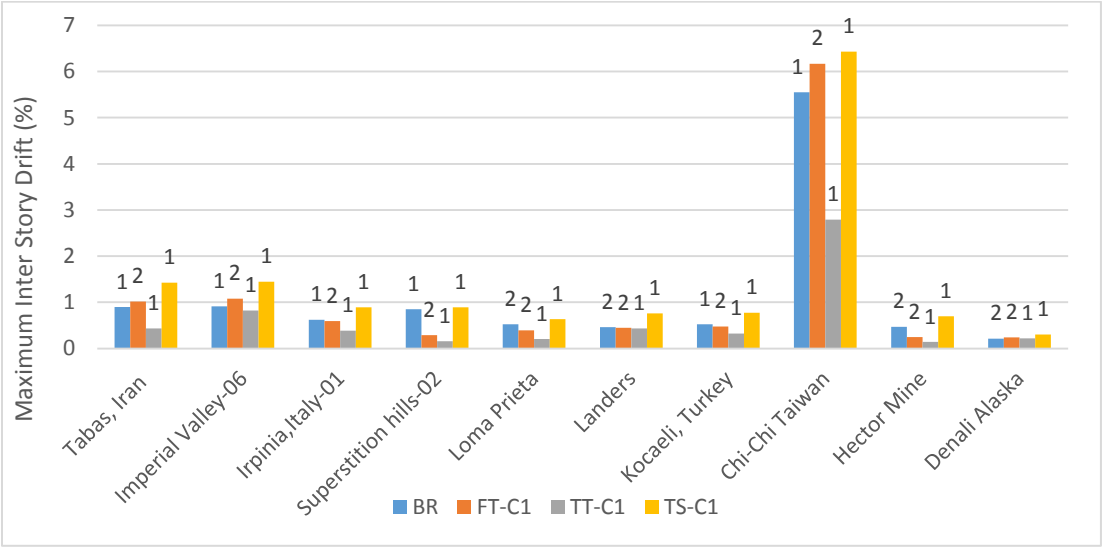

(b)

Figure 3.23: Maximum inter story drift demand for YSPD category-01 (a. for fault normal, b. for fault parallel)

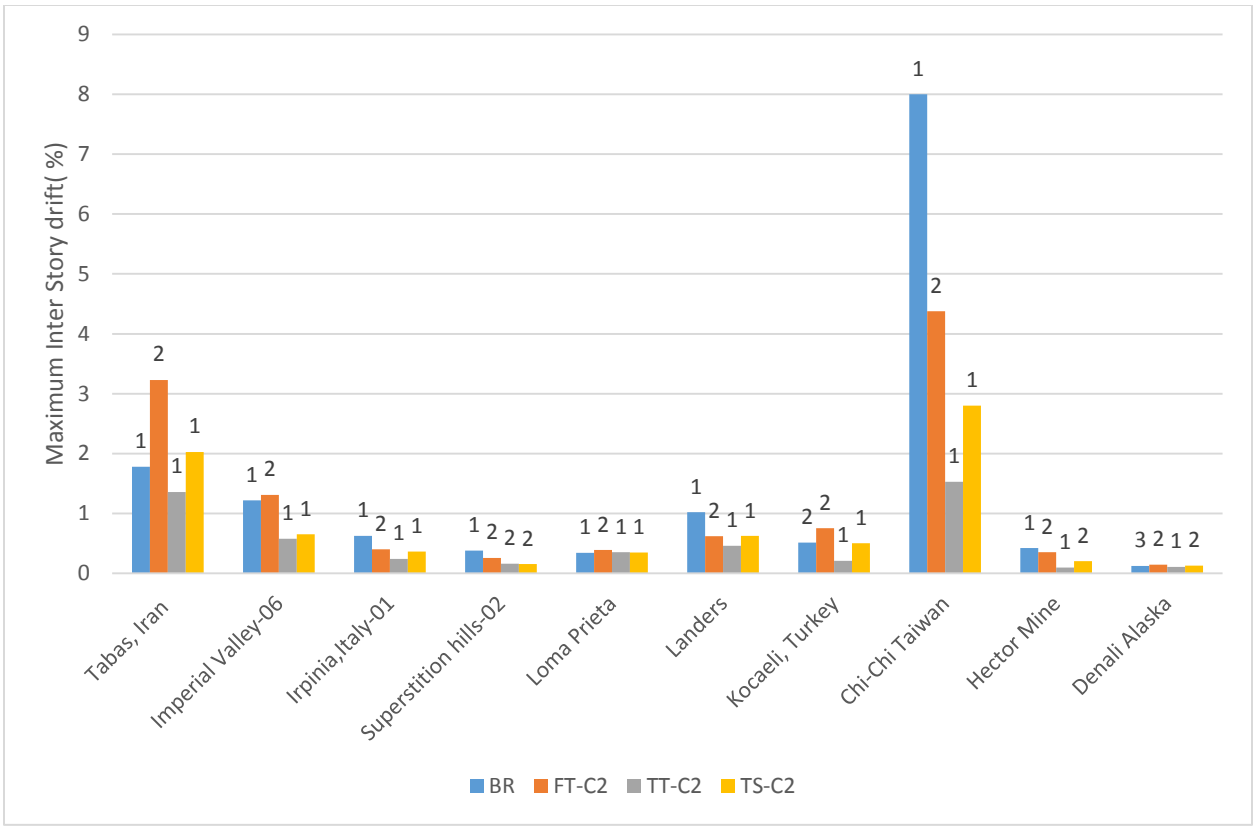

(a)

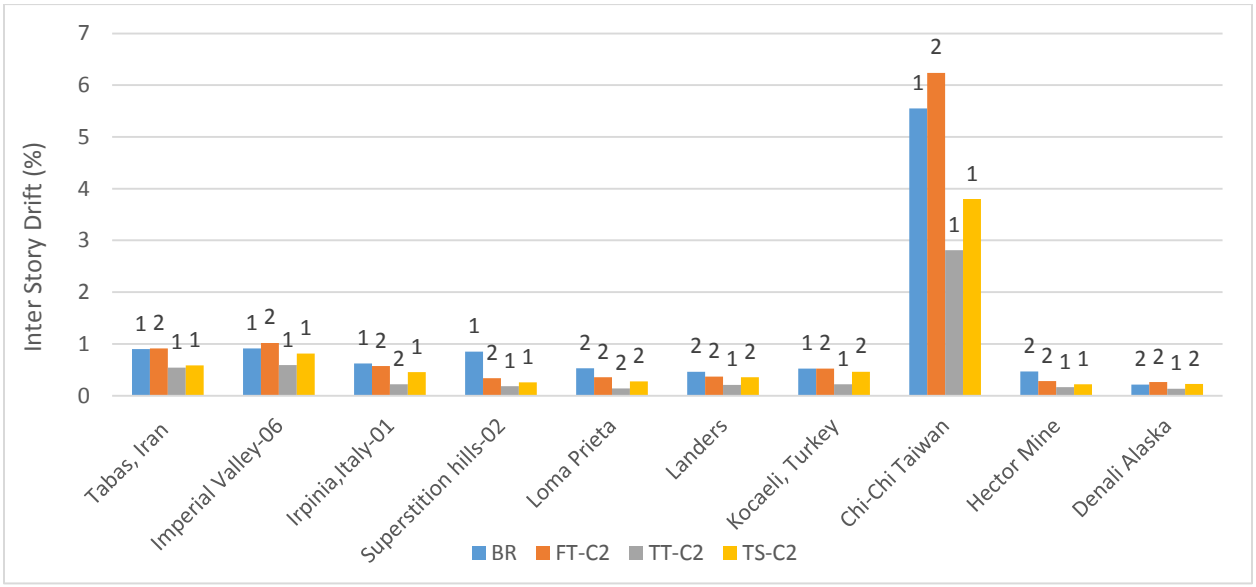

(b)

Figure 3.24: Maximum inter story drift demand for YSPD category-02 (a. for fault normal, b. for fault parallel)

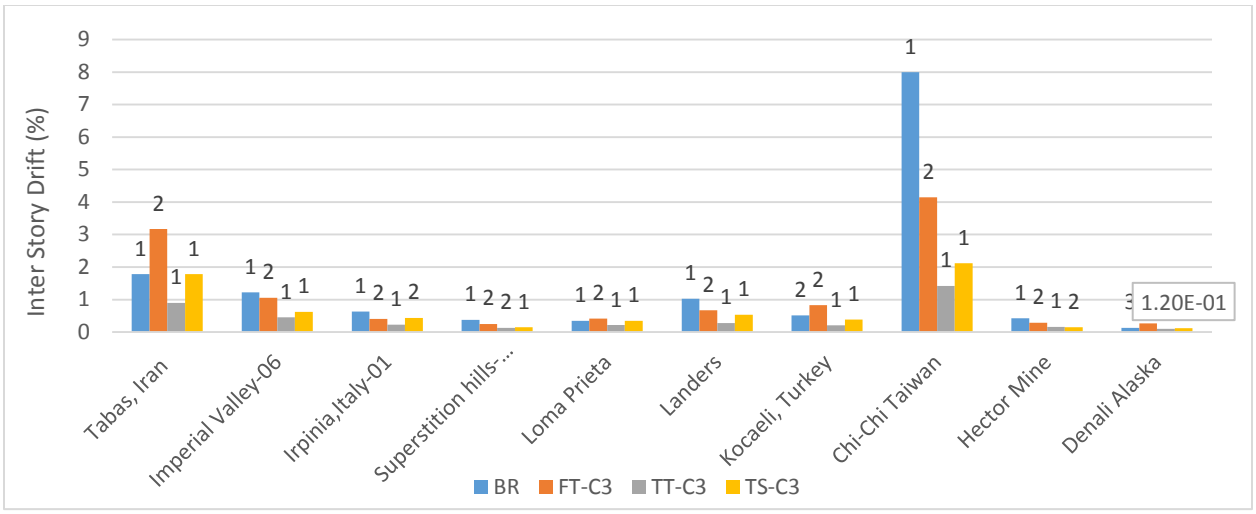

(a)

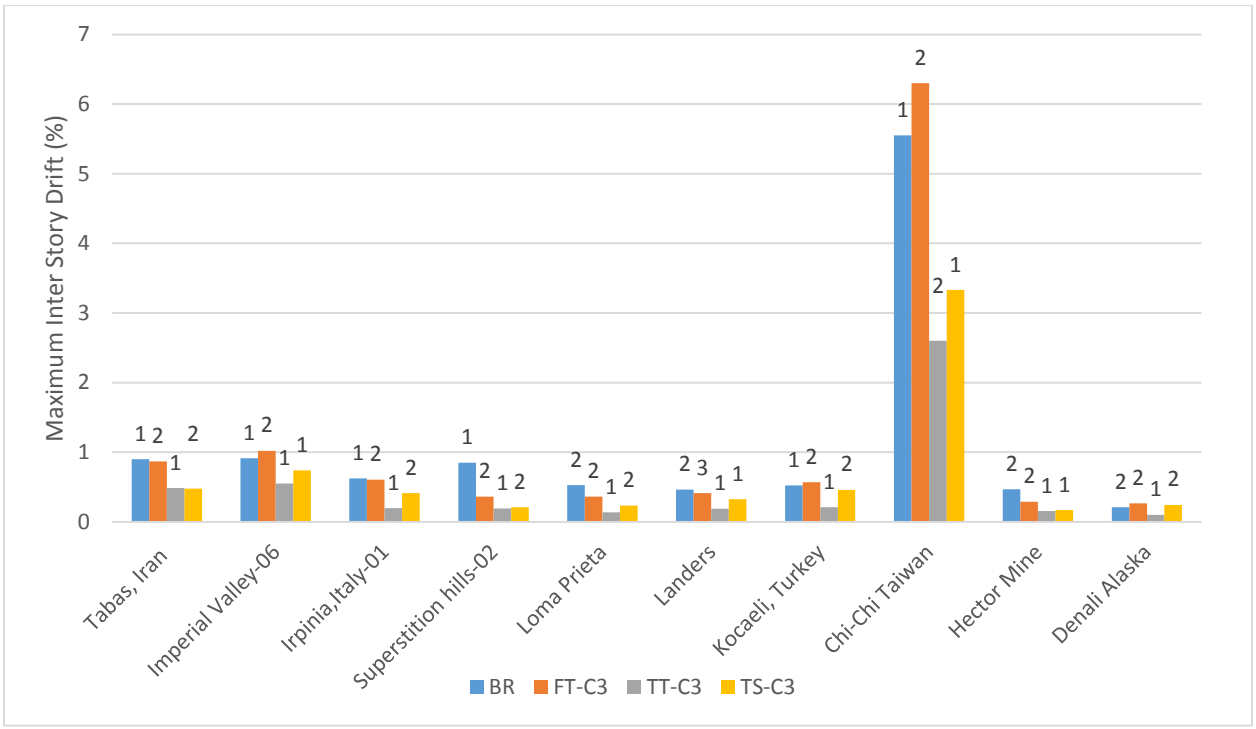

(b)

Figure 3.25: Maximum inter story drift demand for YSPD category-03 (a. for fault normal, b. for fault parallel)

Table 3.6 illustrates the average of maximum inter story drift (%) for ten types of frames along with the different categories of earthquakes. It is observed from the Table 3.6 that the FT shows lower average value of maximum inter story drift than the bare frame. TS shows lower average value of the maximum inter story drift than FT except for the case of TS-C1. TTs shows lower value than the TS arrangements. Again it is found that increasing the sizes of YSPDs decreases the average value of maximum inter story drift.

Table 3.6: Average of maximum inter story drift demand (%) for different types of frames along with the different categories of YSPDS.

Frame Types	Average inter story drift (%) for fault normal	Average inter story drift (%) for fault parallel
BR	1.44	1.10
FT –C1	1.25	1.09
TS-C1	1.69	1.42
TT-C1	0.70	0.59
FT-C2	1.18	1.08
TS-C2	0.78	0.74
TT-C2	0.51	0.52
FT-C3	1.14	1.07
TS-C3	0.66	0.66
TT-C3	0.40	0.48

The Figures 3.26, 3.27, 3.28 represents the roof demand of the three categories of YSPDs along with ten different types of frames against ten different earthquake data along with fault normal and fault parallel. From the Figures 3.26, 3.27, 3.28 it is observed that the roof drift demand is decreased for most of the cases if FT arrangement is compared with the bare frame. Only for first two earthquake data in case of fault normal values the FT arrangements shows slight large roof demand compared with bare frame. For TS arrangements roof demand decreases than the bare frame for TS-C2 and TS-C3 arrangements. For TS-C1 arrangement roof demand decreases than the bare frame for most of the earthquakes except for three FN earthquakes and two FP earthquakes. If TT arrangements is considered the roof demand shows lower demand

than the bare frame. As well as the roof demand is also lower than the FT arrangements. It is valid for both fault normal and fault parallel values.

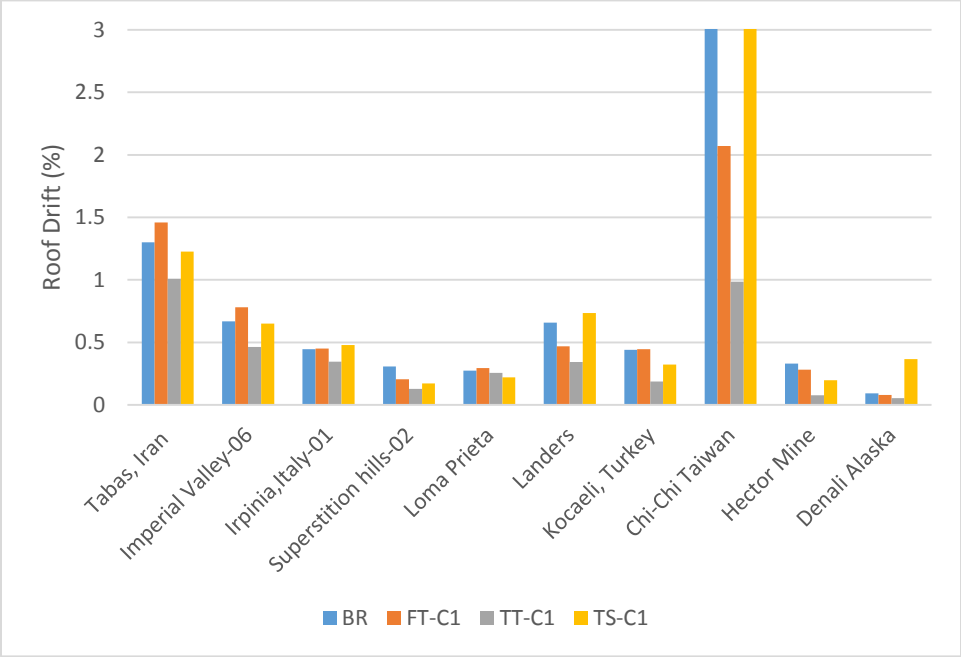

(a)

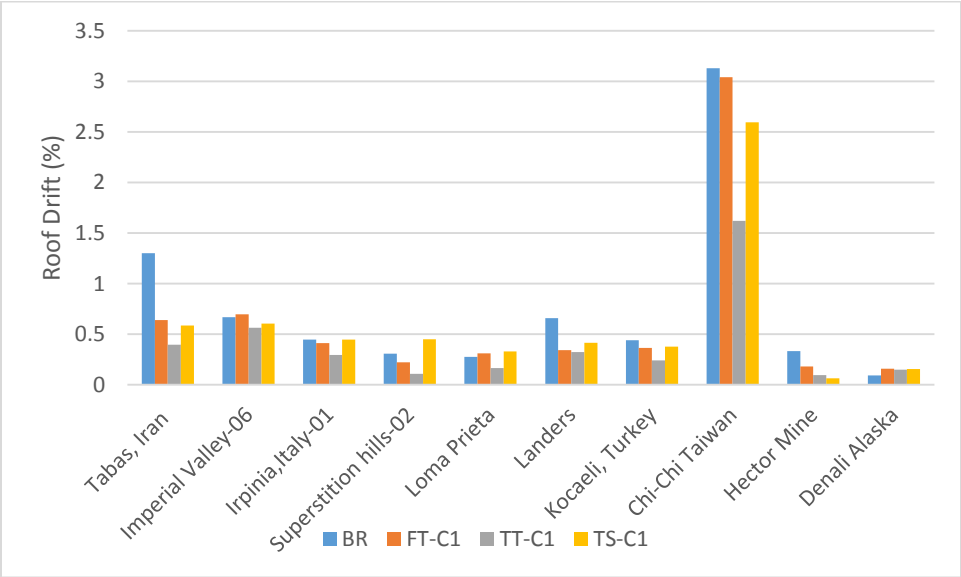

(b)

Figure 3.26: Roof drift demand for YSPD category-01 (a. for fault normal, b. for fault parallel)

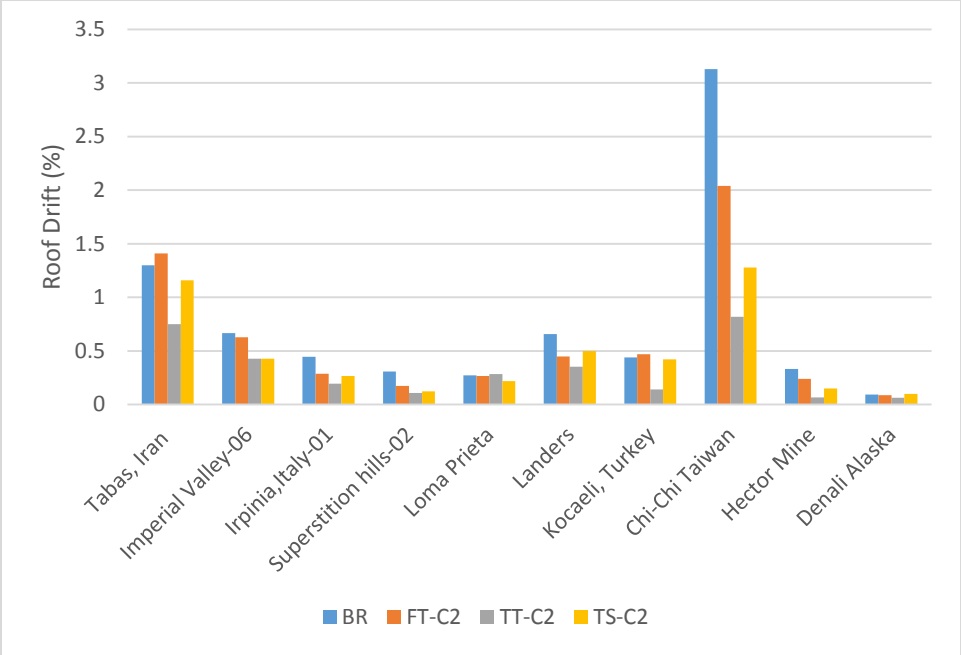

(a)

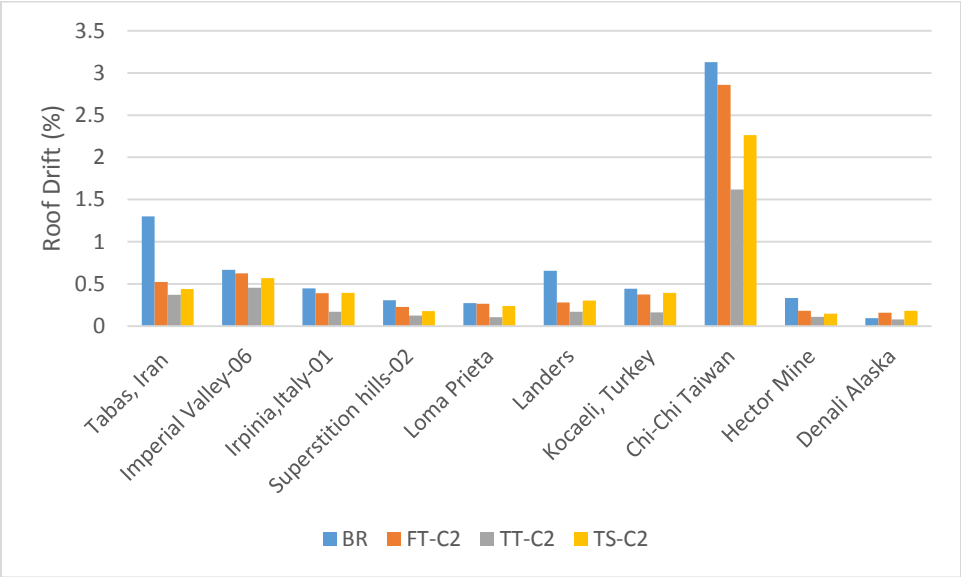

(b)

Figure 3.27: Roof drift demand for YSPD category-02 (a. for fault normal, b. for fault parallel)

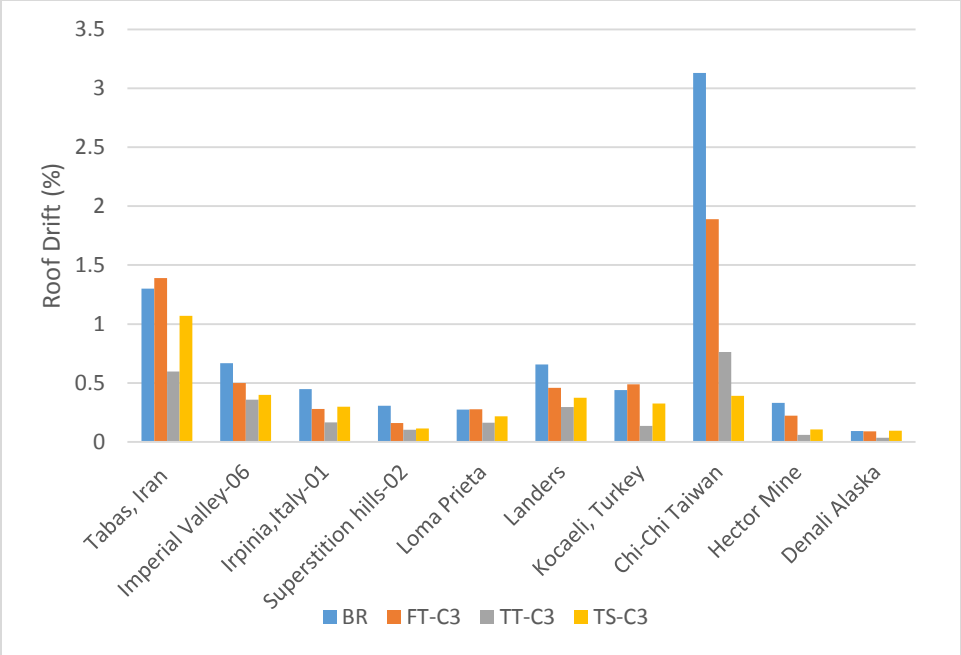

(a)

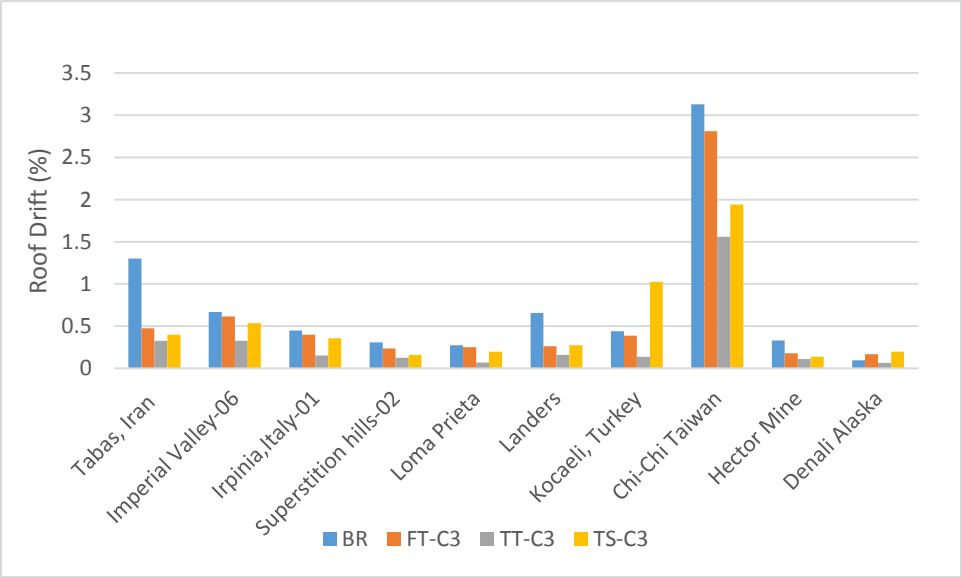

(b)

Figure 3.28: Roof drift demand for YSPD category-03 (a. for fault normal, b. for fault parallel)

Table 3.8 illustrates the average of roof drift (%) for ten types of frames along with the different categories of earthquakes. It is observed that the FT show lower average value of roof drift than the bare frame. TS shows lower average roof drift than bare frame and FT. Moreover, TT

shows lower value than the TS, FT and bare frame. Increased sizes of YSPDs are capable to decrease the average value of roof drift.

Table 3.7: Average roof drift demand (%) for different types of frames along with the different categories of YSPDS.

Frame Types	Average inter story drift (%) for fault normal	Average inter story drift (%) for fault parallel
BR	0.76	0.76
FT-C1	0.65	0.63
TS-C1	0.74	0.60
TT-C1	0.38	0.39
FT-C2	0.60	0.58
TS-C2	0.46	0.51
TT-C2	0.32	0.33
FT-C3	0.57	0.57
TS-C3	0.33	0.52
TT-C3	0.26	0.30

3.7 Incremental dynamic analysis

In recent years different types of methods are used for evaluating the seismic performance of civil engineering structures. Among them cloud analysis and Incremental Dynamic Analysis (IDA) are two advanced structural analysis methods. The difference is that in case of performing cloud analysis unscaled ground motions are used and for IDA scaled ground motions are used. For this reason IDA requires more time to complete compared to cloud analysis. Although IDA is time consuming, it can evaluate the relationship between intensity measures and demand parameters considering a large range of Intensity Measure (IM) **[69]**. IDA is a non-linear analysis method used to evaluate the seismic performance of the structure. In this method a series of non-linear dynamic analyses are performed for multiple scaled ground motion data. It is widely used to predict demand

against capacity capability of structure under seismic loading. The probability of the structural demand against given seismic intensity can be find out through IDA method **[70]**.

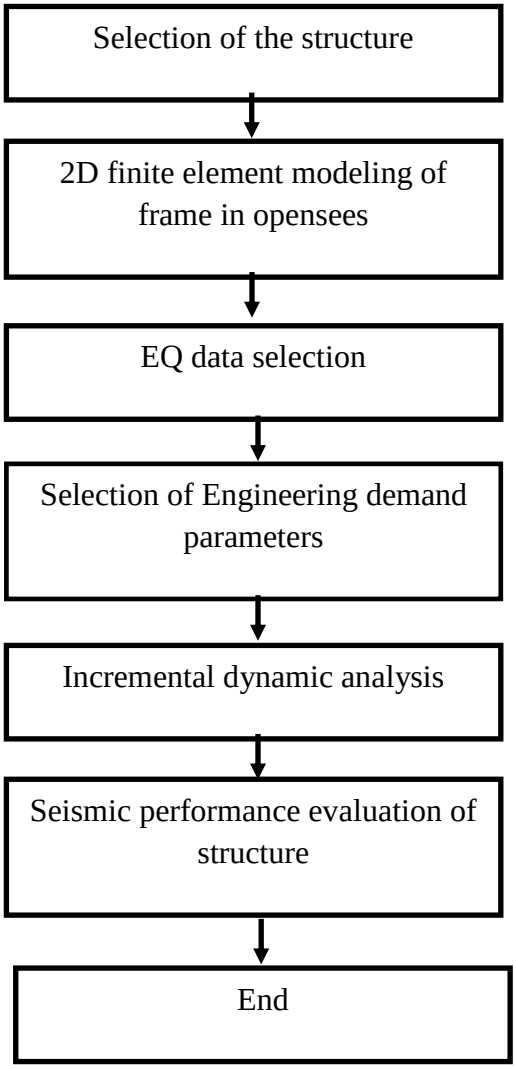

Figure 3.29: Steps of incremental dynamic analysis.

The Figure 3.29 shows the analysis steps are followed to complete IDA analysis. Ten different types of frames are taken for the analysis. Frame with three different arrangements and three different sizes of YSPDs and bare frame are considered for the analysis to find out the suitability of YSPDs in case of energy dissipation.

IDA have been performed for total ten earthquakes including fault normal and fault parallel data. For ten different types of frames have been taken for the analysis. Figure 3.30 to Figure 3.39 show the IDA curves for the ten different types of frames. The results of the IDA have been interpreted using the parameters found from the statistical analysis of post-seismic data i.e. Maximum Considered Earthquake (MCE), Design Basis Earthquake (DBE). MCE is the 2% probability of exceedance of peak horizontal acceleration in 50 years. DBE is the 10% probability of exceedance of peak ground acceleration in 50 years. For Los Angeles site class D the MCE is 0.8 g and DBE is 0.5 g. Initially the IDA curves show the straight line representing the linear elastic behavior and then the change in the straight lines depict the nonlinear behavior.

Figure 3.30 (a) depicts that for the BR subjected to FN earthquake data 8 of the 10 ground motion caused collapse of the frame at MCE ground motion level and 3 of the 10 ground motion caused collapse of the frame at DBE ground motion level. From the figure 3.30 (b) it is observed that for the FP EQ data the number of collapse reduces to 5 of 10 ground motion at MCE level and 2 of 10 at DBE level.

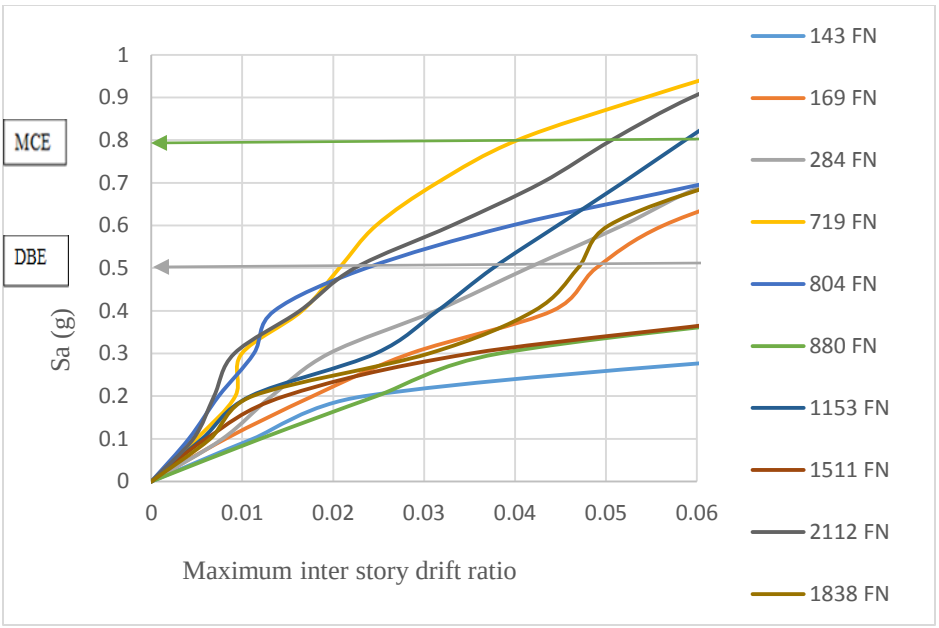

(a)

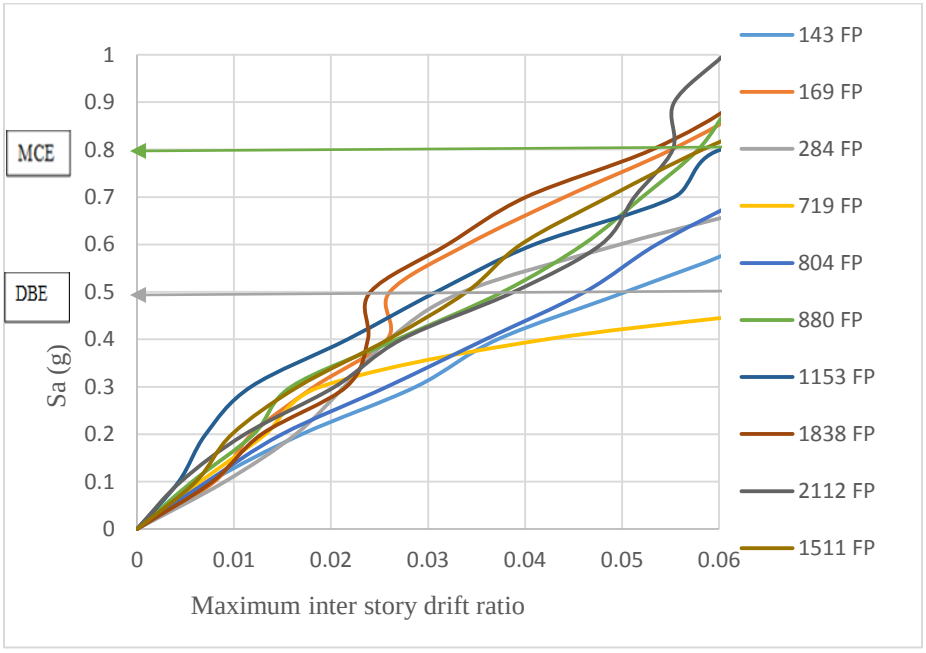

(b)

Figure 3.30: IDA curves for BR (a. Fault normal, b. Fault parallel)

Figure 3.31 shows that for most of the earthquakes drift demand is lower for FT-C1 than the bare frame. With the increase of the size of YSPDs the more reduction in the drift demands have also been observed, shown in Figure 3.31 to 3.33. After installation of YSPDs in the FT-C1 the number

reduces more i.e. 3 of 10 motion caused collapse at MCE level and 2 of 10 at DBE level for FN. Figure 3.31 shows that for FP 3 of 10 ground motion caused collapse at MCE and 1 of 10 at DBE level. The performance improves for the increased size of YSPDs in case of FT arrangements, shown in Figure 3.32, 3.33.

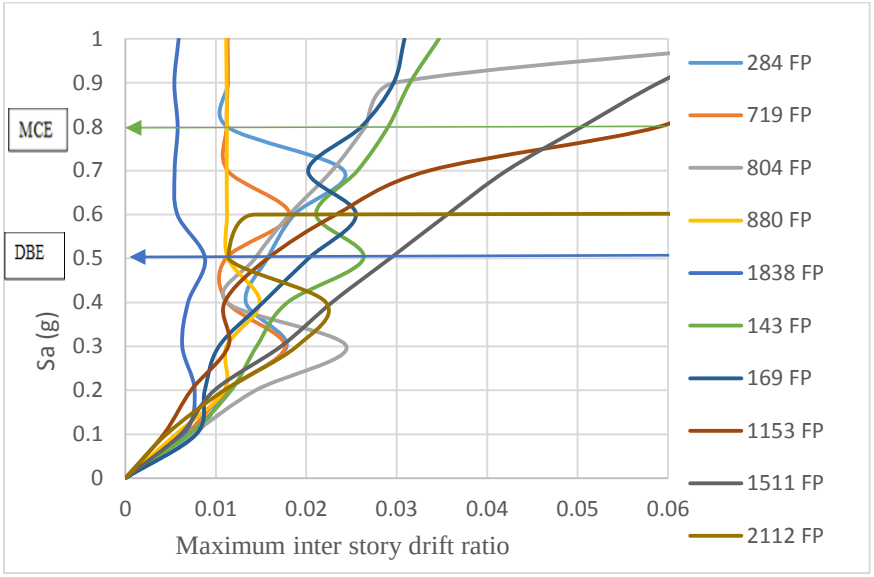

(a)

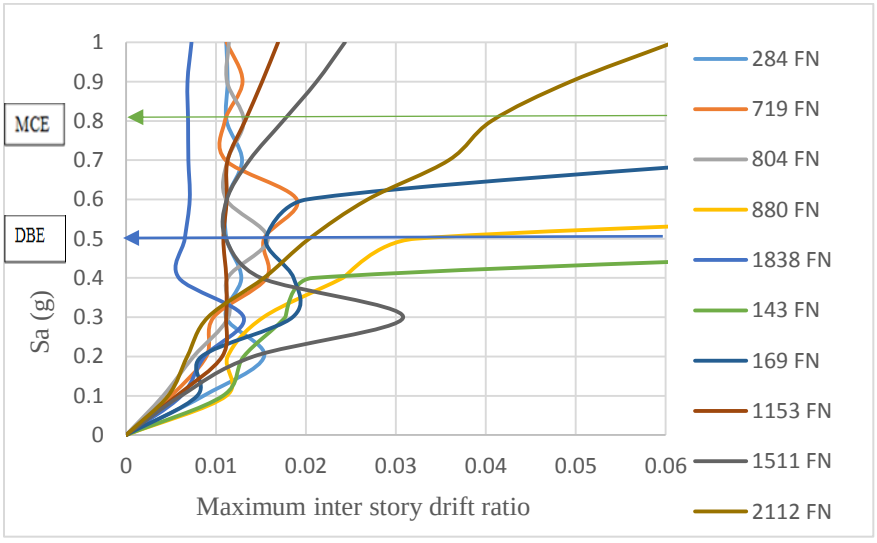

(b)

Figure 3.31: IDA curves for FT-C1 (a. Fault normal, b. Fault parallel)

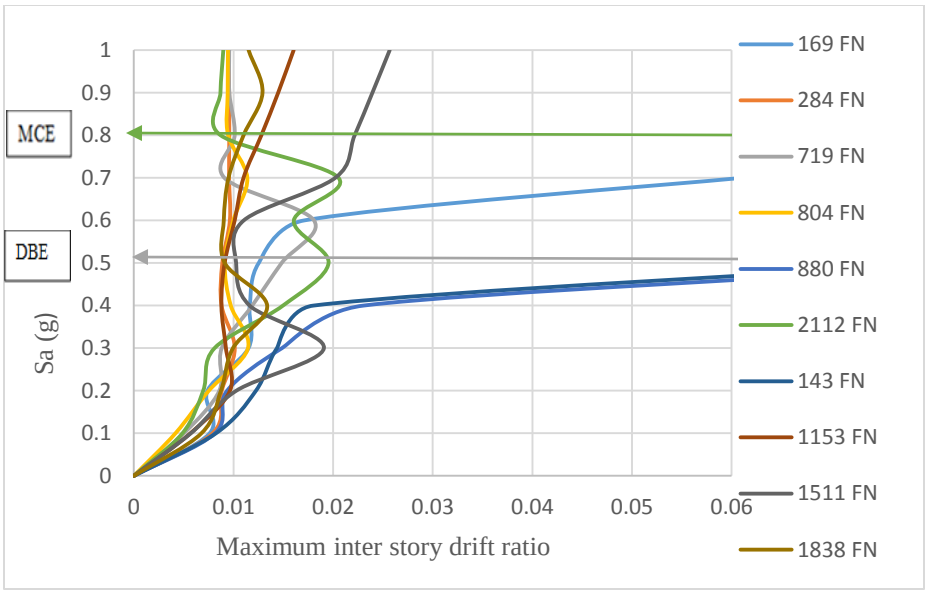

(a)

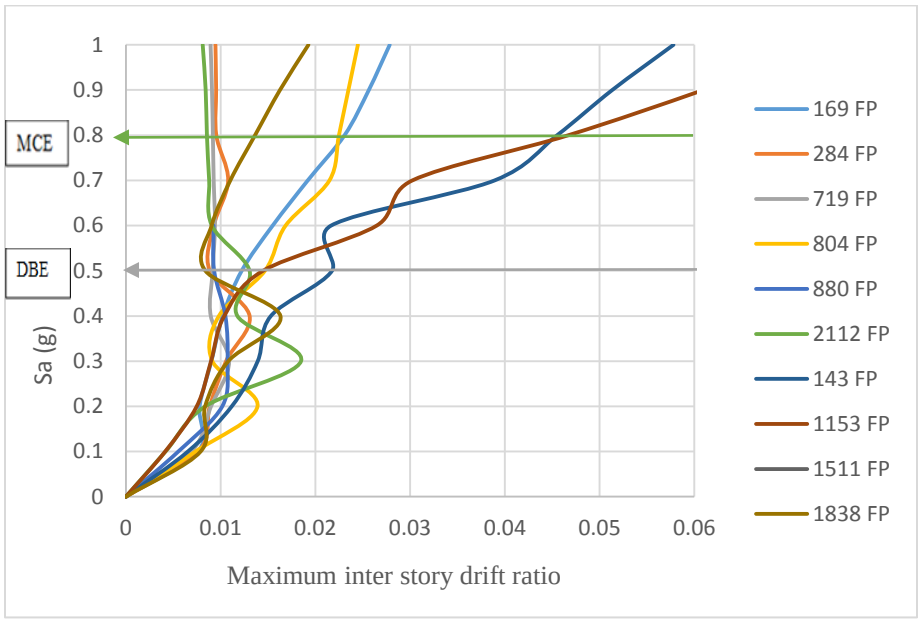

(b)

Figure 3.32: IDA curves for FT-C2 (a. Fault normal, b. Fault parallel)

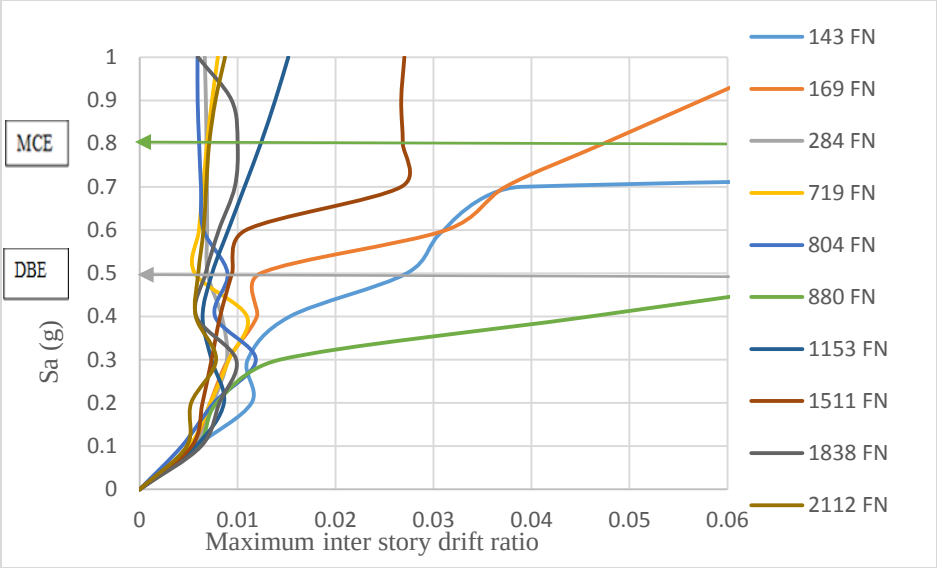

(a)

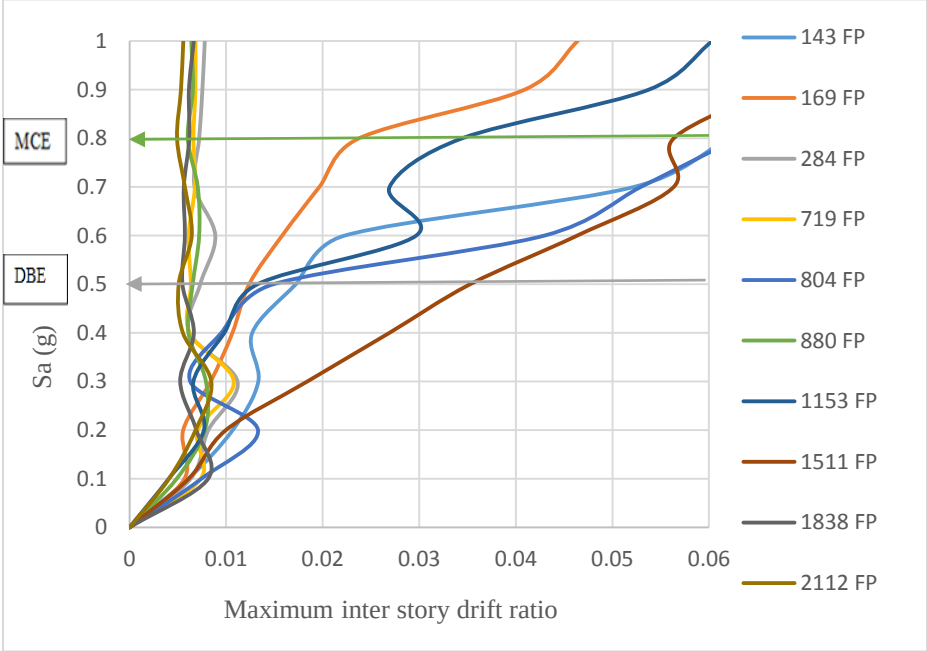

(b)

Figure 3.33: IDA curves for FT-C3 (a. Fault normal, b. Fault parallel)

Figure 3.34 shows that for most of the earthquakes drift demand is lower for TS-C1 than the bare frame. Figure 3.34 to 3.36 show that with the increase of the size of YSPDs the more reduction in the drift demands have also been observed. For TS arrangement 2 of 10 ground motion caused

collapsed of the frames at MCE ground motion level for FN earthquake data and no ground motion caused failure at DBE level, shown in Figure: 3.34(a), 3.35(a), 3.36(a). Figure: 3.34(b), 3.35(b), 3.36(b) depict that for FP earthquake data TS arrangement shows no failure at MCE and DBE level

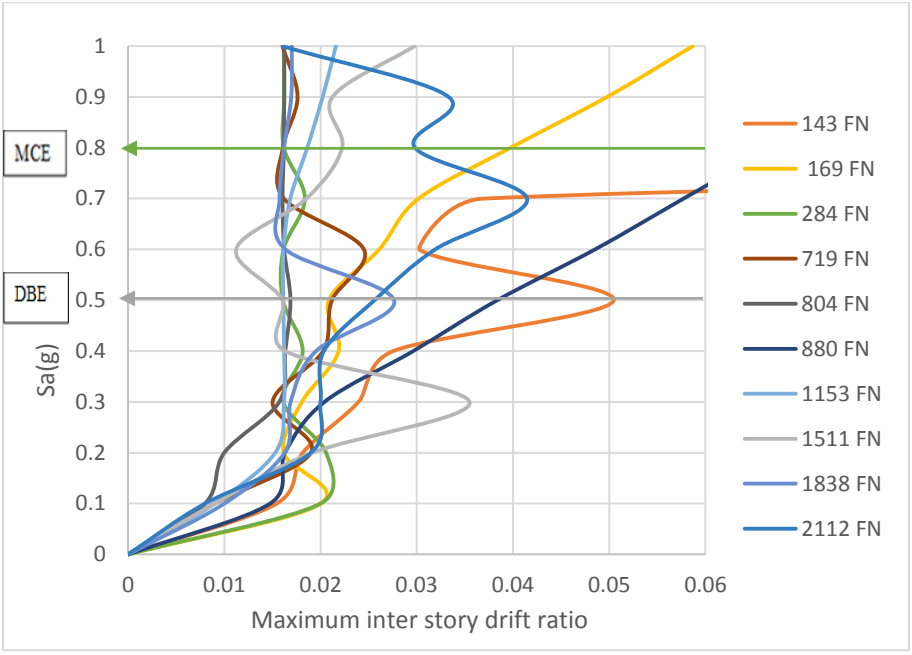

(a)

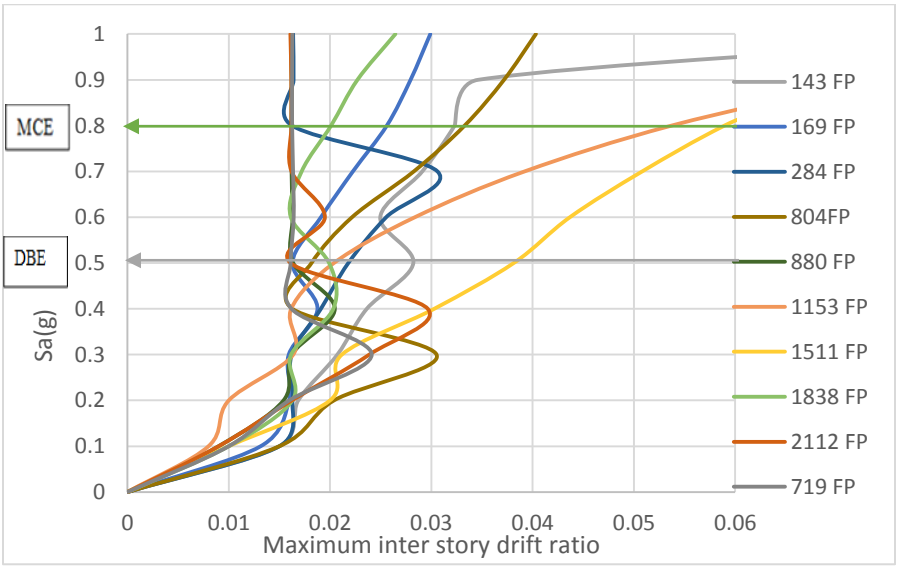

(b)

Figure 3.34: IDA curves for TS-C1 (a. Fault normal, b. Fault parallel)

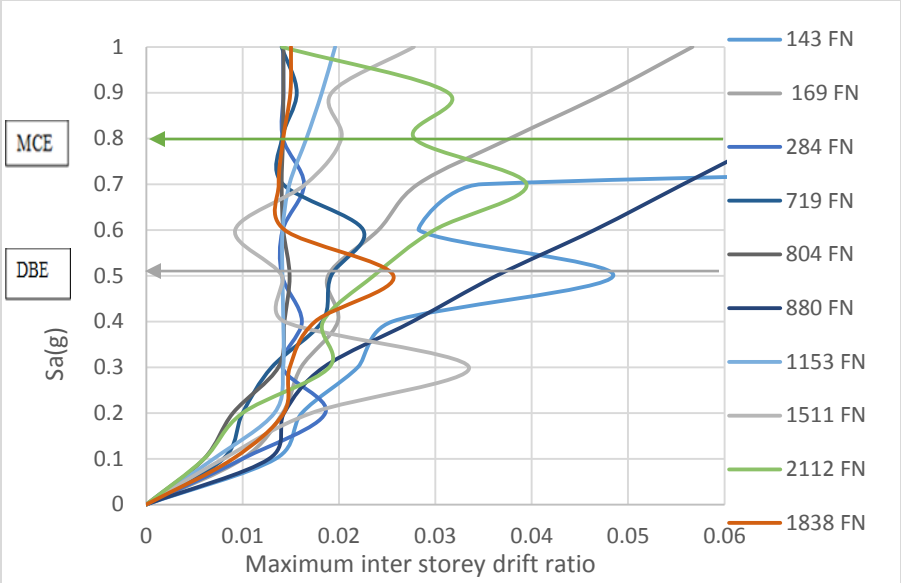

(a)

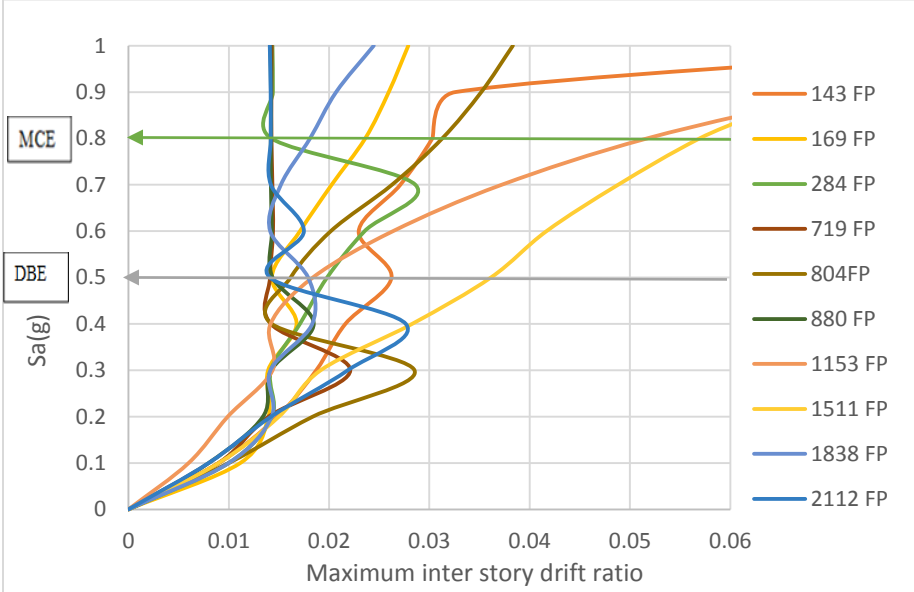

(b)

Figure 3.35: IDA curves for TS-C2 (a. Fault normal, b. Fault parallel)

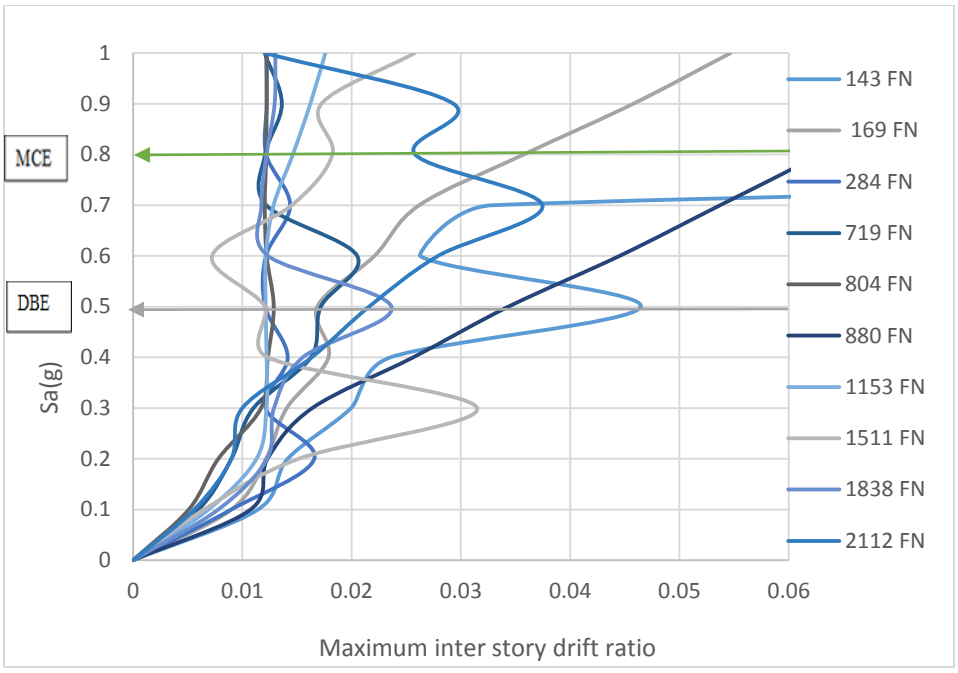

(a)

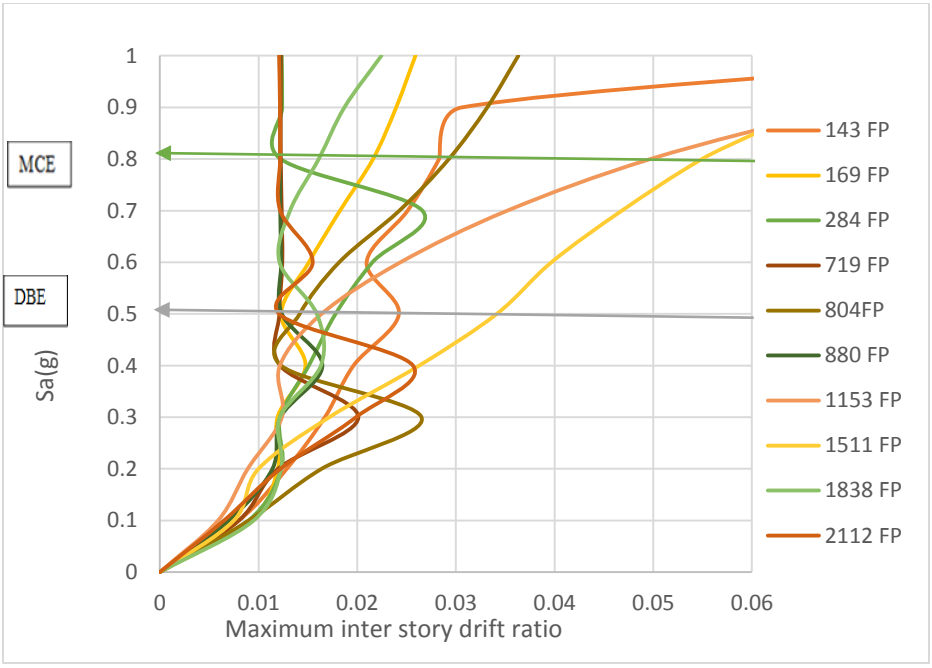

(b)

Figure 3.36: IDA curves for TS-C3 (a. Fault normal, b. Fault parallel)

After installation of YSPDs inter story drift demand is reduced more for TT arrangements in comparison of FT, TS and bare frame. The better energy dissipation capacities have been observed for the TT arrangements than the FT and TS arrangements. For the TT arrangement all most no ground motion caused failure both in MCE and DBE level, observed from Figure 3.37, 3.38, 3.39.

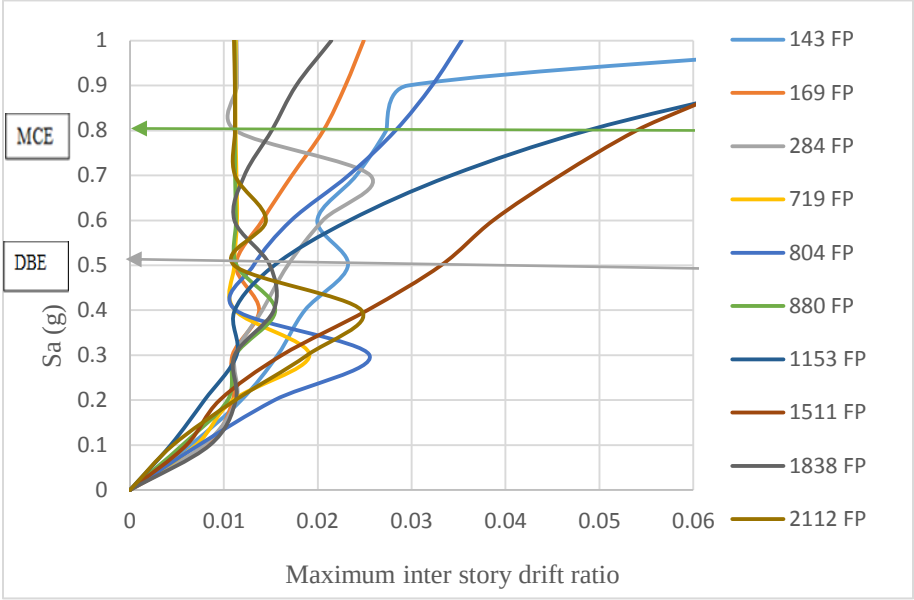

(a)

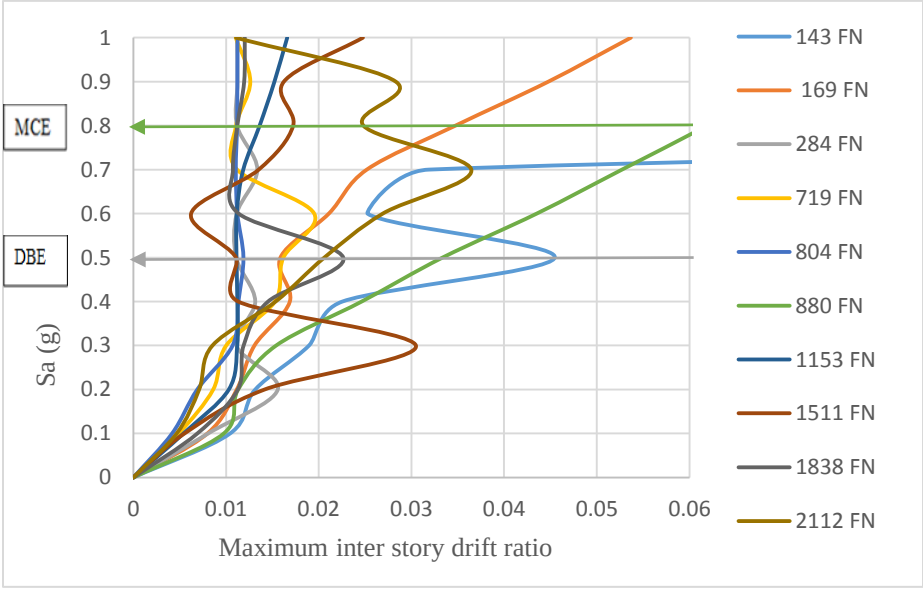

(b)

Figure 3.37: IDA curves for TT-C1 (a. Fault normal, b. Fault parallel)

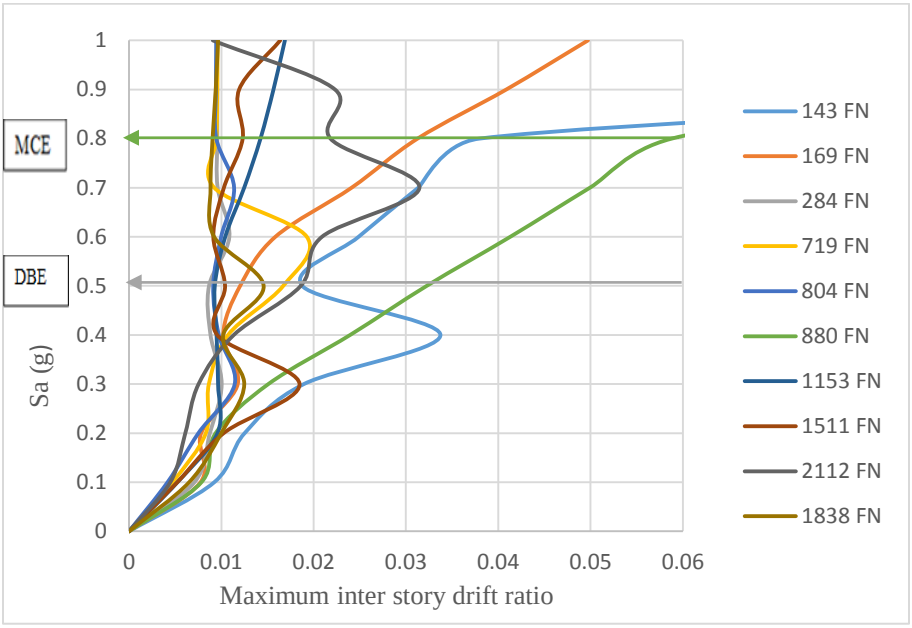

(a)

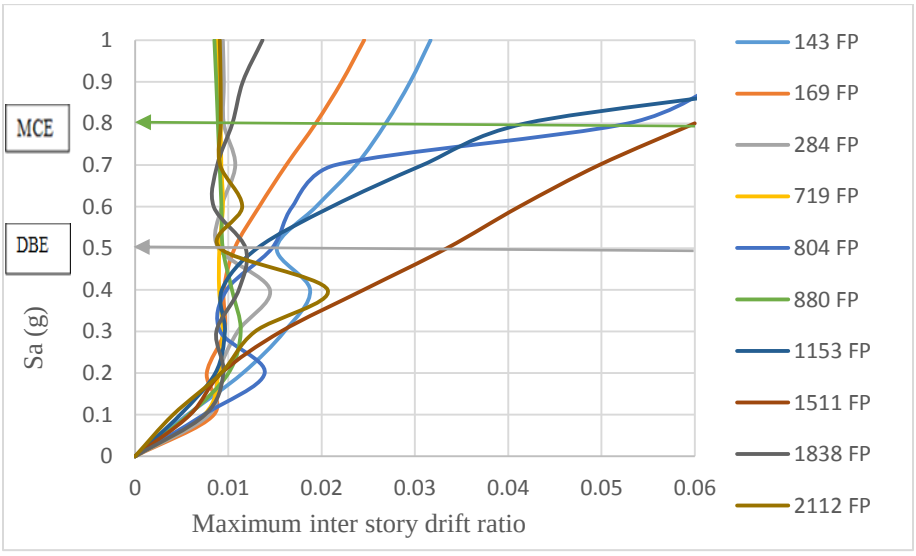

(b)

Figure 3.38: IDA curves for TT-C2 (a. Fault normal, b. Fault parallel)

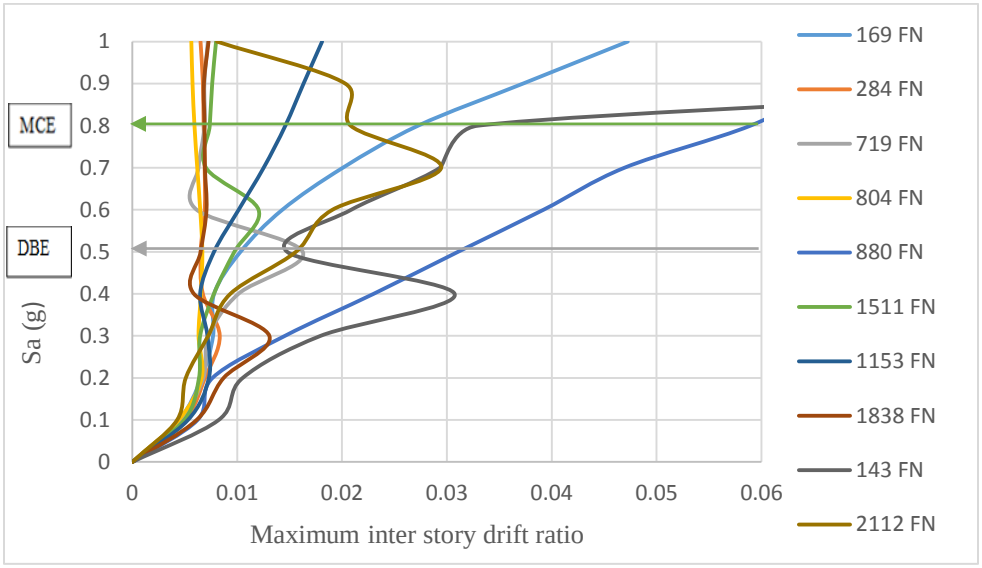

(a)

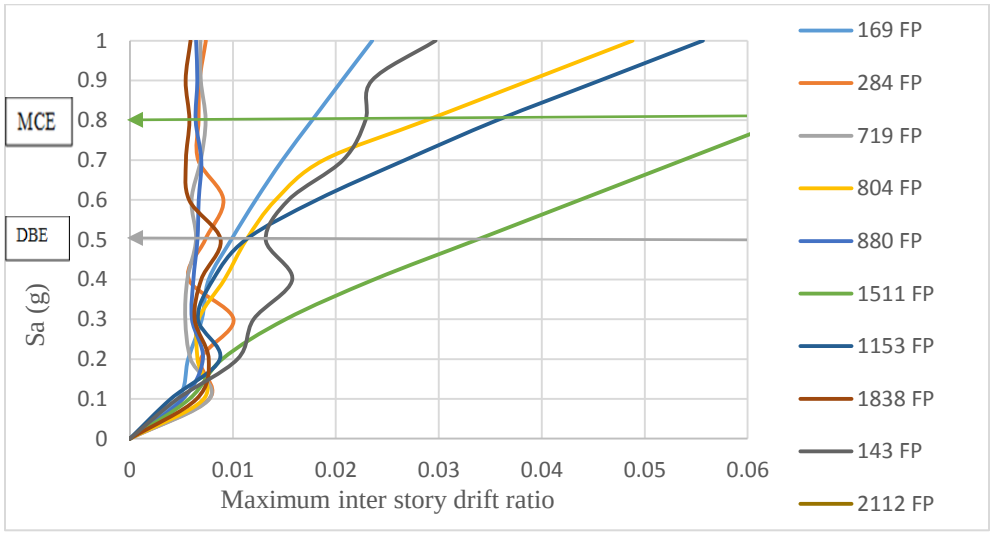

(b)

Figure 3.39: IDA curves for TT-C3 (a. Fault normal, b. Fault parallel)

3.8 Fragility analysis

Fragility analysis has been conducted to evaluate the risk based seismic performance of the structures. IDA analysis results are used to perform fragility analysis. Vulnerability of the structures are explained through limit states capacities. For IO and LS limit states β_c is equal to 0.25 and for CP limit states β_c is 0.15 [**13**]. The median fragility values of different combinations are shown in Table 3.8. From the Table 3.8 it can be observed that the system fragility is decreasing and median fragility is increasing after installing YSPD for TS and TT combinations. Though for FT combination the fragility analysis has not shown better performance. TS and TT combination show better performance than bare frame for all three limit states capacities. Such as for TT-C1 median fragility increases in comparison to the bare frame from 0.16g to 0.33g for IO, 0.28g to 0.64g for LS and 0.44g to 1.01g for CP limit states.

Table 3.8: Seismic demand statistics and median fragility values for bare frame and frames with YSPD

Frames	$\beta_{D\|Sa}$	β_R			S_a(g)		
		IO	LS	CP	IO	LS	CP
BR	0.53	0.59	0.59	0.55	0.16	0.28	0.44
FTC_1	0.55	0.62	0.62	0.60	0.17	0.27	0.42
FTC_2	0.54	0.60	0.60	0.58	0.18	0.30	0.45
FTC_3	0.52	0.57	0.57	0.55	0.19	0.32	0.46
TSC_1	0.47	0.53	0.53	0.48	0.26	0.55	0.96
TSC_2	0.43	0.51	0.51	0.46	0.28	0.58	0.98
TSC_3	0.42	0.50	0.50	0.46	0.30	0.61	0.99
TTC_1	0.41	0.50	0.50	0.44	0.33	0.64	1.01
TTC_2	0.42	0.49	0.49	0.43	0.37	0.67	1.04
TTC_3	0.40	0.47	0.47	0.43	0.40	0.82	1.06

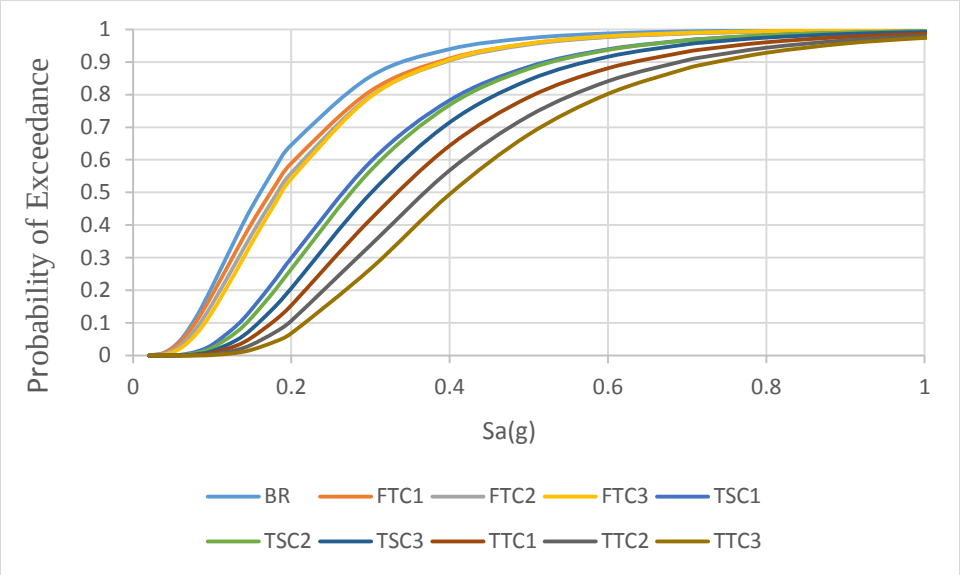

Figure 3.40: Fragility curves for IO

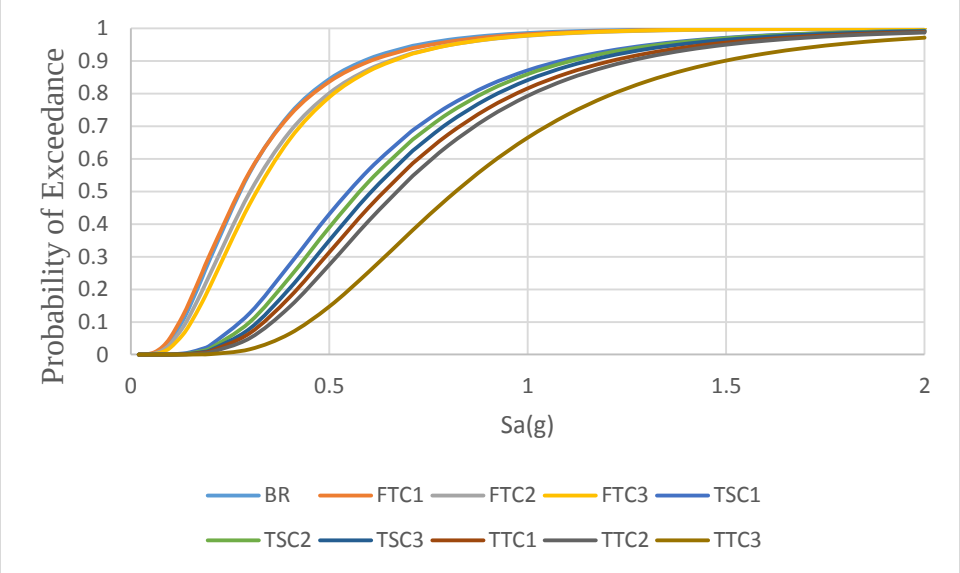

Figure 3.41: Fragility curves for LS

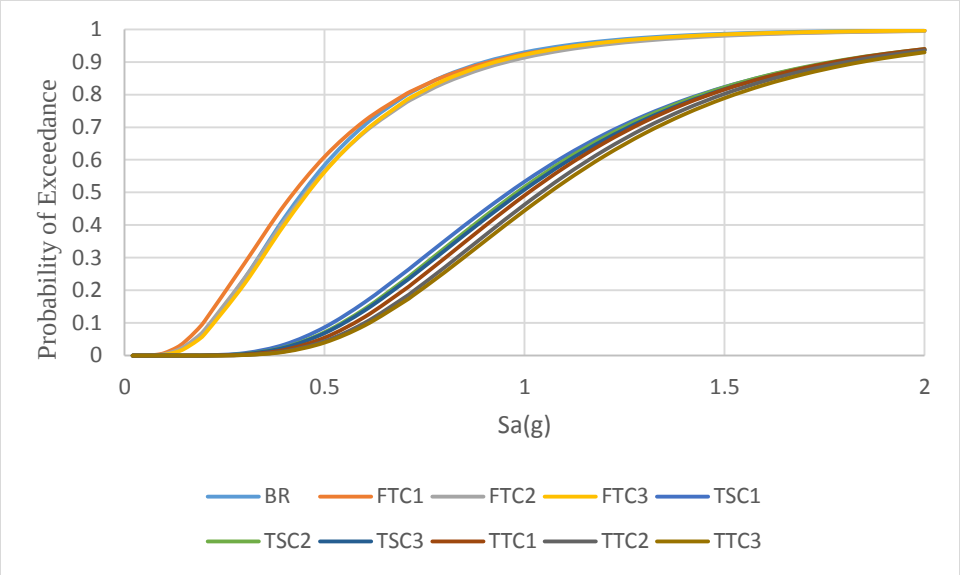

Figure 3.42: Fragility curves for CP

Figure 3.40, 3.41, 3.42 show the fragility curves for the bare frames and the frames with YSPDs. Fragility curves have been drawn for IO, LS, and CP limit states capacities. Significant reduction in fragility is observed after installation of YSPDs except some variation for FT combination. TT combination has demonstrated better performances over FT and TS arrangements. Better performances have been observed with the increase of the size of the YSPDs. TT-C3 arrangements shows the best results among all the combination and arrangements.

3.9 CONCLUSION

The structure chosen for this current research is a low ductility RC building which is very common in eastern and central U.S. The structure is very vulnerable to earthquake as during design no earthquake loads are considered. To strengthen the structure against seismic loading YSPDs are installed. From the pushover analysis it is observed that the capacity of the structure is increased after installing YSPDs. The increase in capacity is higher for the large size of YSPDs. Furthermore it is observed that the use of YSPD in three story three bay is more effective than other two arrangements. The results shows that inter story drift demand is decreased after installing YSPD in three story three bay of the structure. In case of first story three bay arrangement the inter story drift demand is decreased largely in the first story but increased higher

in the second story. For TS arrangements inter story drift demand were lower than the bare frame except for the case of TS-C1. With the increased size of YSPDs both the average maximum inter story drift and roof drift are also reduced. From the static, dynamic and fragility analysis it is observed that the three story three bay arrangements shows better result and the highest size of YSPDs along with this arrangement show best result.

Chapter 4: CONCLUSION AND RECOMMENDATION

4.1 General

The structure chosen for this current research is a low ductility RC building which is very common in Bangladesh. The structure is highly vulnerable to earthquake since no earthquake load is considered in the design of such structures. YSPD, a passive control device, can be installed to strengthen the structure against seismic loading. In the current study, the sizes of the YSPDs were varied and the arrangements were changed to find out the best performance. Total three different sizes of YSPDs with three different orientations were used for evaluating the performance of YSPDs.

4.2 Conclusions

The results found from the analysis are given bellow:

- Pushover analysis has been conducted in order to assess the base shear capacity of the structure against static load after installing YSPDs. The results of the pushover analysis show that after installing YSPDs the base shear capacity of the structure increases, with varying degree of performance has been observed for different orientations and sizes of YSPDs. For FT arrangements the increase in the size of YSPDs does not affect much in case of base shear capacities but for the TS and TT combination increase size of the YSPDs has greater impact in performance. The order of performance (in descending order), as observed in the current study, can be summarized as TS > FT > bare frame. The best performance among three arrangements are observed for TT arrangements. Inter story drift after installing YSPDs for FT arrangements at first floor level decreased to a large amount than the bare frame but increased for other two level. For TS and TT arrangements inter story drift decreased from the bare frame at all floor levels except for the case of TS-C1.
- Time history analysis have been performed for ten different kinds of earthquakes. Results are described in terms of inter story drift, roof drift, location of the maximum inter story drift, average value of the maximum inter story and roof drift. For FT arrangements inter story drift decreases in the first story but increases in the second story. For TS, TT arrangement inter story drift decreases than the bare frame except for the case of TS-C1.

For TS-C1 case, inter story drift increases at first story and decreases in the other two stories. The average maximum inter story drift decreases gradually after installing YSPDs in FT, TS and TT arrangements except for the case of TS-C1. Roof drift also decreases after installing YSPDs for FT, TT and TS arrangements. The best performance has been observed for TT arrangement from the time history analysis also. The locations of maximum inter story drift have been observed for Bare frame, TS and TT is first story and for FT is second story for most of the cases.

- Incremental dynamic analysis and fragility analysis have also been performed to assess the performance of the structure before and after installing YSPDs. From the results of the incremental dynamic analysis it is observed that the curves are becoming stiffer after installation of the YSPDs which indicates lower drift demands. For bare frame the incremental dynamic analysis shows that for 8 earthquakes the structure is vulnerable to collapse at MCE level and for three earthquakes at DBE level. But after installation of the YSPDs the number decreases for FT, TT arrangements and almost no failure for TT arrangement have been observed. Fragility analysis shows that system fragility decreases and median fragility increases after installing YSPDS. Significant reduction in fragility have been observed for TT arrangement.

4.3 Limitation of this research work and future recommendation

- The present study is only limited to numerical analysis. Experimental testing using shake table test is recommended for future to see the variation of performance of YSPDs in case of RC building.
- Life cycle cost analysis has not been done for the current structure with two different arrangements of frames with YSPDs which is recommended for further study.
- The beam column joints are modeled as rigid which does not permit any rotation that might occur in the joint. To simulate the better response of the joint a better joint representation may be used in future.

References

[1] "USGS Real-time Earthquake Map with exact dates and live earthquake reports". United States Geological Survey.

[2] https://en.wikipedia.org/wiki/List_of_earthquakes_in_2016

[3]https://www.google.com/lpsyab.3...103933.107223.0.107532.12.11.0.0.0.0.690.1600.0j1j1j0j1j1.4.0....0...1.1.64.psy-ab..8.2.845...0i8i30k1.aXWiqFNuXlg#imgrc=eJXgrrjjf7heYM

[4] Erberik, M. A., Cullu, S., (2005), "Seismic Fragility studies on Low-Rise and Mid-Rise Reinforced Concrete Frame Building Using Duzce Database"

[5] Ellingwood, B. R., Celik, O. C., Kinali, K., (2007), "Fragility assessment of building structural systems in Mid-America." Earthquake Engineering and Structures Dynamics, pp: 1935-1952.

[6] Tekie, P.B., Ellingwood, B.R., (2003), "Seismic fragility assessment of concrete gravity dams" Earthquake Engineering and Structural Dynamics 2003; 2003; pp: 2221-2240.

[7] Manzur, T. and Noor, M. A., (2006), "Displacement based fragility curves for R.C.C frame structures in contest of Dhaka, Bangladesh." Proceedings of the Asia-Pacific Strucrural Engineering and Contruction Conference.

[8] Shinizuka, M., Grigoriu, M., Ingraffea, a. r., Billington, S.L., Feenstra, P., Soong, T.T., (2000), "Development of fragility information for structures and nonstructural components."

[9] Nielson, B.G., (2005), "Analytical Fragility Curves for Highway Bridges in Moderate Seismic Zones"

[10] Basoz, N., Kiremidjian, A.S., (1997), "Evaluation of bridge damage data from the Prieta and Northridge, CA earthquakes." Report No. 127. Stanford: John A Blume Earthquake Engineering Center, Stanford University.

[11] Karim, K.R., Yamazaki, F., (2001) "Effect of earthquake ground motions on fragility curves of highway bridge piers based on numerical simulation." Earthquake Engineering and Structural Dynamics, pp: 1839-1856.

[12] Shinoj, A., Kurian, S. k., Dutta, D.A., (2006), "Seismic Vulnerability Assessment of a Railway Overbridge Using Fragility Curves" 4th International Conference on Earthquake Engineering Taipei, Taiwan, pp: 12-13.

[13] Nielson, B.G., DesRoches, R., (2007), "Analytical Seismic Fragility Curves for Typical Bridges in the Central and Southeastern United States."

[14] Kibboua, A., Naili, M., Benouar, D., Kehila, F., (2011), "Analytical Fragility Curves for Typical Algerian Reinforced Concrete Bridge Piers" Structural Engineering and Mechanics, Vol.39, No.3, pp: 411-425.

[15] Mander, J.B., (1999) "Fragility Curve Development for Assessing the seismic Vulnerability of Highway Bridges."

[16] Sbinozuka, M. and Kim, S.H., (2012), "Development Fragility Curves for Concrete Bridges Retrofitted with Steel Jacketing"

[17] Elnashai, A.S., Borzi, B., Vlachos, S., (2003), "Deformation-based vulnerability function for RC bridges." Journal of Structural Engineering.

[18] Mackie, K. and Stojadinovic, B., (2004), "Fragility Curves for Reinforced Concrete Highway Overpass Bridges." 13th World Conference on Earthquake Engineering.

[19] Kibboua, A., Kehila, F., Bechtoula, H., Mehani, Y., Remki, M., (2014), "Development of fragility curves for seismic evaluation of a reinforced concrete Bridge." Second European Conference on Earthquake Engineering and Seismology, pp: 25-29.

[20] Billah, A.H.M.M, Alam, M.S., (2012), "Development of fragility curves for retrofitted multi-column bridge bent subjected to near fault ground motion" 15 WCEE.

[21] Padgett, J. E. and DesRoches, R., (2008), "Methodology for the development of analytical fragility curves for retrofitted bridges." Earthquake Engineering and Structures Dynamics, 37, pp: 1157-1174.

[22] Choi, E., DesRoches, R., Nielson, B., (2004), Seismic fragility of typical bridges in moderate seismic zones. Engineering Structures, pp: 187-199.

[23] Hwang, H., Liu, J.B., Chiu, Y.H., (2000), Seismic fragility analysis of highway bridges. MAEC RR-4, C enter for Earthquake Research Information.

[24] MacKie, K.R., Stojadinovic, B.R., (2007), "Factor parameterized bridge damage fragility curves". Journal of Bridge Engineering, pp: 500-510.

[25] Federal emergency management agency [FEMA 356], November, 2000.

[26] Hossain, M. R., Ashraf, M., Albermani, F., (2009), "Numerical evaluation of yielding shear panel device: a sustainable technique to minimize structural damages due to earthquakes" Universitas 21 International Graduate Research Conference: Sustainable Cities for the Future, pp: 65-68.

[27] Ranjan., P. and Dhiman., P., (1991), " Retrofitting of column of an existing building by RC, FRP, and SFRC jacketing techniques" IOSR Journal of Mechanics and Civil Engineering, e-ISSN : 2278-1684, P-ISSN :2320-334X.

[28] Kunisue., A., Koshika., N., Kurokawa., Y., Suzuki., N., Agami., j., Sakamoto., M., (2007), " Retrofitting method of existing reinforced concrete buildings using elasto-plastic steel dampers" 12 WCEF.

[29] Oliveto., G., Marletta., M., (2005), "Seismic retrofitting of reinforced concrete buildings using traditional and innovation techniques" ISET Journal of Earthquake Technology,paper no : 454, vol : 42, no: 2-3, pp :21-46.

[30] Rizkalla., S. and Hassan., T., (2001), " Various FRP strengthening techniques for retrofitting concrete structures"

[31] Vaghani., M., Vasanwala., S.A., Desai. A. K., (2014), "Advanced Retrofitting Techniques for RC Building: A state of an art review" International Journal of Current Engineering and Technology, E-ISSN 2277-4106, P- ISSN 2347-5161.

[32] Chan, R.W.K. and Albermani, F., (2008), "Experimental study of steel slit damper for passive energy dissipation". Engineering Structures 30, pp: 1058-1066.

[33] Hossain, M. R. and Ashraf, M., (2012), "Mathematical modeling of yielding shear panel device." Thin-walled Structures, 59, pp: 153-161.

[34] Chan, R. W. K. (2008), "Metalic yielding deices for passive dissipation of seismic energy" University of Queensland

[35] Soong, T. T. and Spencer, B. F., (2002), "Supplemental energy dissipation: state-of-the-art and state-of-the-practice." Engineering Structures, 24, pp: 243-259.

[36] Ismail, M., Ikhouane, F., Rodellar, J., (2009), "The hysteresis Bouc-Wen model, a asymmary"

[37] Pall, A. S., Marsh, C., Fazio, P., (1980), "Friction joints for seismic control of large panel structures", Journal of the prestressed concrete institution,Vol. 25, No. 6, pp : 38-61

[38] Pall, A. S. and Marsh, C., (1982), "Response of friction damper braced frames" Journal of the structural division, ASCE, Vol. 108, No, ST6, pp: 1313-1323.

[39] Filiatrault, A. and Cherry, S., (1988), "Comparative performance of friction damped syatems and base isolation syatems for earthquake retrofit and aseismic design." Earthquake engineering structural dynamics, Vol. 16, pp: 389-416.

[40] Roik, K., Dorka, V., Dechent, P., (1988), "Vibration control of structures under earthquake loading by three-stage-grip elements." Earthquake engineering structural dynamics, Vol.16, pp: 501-521.

[41] FitzGerald, T. F., Anagnos, T., Goodson, M., Zsutty, T., (1989), "Slotted bolted connections in aseismic design for concentrically braced connections." Earthquake spectra, Vol. 5, No. 9, pp: 383-391.

[42] Ashour, S. A. and Hanson, R. D. (1987), "Elastic seismic response of buildings with supplemental damping, Technical report UMCE 87-01, The University of Michigan, Ann Arbor..

[43] Su, Y-F and Hanson, R. D., (1990), " Seismic response of building structures with mechanical damping devices, Technical report UMCE 90-02", The University of Michigan, Ann Arbor, MI.

[44] Lin, R.C., Liang, Z., Soong, T.T., Zhang, R. h., (1991), "An experimental study on seismic structural response study on seismic structural response with added viscoelastic dampers." Engineering structures, Vol. 13, pp: 75-84.

[45] Chang, K. C., Soong, T. T., Oh, S.T., Lai, M. l., (1995), "Seismic behavior of steel frame with added viscoelastic dampers." Journal of structural engineering, ASCE, Vol. 121, No. 10, pp: 1418-1426.

[46] Chang, K. C., Shen, K. L., Soong, T. T., Lai, M.L., (1994), "Seismic retrofit of a concrete frame with added viscoelastic dampers," Proceedings of the fifth national conference on earthquake engineering, Chicago, IL.

[47] Chan, R.W.K., Albermani, F., Williams, M.S., (2009), "Evaluation of yielding shear panel device for passive energy dissipation." Journal of Construction Steel Research, 65, pp: 260-280.

[48] Aiken, I. D., Whittaker, A. S., Kelly, J. M. (1993), "Testing of passive energy dissipation system" Earthquake Spectra, 9.

[49] Tsai. K.C. and Hong, C.P. (1992), "Steel triangular plate absorber for earthquake-resistant buildings" Constructional Steel Design: World Developments. Elsevier Applied Science.

[50] Soong, T. and Dargush, G., (1997), "Passive energy dissipation systems in structural engineering"

[51] Bracci, J. M., Reinhorn, A. M., Mander, J. B., (1996), "Seismic resistance of reinforced concrete frame structures designed for gravity loads: performance of structural system." ACI Journal, 92(5), pp: 597-608.

[52] Schmidt, K. Dorka, U. E., Taucer, F., Magnonette, G., (2004), " Seismic retrofit of a steel frame and an Rc frame with hyde syatems, " Institute for the protection and security of the citizen European laboratory for structural assessment, European commission joint research centre.

[53] Williams, M. and Albermani, F., (2003), "Monotonic and cyclic tests on shear diaphragm dissipators for steel frames," Civil engineering bulletin No. 23, Department of civil engineering, University of Queensland, Australia.

[54] Baber, T. and Noori, M., (1986), "Modelling general hysteresis behavior and random vibration application" J Vib Acoust Stress Reliab Des; pp: 108:411-20.

[55] Chan, R.W.K., Albermani, F., Kitipornchai, S., (2013), "Experimental study of perforated yielding shear panel device for passive energy dissipation." 91, pp: 14-25.

[56] Li Zhengying, Faris Albermani, Ricky W.K. Chan, S. Kitipornchai (2011), "Pinching hysteretic response of yielding shear panel device." Engineering Structures, 33, pp: 993-1000.

[57] Wada, A., Haung, Y.H., Iwata, M., (2000), "Passive damping technology for buildings in Japan, Prog Struct Engng Mater, 2, pp: 335-350.

[58] Hossain, M. R., Ashraf, M., Padgett, J. E., (2012) "Probabilistic seismic performance evaluation for yielding shear panel design". Australasian Structural Engineering Conference The past, present and future of Structural Engineering. Barton, A.C.T.: Engineers Australia, pp: 58-65.

[59] Freddi, F., Padgett, J. E., Asta, A.D., (2016), "Probabilistic seismic demand modeling of local level response parameters of an RC frame." Springer Science + Business Media Dordrecht.

[60] Ranjan., P. and Dhiman., P., (1991), " Retrofitting of column of an existing building by RC, FRP, and SFRC jacketing techniques" IOSR Journal of Mechanics and Civil Engineering, e-ISSN : 2278-1684, P-ISSN :2320-334X.

[61] Sakina, K. and Sun, Y., (2000), "Steel jacketing for improvement of column strength and ductility" 12WCEE, pp: 2525.

[62] Tsonos, A. G. (2004), "Effectiveness of CFRP-Jackets and Rc- jackets in post- earthquake and pre-earthquake retrofitting of beam-column subassemblies." 13WCEE, pp: 2558

[63] Chan, R. W. K., Yuen, J. K. K., Lee, E. W. M., Arashpour, M., (2015), "Application of Nonlinear-Autoregressive-Exogenous model to predict the hysteretic behavior of passive control system." Engineering Structures, 85, pp: 1-10.

[64] Habibi, A., Chan, R. W. K., Albermani, F., (2013), "Energy-based design method for seismic retrofitting with passive energy dissipation systems. "Engineering Structures, 46, pp: 77-86.

[65] Scott, M. H. and Fenves, G. L., (2006), "Plastic hinge integration methods for force-based beam-column elements." J Struct Eng 132, pp: 244-252.

[66] Panagiotakos, T.B. and Fardis, M.N., (2001), "Deformation of reinforced concrete members at yielding and ultimate" ACI Struct J 98, pp: 135-148.

[67] Baber, T. and Noori, M., (1986) "Modelling general hysteresis behavior and random vibration application" J Vib Acoust Stress Reliab Des, pp: 411-20.

[68] Hossain, M. R., Ashraf, M., Albermani, F., (2011), "Theoretical evaluation of yielding shear panel device for passive energy dissipation" IIECCOMAS Thematic Conference, pp: 25-28.

[69] Vamvatsikos, D.O., Cornell, C.A., (2002), "Incremental dynamic analysis" Earthquake Engineering and Structural Dynamics, pp: 491-541.

[70] Vamvatsikos, D.O., Cornell, C.A., (2011), "The incremental dynamic analysis and its application to performance-based earthquake engineering" 12th European Conference on Earthquake Engineering, Elsevier Science Ltd, pp: 479.

[71] Hossain, M. R., Asraf, M., Padgett, J.E., (2013) "Risk-based seismic performance assessment of Yielding Shear Panel Device." Engineering Structures, 56, pp 1570-1579.

Appendices

Appendix A

Modeling of the frame along with YSPDs in three story three bay

```
# Prototype Model

# (Units mm, N, MPa)


# Model with craked stiffness for the elastic part of the elements, rigid joints,

# Hysteretic materials for the rebars, T section considering the whole slab, masses

# applied on the beam-column intersections, median value among the concrete characteristics considered,

# 0.05 as last deformation of the concrete to avoid localization of the plasticization,

# Rayleg damping 3 %


wipe

model BasicBuilder -ndm 2 -ndf 3;

set dataDir Data;

file mkdir $dataDir;



# Start of model generation

# ========================
```

```
# Create ModelBuilder

model  BasicBuilder  -ndm  2  -ndf  3


#     Node        xCrd      yCrd

node    101        0            0


node    102        0            3429

node    1021     0            3200.4

node    1022     152.4     3429

node    1023     0            3657.6


node    103        0            7086.6

node    1031     0            6858

node    1032     152.4     7086.6

node    1033     0            7315.2


node    104      0            10744.2

node    1041     0            10515.6

node    1042     152.4     10744.2
```

node 105 5486.4 0

node 106 5486.4 3429

node 1061 5486.4 3200.4

node 1062 5638.8 3429

node 1063 5486.4 3657.6

node 1064 5334 3429

node 107 5486.4 7086.6

node 1071 5486.4 6858

node 1072 5638.8 7086.6

node 1073 5486.4 7315.2

node 1074 5334 7086.6

node 108 5486.4 10744.2

node 1081 5486.4 10515.6

node 1082 5638.8 10744.2

node 1084 5334 10744.2

node 109 10972.8 0

node 110 10972.8 3429

node 1101 10972.8 3200.4

node 1102 11125.2 3429

node 1103 10972.8 3657.6

node 1104 10820.4 3429

node 111 10972.8 7086.6

node 1111 10972.8 6858

node 1112 11125.2 7086.6

node 1113 10972.8 7315.2

node 1114 10820.4 7086.6

node 112 10972.8 10744.2

node 1121 10972.8 10515.6

node 1122 11125.2 10744.2

node 1124 10820.4 10744.2

node 113 16459.2 0

node 114 16459.2 3429

node 1141 16459.2 3200.4

```
node    1143    16459.2         3657.6

node    1144    16306.8         3429


node    115      16459.2        7086.6

node    1151    16459.2         6858

node    1153    16459.2         7315.2

node    1154    16306.8         7086.6


node    116      16459.2        10744.2

node    1161    16459.2         10515.6

node    1164    16306.8         10744.2


#setting up the parameters


set IDctrlNode 104;             # node where displacement is read for displacement control

set IDctrlDOF 1;                # degree of freedom of displacement read for displacement control

set NStory 3;           # number of stories above ground level

set NBay 3;             # number of bays
```

#Building height

set LBuilding 10744.2;

Intermediate Node for YSPDs

Node xCrd yCrd

node 1 2743.2 3429;

node 2 8229.6 3429;

node 3 13716 3429;

node 4 2743.2 7086.6;

node 5 8229.6 7086.6;

node 6 13716 7086.6;

node 7 2743.2 10744.2;

node 8 8229.6 10744.2;

node 9 13716 10744.2;

Intermediate Node for Bracing

Node xCrd yCrd

```
node    11      2743.2  3329
node    22      8229.6  3329
node    33      13716   3329
node    44      2743.2  6986.6
node    55      8229.6  6986.6
node    66      13716   6986.6
node    77      2743.2  10644.2
node    88      8229.6  10644.2
node    99      13716   10644.2


# Define Single Point Constraints
# SPC tag Dx Dy Rz
fix     101     1       1       1
fix     105     1       1       1
fix     109     1       1       1
fix     113     1       1       1


# Define nodal masses
# Nodetag         mx      my   mIz
```

```
mass     102     13.77   13.77   0
mass     103     13.77   13.77   0
mass     104     13.77   13.77   0
mass     106     13.77   13.77   0
mass     107     13.77   13.77   0
mass     108     13.77   13.77   0
mass     110     13.77   13.77   0
mass     111     13.77   13.77   0
mass     112     13.77   13.77   0
mass     114     13.77   13.77   0
mass     115     13.77   13.77   0
mass     116     13.77   13.77   0

##########################################################################################################################################################################################

# Define materials

# 2   Column 1 and 3

# 3   Column 2 and 4

# 4   Columns Subassemblages

# 5   Beams Subassemblages
```

6 Concrete Complete Structure

Material Concrete02 matTag fc' epsc0 fcu' epsu lambda ft Ets

uniaxialMaterial Concrete02 2 -24.81 -0.0025 -7.44 -0.05 0.05 0.0 0.5

uniaxialMaterial Concrete02 3 -30.13 -0.0021 -9.04 -0.05 0.05 0.0 0.5

uniaxialMaterial Concrete02 4 -31.58 -0.0029 -11.15 -0.05 0.05 0.0 0.5

uniaxialMaterial Concrete02 5 -34.60 -0.0022 -6.50 -0.05 0.05 0.0 0.5

uniaxialMaterial Concrete02 6 -27.68 -0.00235 -6.53 -0.05 0.05 0.0 0.5

10 Steel gauge12 (slab reinforcements)

11 Steel D4 (beam and column reinforcements)

12 Steel D5 (upper reinforcements lateral beams)

Material Steel02 matTag Fy E b R0 cR1 cR2 <a1 a2 a3 a4> <sig0>

uniaxialMaterial Steel02 10 276.00 214080.4 0.004175 18.5 0.925 0.15 0.0 1.0 0.0 1.0 0.0

Material Steel01 matTag Fy E b a1 a2 a3 a4

uniaxialMaterial Steel01 11 276.00 214080.4 0.003 0.0 1.0 0.0 1.0

uniaxialMaterial Steel01 12 276.00 214080.4 0.003 0.0 1.0 0.0 1.0

20 Steel Hysteretic gauge12 (slab reinforcements) #3

21 Steel Hysteretic D4 base column reinforcements (lap splice) #6

22 Steel Hysteretic D4 first floor column reinforcements (no lap splice) #6

23 Steel Hysteretic D4 Subassemblages #6

24 Steel Hysteretic D5 (upper reinforcements lateral beams) #5

Material Hysteretic matTag s1p e1p s2p e2p s1n e1n s2n e2n pinchX pinchY damage1 damage2 <$beta>

uniaxialMaterial Hysteretic 20 276.00 0.00129 364.23 0.100 373.16 0.11 -276.00 -0.00129 -364.23 -0.100 -373.16 -0.11 0.0 0.0 0 0 0

uniaxialMaterial Hysteretic 21 276.00 0.00129 339.40 0.100 345.82 0.11 -276.00 -0.00129 -339.40 -0.100 -345.82 -0.11 0.4 0.6 0 0 0.8

uniaxialMaterial Hysteretic 22 276.00 0.00129 339.40 0.100 345.82 0.11 -276.00 -0.00129 -339.40 -0.100 -345.82 -0.11 0.2 0.6 0 0 0

uniaxialMaterial Hysteretic 23 276.00 0.00129 339.40 0.100 345.82 0.11 -276.00 -0.00129 -339.40 -0.100 -345.82 -0.11 0.0 0.6 0 0 0

uniaxialMaterial Hysteretic 24 276.00 0.00129 339.40 0.100 345.82 0.11 -276.00 -0.00129 -339.40 -0.100 -345.82 -0.11 0.0 0.3 0 0 0

```
##########################################################################
##########################################################################
########################################

# Define section(s)

# 2   Column

# 3   Beam internal

# 4   Beam external

#         Section           secTag

section Fiber             2         {

          patch quad        6     120       1    -152.4 -152.4  152.4 -152.4 152.4  152.4  -152.4
        152.4

          layer  straight  23      2         283.87          114.3          114.3  114.3  -114.3

          layer  straight  23      2         283.87          -114.3         114.3  -114.3 -114.3

}

#         Section           secTag
```

```
section Fiber        3      {

        patch quad      6    120   1          -228.6     -114.3 228.6  -114.3 228.6   114.3
      -228.6  114.3

        patch quad      6    40      1        76.2         114.3        228.6   114.3 228.6
1828.8 76.2     1828.8

        patch quad      6    40      1        76.2         -1828.8      228.6  -1828.8
      228.6  -114.3  76.2    -114.3

        layer straight 23    3      283.87 190.5  76.2   190.5  -76.2

        layer straight 23    2        141.94      -190.5 76.2   -190.5 -76.2


        layer straight 20    8        70.97         190.5  1798.8       190.5   144.3

        layer straight 20    8        70.97         190.5 -144.3 190.5  -1798.8

        layer straight 20    8        35.48         114.3  1798.8       114.3   144.3

        layer straight 20    8        35.48         114.3 -144.3 114.3  -1798.8

}
```

```
#         Section          secTag

section Fiber            4         {

          patch quad        6     120    1            -228.6      -114.3 228.6  -114.3 228.6    114.3
        -228.6   114.3

          patch quad        6     40        1          76.2          114.3          228.6    114.3  228.6
1828.8  76.2       1828.8

          patch quad        6     40        1          76.2          -1828.8        228.6   -1828.8
        228.6   -114.3   76.2     -114.3

          layer  straight  24      2       283.87 190.5   76.2     190.5   -76.2

          layer  straight  23      2          141.94       -190.5  76.2     -190.5  -76.2



          layer  straight  20      8          70.97          190.5  1798.8         190.5    144.3

          layer  straight  20      8          70.97          190.5 -144.3  190.5   -1798.8

          layer  straight  20      8          35.48          114.3  1798.8         114.3    144.3

          layer  straight  20      8          35.48          114.3 -144.3  114.3   -1798.8

}
```

```
##########################################################################
##########################################################################
########################################
```

```
# Define geometric transformation(s)
# GeoTran    type    tag
geomTransf  Linear       1
geomTransf  PDelta       2

set Econc_el  24178;
set Acolumns  92880;
set Abeams    627093;

set IzBeams   425250572.6    ;

# Define element(s)
# Element                              eleTag   NodeI NodeJ  secTagI      Lpi   secTagJ    Lpj
E          A          Iz                    geoTranTag    <-mass massDens>    <-iter maxIters tol>
# Columns
element  beamWithHinges   1     101  1021     2     192.024    2     192.024 $Econc_el  $Acolumns
305874278.97          1                -mass +0.000000E+000  -iter   25  +1.000000E-008
```

```
element beamWithHinges 2 105 1061 2 192.024 2 192.024 $Econc_el $Acolumns
381202475.60 1 -mass +0.000000E+000 -iter 25 +1.000000E-008

element beamWithHinges 3 109 1101 2 192.024 2 192.024 $Econc_el $Acolumns
381202475.60 1 -mass +0.000000E+000 -iter 25 +1.000000E-008

element beamWithHinges 4 113 1141 2 192.024 2 192.024 $Econc_el $Acolumns
305874278.97 1 -mass +0.000000E+000 -iter 25 +1.000000E-008


element beamWithHinges 5 1023 1031 2 192.024 2 192.024 $Econc_el $Acolumns
283830488.14 1 -mass +0.000000E+000 -iter 25 +1.000000E-008

element beamWithHinges 6 1063 1071 2 192.024 2 192.024 $Econc_el $Acolumns
336029788.41 1 -mass +0.000000E+000 -iter 25 +1.000000E-008

element beamWithHinges 7 1103 1111 2 192.024 2 192.024 $Econc_el $Acolumns
336029788.41 1 -mass +0.000000E+000 -iter 25 +1.000000E-008

element beamWithHinges 8 1143 1151 2 192.024 2 192.024 $Econc_el $Acolumns
283830488.14 1 -mass +0.000000E+000 -iter 25 +1.000000E-008


element beamWithHinges 9 1033 1041 2 192.024 2 192.024 $Econc_el $Acolumns
258044546.66 1 -mass +0.000000E+000 -iter 25 +1.000000E-008

element beamWithHinges 10 1073 1081 2 192.024 2 192.024 $Econc_el
$Acolumns 293582234.48 1 -mass +0.000000E+000 -iter 25 +1.000000E-008

element beamWithHinges 11 1113 1121 2 192.024 2 192.024 $Econc_el
$Acolumns 293582234.48 1 -mass +0.000000E+000 -iter 25 +1.000000E-008

element beamWithHinges 12 1153 1161 2 192.024 2 192.024 $Econc_el
$Acolumns 258044546.66 1 -mass +0.000000E+000 -iter 25 +1.000000E-008
```

Beams

element beamWithHinges 13 1022 1 4 283.464 4 283.464 $Econc_el $Abeams $IzBeams 1 -mass +0.000000E+000 -iter 25 +1.000000E-008

element beamWithHinges 14 1 1064 4 283.464 3 283.464 $Econc_el $Abeams $IzBeams 1 -mass +0.000000E+000 -iter 25 +1.000000E-008

element beamWithHinges 15 1062 2 3 283.464 3 283.464 $Econc_el $Abeams $IzBeams 1 -mass +0.000000E+000 -iter 25 +1.000000E-008

element beamWithHinges 16 2 1104 3 283.464 3 283.464 $Econc_el $Abeams $IzBeams 1 -mass +0.000000E+000 -iter 25 +1.000000E-008

element beamWithHinges 17 1102 3 3 283.464 4 283.464 $Econc_el $Abeams $IzBeams 1 -mass +0.000000E+000 -iter 25 +1.000000E-008

element beamWithHinges 18 3 1144 4 283.464 4 283.464 $Econc_el $Abeams $IzBeams 1 -mass +0.000000E+000 -iter 25 +1.000000E-008

element beamWithHinges 19 1032 4 4 283.464 4 283.464 $Econc_el $Abeams $IzBeams 1 -mass +0.000000E+000 -iter 25 +1.000000E-008

element beamWithHinges 20 4 1074 4 283.464 3 283.464 $Econc_el $Abeams $IzBeams 1 -mass +0.000000E+000 -iter 25 +1.000000E-008

element beamWithHinges 21 1072 5 3 283.464 3 283.464 $Econc_el $Abeams $IzBeams 1 -mass +0.000000E+000 -iter 25 +1.000000E-008

element beamWithHinges 22 5 1114 3 283.464 3 283.464 $Econc_el $Abeams $IzBeams 1 -mass +0.000000E+000 -iter 25 +1.000000E-008

element beamWithHinges 23 1112 6 3 283.464 4 283.464 $Econc_el $Abeams $IzBeams 1 -mass +0.000000E+000 -iter 25 +1.000000E-008

```
element beamWithHinges 24 6 1154 4 283.464 4 283.464 $Econc_el $Abeams
$IzBeams 1 -mass +0.000000E+000 -iter 25 +1.000000E-008

element beamWithHinges 25 1042 7 4 283.464 4 283.464 $Econc_el $Abeams
$IzBeams 1 -mass +0.000000E+000 -iter 25 +1.000000E-008

element beamWithHinges 26 7 1084 4 283.464 3 283.464 $Econc_el $Abeams
$IzBeams 1 -mass +0.000000E+000 -iter 25 +1.000000E-008

element beamWithHinges 27 1082 8 3 283.464 3 283.464 $Econc_el $Abeams
$IzBeams 1 -mass +0.000000E+000 -iter 25 +1.000000E-008

element beamWithHinges 28 8 1124 3 283.464 3 283.464 $Econc_el $Abeams
$IzBeams 1 -mass +0.000000E+000 -iter 25 +1.000000E-008

element beamWithHinges 29 1122 9 3 283.464 4 283.464 $Econc_el $Abeams
$IzBeams 1 -mass +0.000000E+000 -iter 25 +1.000000E-008

element beamWithHinges 30 9 1164 4 283.464 4 283.464 $Econc_el $Abeams
$IzBeams 1 -mass +0.000000E+000 -iter 25 +1.000000E-008

set ARigid 1.00E+09;

set ERigid 34000;

set IzRigid 1.00E+15;

# Element eleTagNodeI NodeJ A E Iz geoTranTag <alpha
d> <-mass massDens>
```

```
# Rigid
element     elasticBeamColumn  1021  1021  102   $ARigid $ERigid   $IzRigid
      1     0.0   0.0     -mass  0.0
element     elasticBeamColumn  1022  102   1022  $ARigid $ERigid   $IzRigid
      1     0.0   0.0     -mass  0.0
element     elasticBeamColumn  1023  102   1023  $ARigid $ERigid   $IzRigid
      1     0.0   0.0     -mass  0.0

element     elasticBeamColumn  1031  1031  103   $ARigid $ERigid   $IzRigid
      1     0.0   0.0     -mass  0.0
element     elasticBeamColumn  1032  103   1032  $ARigid $ERigid   $IzRigid
      1     0.0   0.0     -mass  0.0
element     elasticBeamColumn  1033  103   1033  $ARigid $ERigid   $IzRigid
      1     0.0   0.0     -mass  0.0

element     elasticBeamColumn  1041  1041  104   $ARigid $ERigid   $IzRigid
      1     0.0   0.0     -mass  0.0
element     elasticBeamColumn  1042  104   1042  $ARigid $ERigid   $IzRigid
      1     0.0   0.0     -mass  0.0

element     elasticBeamColumn  1061  1061  106   $ARigid $ERigid   $IzRigid
      1     0.0   0.0     -mass  0.0
element     elasticBeamColumn  1062  106   1062  $ARigid $ERigid   $IzRigid
      1     0.0   0.0     -mass  0.0
```

```
element     elasticBeamColumn  1063  106   1063  $ARigid $ERigid   $IzRigid
      1     0.0   0.0    -mass  0.0

element     elasticBeamColumn  1064  1064  106   $ARigid $ERigid   $IzRigid
      1     0.0   0.0    -mass  0.0


element     elasticBeamColumn  1071  1071  107   $ARigid $ERigid   $IzRigid
      1     0.0   0.0    -mass  0.0

element     elasticBeamColumn  1072  107   1072  $ARigid $ERigid   $IzRigid
      1     0.0   0.0    -mass  0.0

element     elasticBeamColumn  1073  107   1073  $ARigid $ERigid   $IzRigid
      1     0.0   0.0    -mass  0.0

element     elasticBeamColumn  1074  1074  107   $ARigid $ERigid   $IzRigid
      1     0.0   0.0    -mass  0.0


element     elasticBeamColumn  1081  1081  108   $ARigid $ERigid   $IzRigid
      1     0.0   0.0    -mass  0.0

element     elasticBeamColumn  1082  108   1082  $ARigid $ERigid   $IzRigid
      1     0.0   0.0    -mass  0.0

element     elasticBeamColumn  1084  1084  108   $ARigid $ERigid   $IzRigid
      1     0.0   0.0    -mass  0.0


element     elasticBeamColumn  1101  1101  110   $ARigid $ERigid   $IzRigid
      1     0.0   0.0    -mass  0.0

element     elasticBeamColumn  1102  110   1102  $ARigid $ERigid   $IzRigid
      1     0.0   0.0    -mass  0.0
```

```
element     elasticBeamColumn  1103  110    1103  $ARigid $ERigid    $IzRigid
    1       0.0   0.0     -mass   0.0

element     elasticBeamColumn  1104  1104   110   $ARigid $ERigid    $IzRigid
    1       0.0   0.0     -mass   0.0


element     elasticBeamColumn  1111  1111   111   $ARigid $ERigid    $IzRigid
    1       0.0   0.0     -mass   0.0

element     elasticBeamColumn  1112  111    1112  $ARigid $ERigid    $IzRigid
    1       0.0   0.0     -mass   0.0

element     elasticBeamColumn  1113  111    1113  $ARigid $ERigid    $IzRigid
    1       0.0   0.0     -mass   0.0

element     elasticBeamColumn  1114  1114   111   $ARigid $ERigid    $IzRigid
    1       0.0   0.0     -mass   0.0


element     elasticBeamColumn  1121  1121   112   $ARigid $ERigid    $IzRigid
    1       0.0   0.0     -mass   0.0

element     elasticBeamColumn  1122  112    1122  $ARigid $ERigid    $IzRigid
    1       0.0   0.0     -mass   0.0

element     elasticBeamColumn  1124  1124   112   $ARigid $ERigid    $IzRigid
    1       0.0   0.0     -mass   0.0


element     elasticBeamColumn  1141  1141   114   $ARigid $ERigid    $IzRigid
    1       0.0   0.0     -mass   0.0

element     elasticBeamColumn  1143  114    1143  $ARigid $ERigid    $IzRigid
    1       0.0   0.0     -mass   0.0
```

```
element     elasticBeamColumn  1144  1144  114   $ARigid $ERigid   $IzRigid
      1     0.0   0.0     -mass   0.0

element     elasticBeamColumn  1151  1151  115   $ARigid $ERigid   $IzRigid
      1     0.0   0.0     -mass   0.0

element     elasticBeamColumn  1153  115   1153  $ARigid $ERigid   $IzRigid
      1     0.0   0.0     -mass   0.0

element     elasticBeamColumn  1154  1154  115   $ARigid $ERigid   $IzRigid
      1     0.0   0.0     -mass   0.0

element     elasticBeamColumn  1161  1161  116   $ARigid $ERigid   $IzRigid
      1     0.0   0.0     -mass   0.0

element     elasticBeamColumn  1164  1164  116   $ARigid $ERigid   $IzRigid
      1     0.0   0.0     -mass   0.0

#Brace Sections

set A_HSS1 1142.0;

set I_HSS1 1831418.0;

set A_HSS2 2174.0;

set I_HSS2 3246605.0;
```

```
set A_HSS3 3884.0;

set I_HSS3 4953154.0;

set E 200000;


#Braces


element elasticBeamColumn 31 101 11 $A_HSS3 $E $I_HSS3 1;

element elasticBeamColumn 32 11 105 $A_HSS3 $E $I_HSS3 1;

element elasticBeamColumn 33 105 22 $A_HSS3 $E $I_HSS3 1;

element elasticBeamColumn 34 22 109 $A_HSS3 $E $I_HSS3 1;

element elasticBeamColumn 35 109 33 $A_HSS3 $E $I_HSS3 1;

element elasticBeamColumn 36 33 113 $A_HSS3 $E $I_HSS3 1;



element elasticBeamColumn 37 102 44 $A_HSS3 $E $I_HSS3 1;

element elasticBeamColumn 38 44 106 $A_HSS3 $E $I_HSS3 1;

element elasticBeamColumn 39 106 55 $A_HSS3 $E $I_HSS3 1;

element elasticBeamColumn 40 55 110 $A_HSS3 $E $I_HSS3 1;

element elasticBeamColumn 41 110 66 $A_HSS3 $E $I_HSS3 1;

element elasticBeamColumn 42 66 114 $A_HSS3 $E $I_HSS3 1;
```

element elasticBeamColumn 43 103 77 $A_HSS3 $E $I_HSS3 1;

element elasticBeamColumn 44 77 107 $A_HSS3 $E $I_HSS3 1;

element elasticBeamColumn 45 107 88 $A_HSS3 $E $I_HSS3 1;

element elasticBeamColumn 46 88 111 $A_HSS3 $E $I_HSS3 1;

element elasticBeamColumn 47 111 99 $A_HSS3 $E $I_HSS3 1;

element elasticBeamColumn 48 99 115 $A_HSS3 $E $I_HSS3 1;

Define material

#uniaxialMaterial material tag alpha Ko n gama beta A q Zetas p Shi deltaShi Lamda tolerance maxNumberIter

uniaxialMaterial BWBN 25 0.012331839 26760 1.213 0.5 0.5 1 0.52 0.96 0.018 0.41 0.00001 0.0300 0.001 1000;

uniaxialMaterial BWBN 26 0.007746219 54220 0.544 0.5 0.5 1 0.38 0.95 0.015 0.27 0.00001 0.0014 0.001 1000;

uniaxialMaterial BWBN 27 0.005240081 93510 0.300 0.5 0.5 1 0.30 0.95 0.012 0.22 0.00001 0.0002 0.001 1000;

```
uniaxialMaterial Elastic 28 1.0e-20;

# Define two node link element

element twoNodeLink 49 1 11 -mat 28 27 28 -dir 1 2 3;
element twoNodeLink 50 2 22 -mat 28 27 28 -dir 1 2 3;
element twoNodeLink 51 3 33 -mat 28 27 28 -dir 1 2 3;

element twoNodeLink 52 4 44 -mat 28 27 28 -dir 1 2 3;
element twoNodeLink 53 5 55 -mat 28 27 28 -dir 1 2 3;
element twoNodeLink 54 6 66 -mat 28 27 28 -dir 1 2 3;

element twoNodeLink 55 7 77 -mat 28 27 28 -dir 1 2 3;
element twoNodeLink 56 8 88 -mat 28 27 28 -dir 1 2 3;
element twoNodeLink 57 9 99 -mat 28 27 28 -dir 1 2 3;

equalDOF 1 11 2;
equalDOF 2 22 2;
equalDOF 3 33 2;
```

```
equalDOF 4 44 2;

equalDOF 5 55 2;

equalDOF 6 66 2;


equalDOF 7 77 2;

equalDOF 8 88 2;

equalDOF 9 99 2;


# Define RECORDERS ----------------------------------------------------------

recorder Drift -file $dataDir/Drift-Story1.out -time -iNode 101 -jNode 102 -dof 1 -perpDirn 2;

recorder Drift -file $dataDir/Drift-Story2.out -time -iNode 102 -jNode 103 -dof 1 -perpDirn 2;

recorder Drift -file $dataDir/Drift-story3.out -time -iNode 103 -jNode 104 -dof 1 -perpDirn 2;

recorder Drift -file $dataDir/Drift-total.out -time -iNode 101 -jNode 104 -dof 1 -perpDirn 2;



################################################################################
##########



# display displacement shape of the column
```

```
recorder display "Displaced shape" 10 10 500 500 -wipe

prp 200. 50. 1;

vup  0  1 0;

vpn  0  0 1;

display 1 5 40



##########################################################################################

# Gravity-analysis

constraints Plain;

#constraints Transformation;

numberer Plain;

system BandGeneral;

#system UmfPack;

test NormDispIncr 1.0e-6 100;

algorithm Newton;

set NstepGravity 10;

set DGravity [expr 1.0/$NstepGravity];

integrator LoadControl $DGravity;
```

```
analysis Static;

analyze $NstepGravity;


# maintain constant gravity loads and reset time to zero

loadConst -time 0.0;

#puts "Model Built";

DYNAMIC ground-motion analysis -------------------------------------------------------------

# create load pattern

set G 9810

timeSeries Path 2 -dt 0.005 -filePath 143_FN.acc -factor $G; # define acceleration vector from file (dt=0.005 is associated with the input file gm)

pattern UniformExcitation 2 1 -accel 2;                    # define where and how (pattern tag, dof) acceleration is applied


# set damping based on first eigen mode

set freq [expr [eigen -fullGenLapack 1]**0.5]

set dampRatio 0.03

rayleigh 0. 0. 0. [expr 2*$dampRatio/$freq]


# create the analysis

wipeAnalysis;                                  # clear previously-define analysis parameters

constraints Plain;                             # how it handles boundary conditions
```

```
numberer Plain;                                 # renumber dof's to minimize band-width
(optimization), if you want to

system BandGeneral;                             # how to store and solve the system of
equations in the analysis

algorithm Linear                                # use Linear algorithm for linear analysis

integrator Newmark 0.5 0.25 ;           # determine the next time step for an analysis

analysis Transient;                             # define type of analysis: time-dependent

analyze 3995 0.01;                              # apply 3995 0.01-sec time steps in analysis



puts "Done!"

wipe
```

Appendix B

Calculation of lateral load for pushover analysis

Beam = 230 x 460 mm^2 = 9 x 18.11 in^2

Column = 300 x 300 mm^2 = 11.811 x 11.811 in^2 and Slab thickness = 6 in

Total slab dead load = 110 psf

Total slab live load = 50 psf

Total slab load = 110 + 50 = 160 psf

Self-weight of beam = (150 x 9 x 18.11) / 144 = 169.78 psf

Total beam weight = (1440 + 169.78) x 18 = 28976.04 lb

Total column weight = (150 x 11.811 x 11.811)/ 144 = 145.3 x 12 = 1743.74 lb

Weight of first story = (1743.74 x 4) / 2 + (1743.74 x 4) / 2 + 3 * 28976.04 = 93903.8 lb

Weight of second story = 93903.08 lb

Weight of third story = (1743.74 * 4) / 2 + 3*28976.04 = 90415.6 lb

Total floor weight = (93903.08 x 2 + 90415.6) = 278221.76 lb

Load at first story = [(93903.08 x 12) / (93903.08 x 12 + 93903.08 x 24 + 90415.6 x 36)] X 278221.76 = 47247.6 lb = 210167.79 N

Load at first story (per node) = 52541.9 N

Load at second story = [(93903.08 x 24) / 6635479.2] * 278221.76 = 94495.22 lb = 420335.52 N

Load at second story (per node) = 105083.88 N

Load at third story = [(90415.6 x 36) / 6635479.2] x 278221.76 = 136478.63 lb = 607086.97 N

Load at third story (per node) = 151771.74 N